



Theses and Dissertations

2018-08-01

Implementation and Optimization of Time Reversal for Use in Nondestructive Evaluation of Stress Corrosion Cracking

Sarah Marie Young
Brigham Young University

Follow this and additional works at: <https://scholarsarchive.byu.edu/etd>

BYU ScholarsArchive Citation

Young, Sarah Marie, "Implementation and Optimization of Time Reversal for Use in Nondestructive Evaluation of Stress Corrosion Cracking" (2018). *Theses and Dissertations*. 7539.

<https://scholarsarchive.byu.edu/etd/7539>

This Thesis is brought to you for free and open access by BYU ScholarsArchive. It has been accepted for inclusion in Theses and Dissertations by an authorized administrator of BYU ScholarsArchive. For more information, please contact scholarsarchive@byu.edu, ellen_amatangelo@byu.edu.

Implementation and Optimization of Time Reversal for Use in
Nondestructive Evaluation of Stress Corrosion Cracking

Sarah Marie Young

A thesis submitted to the faculty of
Brigham Young University
in partial fulfillment of the requirements for the degree of
Master of Science

Brian E. Anderson, Chair
Kent L. Gee
Jonathan D. Blotter

Department of Physics and Astronomy
Brigham Young University

Copyright © 2018 Sarah Marie Young

All Rights Reserved

ABSTRACT

Implementation and Optimization of Time Reversal for Use in Nondestructive Evaluation of Stress Corrosion Cracking

Sarah Marie Young
Department of Physics and Astronomy, BYU
Master of Science

The time reversal (TR) process manipulates a system's impulse response in order to focus a peak of acoustic energy at a specific location in space and time. This technique has been implemented in both fluid and solid media for purposes ranging from communications to source localization. This thesis will examine both the implementation and processing of TR for nondestructive evaluation in steel, specializing in nonlinear detection methods. A series of steel samples are inspected for stress corrosion cracking (SCC) using TR focusing to excite nonlinearities inherent in cracks. It is determined that SCC exists in the expected regions of the steel samples and that an induced increase in SCC corresponds to an increase in detected nonlinearity. In addition to this, a study is shown wherein TR signal processing is optimized for the detection of cracks. The TR impulse response is modified in a number of ways with the primary goal of increasing the amplitude of the TR focus. Each of these modifications is experimentally scrutinized for characteristics necessary for application to nondestructive evaluation, and ultimately one is chosen that amplifies TR focusing without increasing system nonlinearity. The optimized technique, decay compensation TR, is employed in the detection of SCC and is found to be as or perhaps even more successful than typical TR nondestructive evaluation methods.

Keywords: time reversal, nondestructive evaluation, stress corrosion cracking

ACKNOWLEDGMENTS

In conjunction with the heady euphoria that accompanies the conclusion of this thesis, I feel compelled to express my overwhelming gratitude for those persons and things that have contributed not only to its completion but to my continued sanity.

First, I wish to thank those who so charitably funded my research: A subcontract through Los Alamos National Laboratory from the Nuclear Energy University Program of the Department of Energy. I also wish to acknowledge and thank T.J. Ulrich, Marcel Remillieux, and Pierre-Yves Le Bas for their educational assistance. I must also, of course, thank BYU, the College of Physical and Mathematical Sciences, and the Department of Physics and Astronomy for their funding as well as making my educational environment remarkable.

Second, the swallows in the parking garage of my abode. If I loved birdsong before, it was a paltry thing compared to the glow I now feel when heralded by these beautiful creatures. It was and will always be a reminder of pure joy for the beauty of living.

Third, the ARG community who allowed me to tease, cajole, and jest my way into positions of abiding friendship. This included a lot of off-topic class-time in PH561 and PH662 and hundreds of jokes via my control of the ARG email. I had more fun writing them than anyone had reading them.

Fourth, to the grad students who let me pester them with questions beyond the typical human capacity to bear. Brent Reichman, Blaine Harker, Michael Denison, and Travis Hoyt, all gentlemen of patience, humor, and vast intelligence.

Fifth, my office-mates who also fit nicely in category four, but whose daily wit, laughter, and stories gave me reason to remember that people are more important than physics. In particular,

Kelli Succo, Joseph Lawrence, Pegah Aslani, and Brian Patchett, all individuals whose character shone brighter than their obvious mastery of physics.

Sixth, my professors here who challenged me to try difficult things, listened intently when I inevitably had questions about the material, humored me when I tried to take the class to some off-topic intellectual adventure (within reasonable limits, of course), gave me steady, heartfelt encouragement to continue, and carried with them a love for God and mankind that lifted souls, mine included.

Seventh, my advisor Dr. Brian Anderson who has personally taught me how to research with exactness, write with clarity, and be patient with each barrier towards progress. I am grateful for the time he was willing to spend training me on how to be an experimentalist because it is the part I now love the most.

Eighth, my former Bishop Tim Smith whose Godly counsel and steadying hand brought me to solace equal to the aching of life; who led me on a journey to the God whose healing love now guides my heart.

Ninth, my parents and sister, Melissa. Their faith, love, patience, joy, encouragement, humor, steadiness, and prayers give me the courage to continue beyond what I think I can bear and bring me joy until I overflow with gladness. In the past, in the present, and forever in the future.

Table of Contents

ABSTRACT.....	ii
ACKNOWLEDGMENTS	iii
Table of Contents	v
List of Figures	vi
List of Tables	ix
Chapter 1 : Introduction to Time Reversal	- 1 -
Chapter 2 : Nonlinearity from stress corrosion cracking as a function of chloride exposure time using the time reversed elastic nonlinearity diagnostic	- 8 -
2.1 Abstract	- 8 -
2.2 Introduction	- 8 -
2.3 Experimental Setup	- 14 -
2.4 Results	- 19 -
2.5 Conclusion.....	- 29 -
Chapter 3 : A comparison of impulse response modification techniques for time reversal with application to crack detection	- 31 -
3.1 Abstract	- 31 -
3.2 Introduction	- 32 -
3.3 Time Reversal and Experimental Setup	- 35 -
3.4 Time Reversal Signal Processing Modification Techniques.....	- 39 -
3.5 Focal Signal Analysis Metrics.....	- 42 -
3.6 Results	- 44 -
3.6.1 Peak Focal Amplitude	- 47 -
3.6.2 Temporal Quality	- 49 -
3.6.3 Spatial Quality.....	- 50 -
3.6.4 Harmonic Generation	- 51 -
3.7 Nonlinear Detection of SCC Using Decay Compensation TR.....	- 54 -
3.8 Conclusion.....	- 58 -
Chapter 4 : Conclusion.....	- 60 -
4.1 Future Work	- 62 -
Bibliography	- 63 -
Appendix A.....	- 71 -
Appendix B.....	- 130 -

List of Figures

- FIG. 1.1. An illustration of the propagation of an impulse through a closed-boundary system from transducer 1 to transducer 2. Time progresses from (a) to (e). (a) The moment an impulse is emitted from transducer 1. (b) The impulse propagates in three directions, a subset of the infinite number of possible paths. (c) The three rays continue to travel, reflecting off boundaries. (d) Two of the rays arrive at transducer 2 while the third is still traveling along a longer path. (e) The three rays have finished traveling from transducer 1 to transducer 2 and an impulse response constitutes a recording of their arrivals and amplitudes. - 3 -
- FIG. 1.2. An illustration of the propagation of the reversed impulse response (RIR) from transducer 2 to transducer 1 in a closed-boundary system. Time progresses from (a) to (f). (a) The moment the RIR has begun to be emitted into transducer 2, beginning with the green peak. (b) The green ray travels in three directions, a subset of the infinite number of possible paths. The red peak is about to be emitted. (c) All three peaks in the RIR have been emitted and travel the three paths, all with appropriate delays. (d) Two of the green rays have arrived at transducer 1 and two pulses are recorded. (e) The first of the red rays has arrived at transducer 1 and is recorded. The third green ray, second red ray, and first yellow ray all arrive simultaneously at transducer 1, creating a focus. (f) All nine rays have arrived at transducer 1 and are recorded. The focus is in the center with symmetrical side lobes. - 5 -
- FIG. 1.3. Three typical time reversal signals obtained using ultrasound in a solid sample, illustrating the many recorded paths. (a) Impulse response. (b) Reversed impulse response. (c) Focal signal. - 6 -
- FIG. 2.1. An image of 304L stainless steel with stress corrosion cracking (SCC) in the heat-affected zone (HAZ) just outside the weld. In this case, SCC has developed in the HAZ and occasionally in the weld. - 13 -
- FIG. 2.2 Example signals used in the time reversal process for the given experiments. (a) Normalized chirp signal used as the initial source excitation (the frequencies shown are intentionally decreased for visualization purposes). (b) Normalized chirp response, measured at the receiver location. (c) Normalized reversed impulse response, generated by a cross correlation of (a) and (b). (d) Focal signal generated at the receiver location. - 16 -
- FIG. 2.3. Photographs of the progression of rods from welded to damaged. (a) Undamaged 12.7 mm long, welded rod. The heat-affected zone (HAZ) is evident in the discoloration. (b) Rods in the 42% solution of hot magnesium chloride ($MgCl_2$). (c) Damaged rod after 14 days exposure in the solution. The $MgCl_2$ bath removes much of the HAZ discoloration. - 17 -
- FIG. 2.4. Photograph of the steel disk chaotic cavity with 8 piezoelectric transducers epoxied to the underside. A rod under test is epoxied to the top of the disk and the laser light (drawn in to visualize it) is coming from the direction of the dashed red line. The silver colored region on the rod is retro-reflective tape used to decrease optical noise. The scan line spans the line between the two dots drawn on the tape. - 18 -

FIG. 2.5. Time-domain focal signals from two scan points on the rod exposed to magnesium chloride for 12 days. (a) Focal signal 14.2 mm from the weld. (b) Focal signal 2 mm from the weld.	20 -
FIG. 2.6. Instantaneous velocity along the length of rod at the moment of time reversal focusing on an unexposed rod. The focus is generated at the location marked by the 'x'....	21 -
FIG. 2.7. Spectra of the focal signals displayed in Fig. 2.5. Amplitude scaling to the Euclidean norm of the spectra within the fundamental bandwidth is applied, shown mathematically in Eq. (2.1). The fundamental bandwidth is outlined by the vertical dash-dot lines. The second harmonic is outlined by the vertical dashed lines.	23 -
FIG. 2.8. The scaled nonlinearity, $\zeta(x, \theta)$, in the second harmonic bandwidth, versus scan position, x (mm). Vertical dashed lines indicate the approximate outer edge of the weld. Data shown in black are from the rod exposed to the magnesium chloride bath for 12 days, while the curves in teal are for the rod exposed for zero days. Data are from a 200 point scan at (a) 0° , (b) 90° , (c) 180° , and (d) 270°	25 -
FIG. 2.9. Left axis: peak focal amplitude, A_p , versus scan position, x . Right axis: scaled nonlinearity, $\zeta(x, \theta)$, versus scan position. The outer edges of the weld are indicated by the vertical dashed lines.	27 -
FIG. 2.10. Total nonlinearity, Z , measured in each rod versus the amount of time the rod was exposed to the hot solution of magnesium chloride ($MgCl_2$).	29 -
FIG. 3.1. Example signals used in the time reversal process. Except for (e), the amplitudes are normalized and are in arbitrary units. (a) Source chirp (with frequencies altered for visualization), (b) chirp response, (c) impulse response, (d) reversed impulse response, (e) focal signal.....	37 -
FIG. 3.2. Experimental setup with scanning laser Doppler vibrometer (SLDV) pointed at a steel disk. The steel disk has a piezoelectric transducer (PZT) epoxied to the bottom....	38 -
FIG. 3.3. Impulse response modification techniques with each starting with a traditional RIR, (a)-(b) deconvolution TR, (c)-(e) one-bit TR with a threshold of 0.2, indicated by the dashed black lines, (f)-(h) clipping TR with a threshold of 0.2, (i)-(k) decay compensation TR with a threshold of 0.06.	41 -
FIG. 3.4. Measured focus signals using (a) traditional, (b) deconvolution, (c) one-bit, (d) clipping, and (e) decay compensation TR. One-bit, clipping, and decay compensation TR all use a threshold value of 0.02.	46 -
FIG. 3.5. Peak focal amplitude, A_p , vs threshold applied obtained from time reversal (TR) focal signals with various TR processing techniques applied. Traditional TR and deconvolution TR do not use a threshold and so are plotted at a threshold of one.-	48 -
FIG. 3.6. Temporal quality, ξ_t , vs threshold applied obtained from time reversal (TR) focal signals with various TR processing techniques applied. Traditional TR and deconvolution TR are plotted at a threshold value of one.	50 -
FIG. 3.7. The focal spectra measured with (a) traditional time reversal (TR), (b) one-bit TR, (c) clipping TR, (d) decay compensation TR. (b)-(d) use a threshold of 0.02 for the impulse response modification. The region between the solid vertical lines is the fundamental	

bandwidth (75-125 kHz). The region between the dashed lines is the second harmonic (150-250 kHz), and the region between the dash-dot lines is the third harmonic (225-375 kHz). - 53 -

FIG. 3.8. Normalized nonlinearity contained in the second harmonic of a focal signal, shown as E_2 on the vertical axis, generated at each of 200 scan locations along a rod with stress corrosion cracking. Traditional time reversal (TR) (gray) and decay compensation TR (black) were used to excite TR foci at each location. Figure 8(a) shows the results when the focal signals were excited with an amplitude of 0.25 V. Figure 8(b) shows the results at an excitation amplitude of 1.5 V. While ultimately unknown, stress corrosion cracking is likely to occur in the region just outside the weld on the rod, called the Heat-Affected-Zone. - 58 -

List of Tables

TABLE 3.1. Spatial quality and full-width-half-max (FWHM) of the spatial scans taken of a focal signal for each time reversal (TR) signal processing technique. A threshold of 0.02 was used for one-bit, clipping, and decay compensation TR techniques.....- 51 -

TABLE 3.2. Harmonic ratios: the ratio of the energy in the fundamental bandwidth to the energy in a higher harmonic, shown below for the second harmonic, R_{12} , and the third harmonic, R_{13} for each of the amplitude-increasing modification techniques and traditional time reversal (TR).....- 54 -

Chapter 1: Introduction to Time Reversal

Time reversal (TR) is a process whereby acoustic energy can be manipulated to create a focus of energy at a single location in space and time.^{1,2} This is done by manipulation of a system's impulse response. The impulse response records the timing of the reflections from an impulse broadcast into a system. The impulse response is then reversed in time and emitted into the system. The reflections retrace their original paths and ultimately constructively interfere, recreating the original impulse. Let us begin by examining this process in more detail.

The first step in TR is to collect the impulse response of a system. In Fig. 1.1, a room is depicted as a rectangle with two transducers, one on either side labeled 1 and 2. Each transducer can both receive and emit a signal. An impulse is sent through transducer 1 and waves spread through the room, shown in Fig. 1.1(b). In a real system, an infinite number of rays should be used to represent the propagation of outward spherical waves, but for the system in Fig. 1.1, three rays are shown that represent a few of the possible paths in this reverberant system. In Fig. 1.1(c) the three rays continue to propagate, and two have reflected off boundaries, following the law of reflections as they rebound. Figure 1.1(d) shows that two of the rays have arrived at transducer 2, and the third ray, which followed the longest path, will soon follow. Figure 1.1(e) illustrates the complete journey of the three rays and to the right, excluding any reflection of these rays from the boundary at transducer 2, the time history of the arrivals of these rays is shown in the impulse response recorded by transducer 2. The impulse response records the time-of-flight for each of the three rays. Three peaks of energy are shown in the impulse response, the first from the wave which traveled directly from transducer 1 to transducer 2, which experienced the least propagation losses (i.e. spherical spreading) and so has the highest amplitude. The second peak in the impulse response records the arrival of the ray which reflected once, off the top boundary, and from there

traveled to transducer 2. The path this ray traveled was slightly longer than the direct ray and so it arrived slightly later in time with a further reduced amplitude. The last and shortest peak indicates the arrival of the ray which followed the longest path, reflecting off two boundaries before reaching transducer 2, and therefore is recorded in the impulse response much later in time than the first two rays. The three peaks of the impulse response are three, time-delayed impulses that are indicative of the paths traveled between transducer 1 and 2. The timing of the impulse arrivals at transducer 2 is dependent on the geometry of the room. Additionally, if either transducer is moved to a new location, the impulse response would also change, and thus the impulse response is source and receiver location dependent.

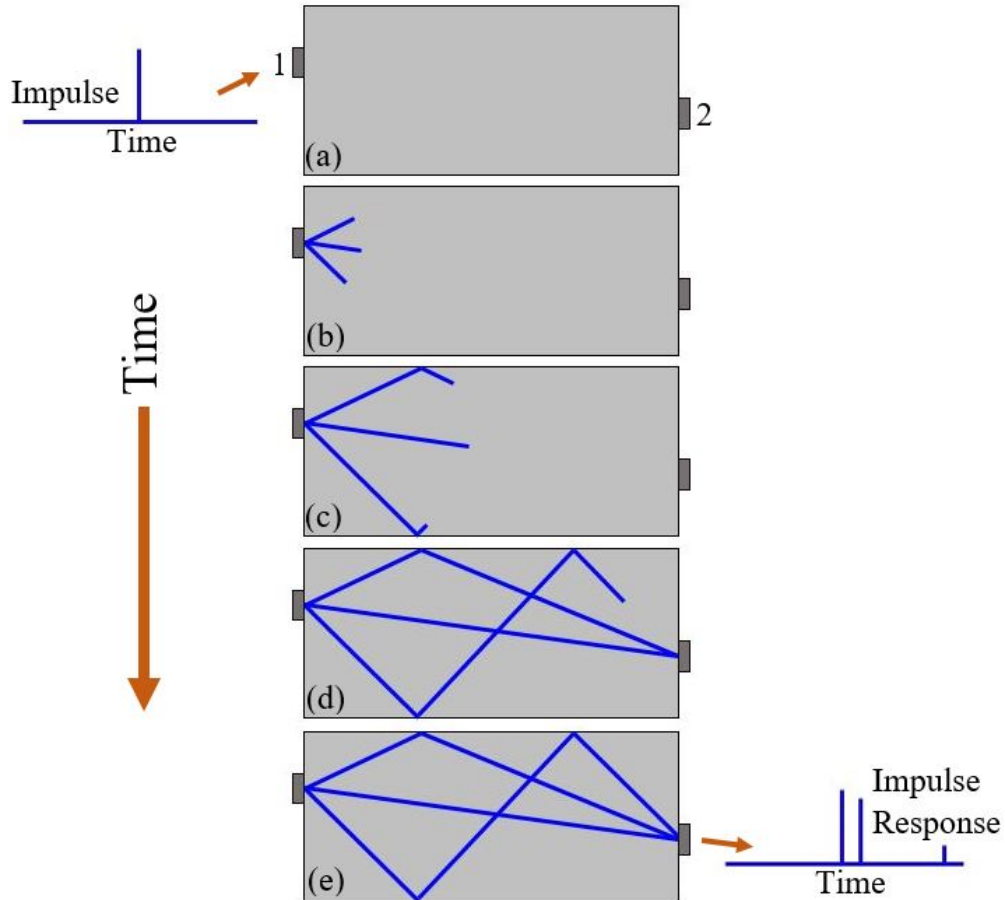


FIG. 1.1. An illustration of the propagation of an impulse through a closed-boundary system from transducer 1 to transducer 2. Time progresses from (a) to (e). (a) The moment an impulse is emitted from transducer 1. (b) The impulse propagates in three directions, a subset of the infinite number of possible paths. (c) The three rays continue to travel, reflecting off boundaries. (d) Two of the rays arrive at transducer 2 while the third is still traveling along a longer path. (e) The three rays have finished traveling from transducer 1 to transducer 2 and an impulse response constitutes a recording of their arrivals and amplitudes.

The process depicted in Fig. 1.1 is referred to as the forward propagation step, where an impulse response is measured between two points in the system. In order for TR to create a focus of energy using the impulse response, another propagation step must occur, a backward propagation step. Prior to this step, the impulse response is reversed in time. In Fig. 1.2, just to the right of (a) is shown the time-reversed impulse response recorded in the process depicted in Fig. 1.1. This reversed impulse response (RIR) will now be emitted through transducer 2 with the

peak representing the longest path emitted first (shown with a green color) and the peak representing the direct path emitted last (shown with a yellow color). The three peaks (and their corresponding paths) have been color coded in order to differentiate the timing of the emitted rays. In Fig. 1.2(b), the green impulse has been broadcast into the medium and is propagating along the same three paths traversed in the forward step. The two remaining peaks in the RIR, red and yellow, have yet to be emitted. In Fig. 1.2(c), all three impulses in the RIR have been emitted, each following the three paths, meaning there will be nine rays arriving at transducer 1. With the time step shown in Fig. 1.2(d), two of those arrivals have occurred. Two of the green rays, emitted much earlier than the other two peaks, have already completed the two shortest paths and a recording of their arrivals is shown to the left of Fig. 1.2(d). In Fig. 1.2(e), the arrival of the first red ray has been recorded after which the last green ray, the second red ray, and the first yellow ray simultaneously arrive at transducer 1, superposing to generate a large peak amplitude. For this to occur, the green, red, and yellow rays that arrived simultaneously had to travel the original paths traversed in the forward step in the order of the reversed timing. In other words the green impulse that traveled the longest path in the forward step had to start traveling that same path in reverse in the backward step, then the red impulse that traveled the path with a single reflection had to travel that same path in reverse, and finally the yellow impulse that traveled directly between the transducers had to travel that same path in reverse to provide the simultaneous arrival of these three rays at transducer 1. The RIR thus contains the proper timing of these emissions. This high-amplitude peak in time, when the time-aligned rays constructively interfere, is called the focus. Figure 1.2(f) shows the completed process, after all rays have arrived and the focus is surrounded by symmetrical low amplitude peaks on either side. The recorded signal shown in Fig. 1.2(f) is called the focal signal. The symmetrical low-amplitude peaks, called side lobes, are the

unavoidable effect of allowing the RIR to follow all possible paths and therefore produce background noise before and after the focus. If the directional information of the arriving rays were recorded and this information were used in the backward propagation step, then side lobes could be reduced.

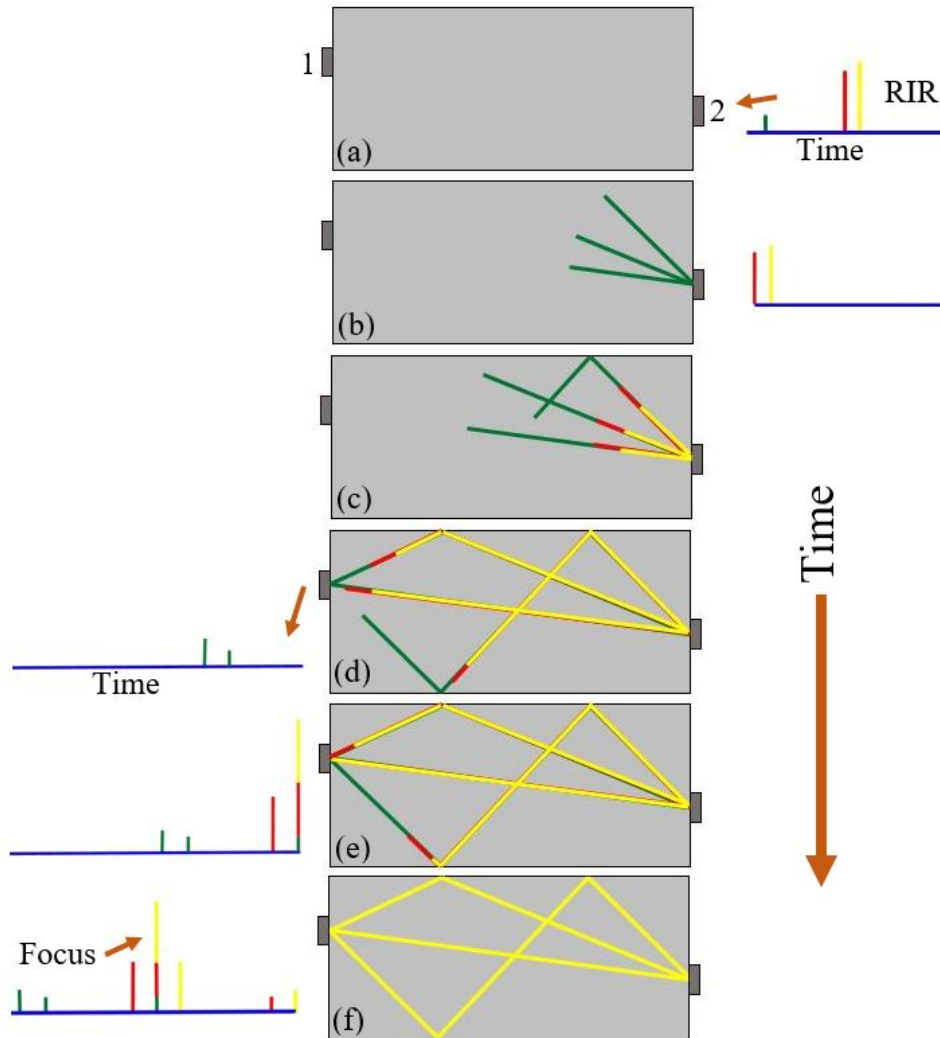


FIG. 1.2. An illustration of the propagation of the reversed impulse response (RIR) from transducer 2 to transducer 1 in a closed-boundary system. Time progresses from (a) to (f). (a) The moment the RIR has begun to be emitted into transducer 2, beginning with the green peak. (b) The green ray travels in three directions, a subset of the infinite number of possible paths. The red peak is about to be emitted. (c) All three peaks in the RIR have been emitted and travel the three paths, all with appropriate delays. (d) Two of the green rays have arrived at transducer 1 and two pulses are recorded. (e) The first of the red rays has arrived at transducer 1 and is recorded. The third green ray, second red ray, and first yellow ray all arrive simultaneously at transducer 1, creating a focus. (f) All nine rays have arrived at transducer 1 and are recorded. The focus is in the center with symmetrical side lobes.

In the example illustrated in Figs. 1.1 and 1.2, only three paths were used to demonstrate the TR process clearly. In a real system, there are an infinite number of paths of sound propagation that may be recorded in the impulse response over a sufficient length of time and each of these recorded arrivals are then subsequently broadcast during the backward propagation step, creating a larger amplitude focus, although side lobes would still be evident. Examples of typical signals recorded during these steps using TR of ultrasonic waves sent throughout a solid sample are shown in Fig. 1.3.

It is important to point out that a spatial focusing of waves also occurs in the TR process as the waves superpose to form the focus. This focus of energy is diffraction limited. In order for TR to be successful the system cannot change. The timing within the impulse response remains accurate only for linear, time-invariant systems. The focus becomes misaligned in time, less spatially localized, and lower in amplitude for weakly nonlinear, or slightly time-variant systems, however the TR focusing still occurs to some degree.

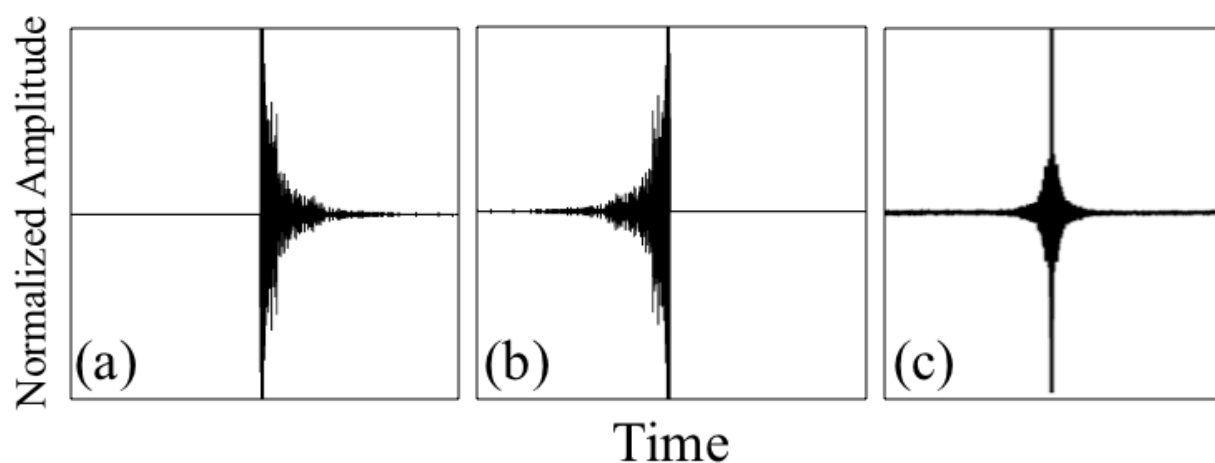


FIG. 1.3. Three typical time reversal signals obtained using ultrasound in a solid sample, illustrating the many recorded paths. (a) Impulse response. (b) Reversed impulse response. (c) Focal signal.

TR has been used for a number of applications in solid media, including high energy focusing, communications, and source localization. Much of the work in high energy focusing involves nondestructive evaluation of damaged materials. The focus of energy at a single time and place excites local properties of a medium, which for a damaged or cracked location will be amplitude dependent and the introduction of nonlinear frequency content occurs, indicating the presence of damage.³ Studies have been conducted to identify various types of damage including surface cracks,⁴ delaminations,⁵ fatigue cracks,⁶ and stress corrosion cracking.⁷ On the destructive end of things, other research studies have used high-amplitude TR to induce controlled cracking in glass⁸ or in lithotripsy for destroying kidney stones.⁹ The use of TR began in 1960 when it was developed for underwater naval communications applications,^{10,11} though communication in solid media has been demonstrated.¹² Extensive research has been conducted using TR for source localization. A significant body of work was developed using TR to locate scatterers,¹³ and ongoing research in this area has included the localization of earthquakes,^{14,15,16} acoustic emissions,^{17,18} and finger taps for touchpad technology.^{19,20}

Chapter 2 will discuss the use of TR to detect stress corrosion cracking in steel that had been subject to a hot magnesium chloride solution. In Chapter 3, a number of techniques to optimize TR for nondestructive evaluation of solids will be explored. This will be followed by conclusions and suggestions for future work.

Chapter 2: Nonlinearity from stress corrosion cracking as a function of chloride exposure time using the time reversed elastic nonlinearity diagnostic

2.1 Abstract

The Time Reversed Elastic Nonlinearity Diagnostic (TREND) has a long history of successful nondestructive detection of cracks in solids using nonlinear indicators. Recent research has implemented TREND to find stress corrosion cracking (SCC) in the heat-affected zone adjacent to welds in stainless steel [Anderson *et al.*, J. Acoust. Soc. Am. **141**(1), EL76-EL81 (2017)]. SCC development around welds is likely to occur due to the temperature and chemical exposure of steel canisters housing spent nuclear fuel. The ideal SCC detection technique would be able to quantify the size and extent of the SCC, rather than just locating it, as TREND has been used for in the past. The current chapter explores TREND's ability to detect an assumed increase in SCC over time using thirteen samples exposed to a magnesium chloride (MgCl_2) bath for different lengths of time. The samples are then scanned with TREND and nonlinearity is quantified for each scan point and each sample. The results suggest that TREND can be used to not only locate SCC in the heat-affected zone, but also track an increase in nonlinearity, and thereby an increase in damage, in samples exposed to the MgCl_2 solution for a longer duration.

2.2 Introduction

Time reversal (TR) focusing has been used for the nondestructive evaluation (NDE) of solid media for just over a decade. TR utilizes the reversed impulse response of a system to

generate a temporal focus of vibration energy at a single location,¹ which can be used to reveal the local system properties upon examination of the focal signal.² Direct excitation of a cracked location is often insufficient for generation of the amplitudes necessary to allow detection of the nonlinear response of the damage. TR focusing can generate up to 30 times higher amplitude than direct excitation and therefore has sufficient amplitude to allow detection of local nonlinear properties.²¹ Analysis of the TR focal signal can reveal nonlinear variations in a number of forms including higher signal amplitude, waveform distortions,^{22,23} or nonlinear harmonic content.^{24,25} For a focus at a cracked location in a medium, all of these indicators and more typically exist.

The earliest methods utilizing TR for NDE detected scattered waves from a defect as an impulse response that could then be reversed in time and focused at the defect to localize it.^{13, 26, 27, 28} This linear process, called DORT (for the decomposition of the time reversal operator), was used for flaw detection in materials such as titanium and duralumin.^{29,30,31,32} An iterative TR technique was also developed to increase the scattered signal strength.^{33,34} The use of TR for the nonlinear detection of cracks was proposed by Guyer³⁵ and numerically verified by Delsanto *et al.*³⁶ and Bou Matar *et al.*³⁷ Sutin *et al.* was able to experimentally confirm a reciprocal TR process where a focus is placed at any location specified by a noncontact receiver, allowing an entire region to be studied without transducer rebonding.^{24,25} Experimental validation of the use of TR for nonlinear detection and imaging of cracks was done for impact damage^{4,38} as well as stress fatigue⁶ and delaminations.^{39,40} In these studies, high-amplitude TR focusing was intentionally used to excite local nonlinearities from damage, and ultimately, a technique termed the Time Reversed Elastic Nonlinearity Diagnostic (TREND) was developed to image damage in a sample.^{3,5,40} Additional recent experiments have used nonlinear techniques in conjunction with TR to study

closed cracks,⁴¹ and use TREND to both locate and study the depth of stress corrosion cracking (SCC) near welds.^{7,42,43}

The TREND technique excites nonlinearities at a specific location by training a high amplitude TR focus of acoustic energy to that location. A series of scan points is selected in a region of interest and a TR focus is generated and measured at each location in turn. The TR focus of energy at a single location, even a cracked one, is still nondestructive since the strain is at least an order of magnitude smaller than the linear strain relationships of the undamaged medium. By evaluating each scan point's focal signal for nonlinear content, a visual map of the quantified nonlinear signature may be produced wherein high amounts of nonlinearity are assumed to imply more damage. Because every hardware system inherently generates some level of nonlinearity, assessments of nonlinearity correlated to damage should be made relative to a measurement at an undamaged location in the sample or to an undamaged sample. This relies on a clear distinction between system and sample nonlinearity, a sometimes difficult requirement not always necessary for linear detection systems, but the success of TREND is partially due to its localized, high focal amplitude, which makes system noise less of a problem. In addition, studies have shown that nonlinear detection methods like TREND are able to find damage in its beginning stages,⁴⁴ whereas linear detection methods (i.e. pulse echo) are only able to find damage in its later stages of development.

Recent research has investigated the use of TREND for nondestructive localization and characterization of SCC with application to steel canisters holding spent nuclear fuel.^{7,43,45} The approximately 3.7 m (12 ft) diameter cylindrical canisters are air-tight and are surrounded by a cylindrical concrete cask with air vents. These canisters are often stored near coastlines and due to heating within, cooling without, the salt-air exposure, and residual stresses, SCC may develop near

welds. Long exposure to these conditions might lead to SCC beginning to threaten the air-tight seal.^{46,47,48}

The development of SCC around welds occurs as a result of residual stress and long-term exposure to moist, chloridic environments.⁴⁹ In austenitic stainless steels, like those used for nuclear fuel storage canisters, the necessarily high heat associated with the welding process adjusts the structure of the steel adjacent to the weld, allowing the base steel to bond to the weld filler material, but also potentially weakening the crystalline framework of the base steel. The steel altered by the heat of welding is called the Heat-Affected Zone (HAZ). After cooling, the HAZ can often be roughly identified by external discoloration caused by oxidation of the steel adjacent to the weld,⁵⁰ although it is impossible to know the true extent of the HAZ without high resolution imaging of the grain structure.⁵¹ Within the HAZ, the grain boundaries at the transition between the base and filler metals can result in a residual stress from the welding process. Given ongoing exposure to high temperatures, humidity, chlorides, or any service-induced stress, SCC is most likely to form within the HAZ, especially along the edge of the weld.^{43,49} An example of SCC in stainless steel is shown in Fig. 2.1 with labels indicating the weld, HAZ, and SCC.

In the study conducted by Anderson *et al.*,⁷ a sample of 304L stainless steel (the subject of the photograph in Fig. 2.1), the same steel used in the storage canisters, was welded and subject to a boiling magnesium chloride ($MgCl_2$) bath to induce SCC in the HAZ. Imaging nonlinearity along the weld with TREND was able to not only identify the location of SCC, but discover clues concerning the depth dependence of the cracking by using various frequency bandwidths for measurement. The external concrete encasing the steel canisters makes inspection difficult, but the TREND system may be able to be employed in the intentional gap (for air flow) left between the

steel canister and concrete cask making it possible to inspect SCC without disturbing the protective barriers.

A number of other nonlinear ultrasound techniques aimed at NDE of SCC have been used in the past. Ohara *et al.* used a Subharmonic Phased Array to detect frequency mixing by SCC on the opposite side of a sample from the transducer⁵² or on the same side of the sample.⁵³ Dynamic Acousto-Elastic Testing was used to compare time-of-flight measurements across a dynamically strained crack.⁵⁴ Nonlinear Resonant Ultrasound Spectroscopy was used to locate SCC from resonance frequency shifts observed for different modes of a globally excited sample.⁵⁵ Morlock *et al.* used Rayleigh waves to excite SCC which are then detected downstream of the crack.⁵⁶ This last experiment was the only one to use multiple samples with differing degrees of SCC, which were induced by applying differing amounts of stress to samples exposed to a corrosive environment for the same amount of time. Thus there has not been a study that exposed several samples to a corrosive environment for differing amounts of time nor a study exposing one sample to corrosion, monitoring it, and then exposing it again and repeating this cycle. This work does the former, exposing multiple samples to corrosion for differing amounts of time. Some of the above techniques were designed for advanced laboratory studies and not for field work (e.g. Dynamic Acousto-Elastic Testing), and some cannot easily localize SCC (e.g. Nonlinear Resonant Ultrasound Spectroscopy).

It is desired to develop TREND to be a robust tool for detecting and imaging SCC for field testing, meaning the ability to detect the depth of SCC and the orientation of the SCC. This information could allow corrective action to be taken before the air-tight seal is compromised. The purpose of this chapter is to experimentally study the ability of TREND to locate SCC in the HAZ of welds, but more importantly, correlate the amount of measured nonlinearity to the assumed

amount of SCC present. By exposing a number of identically welded steel samples to a hot $MgCl_2$ solution for varying amounts of time, a series of samples are created with an expected, successive increase in SCC with longer exposure time. Using TREND, each of these samples is nondestructively examined and it is found that, with some variation, the longer a sample is exposed to the solution of $MgCl_2$, the more nonlinearity is measured in the HAZ.

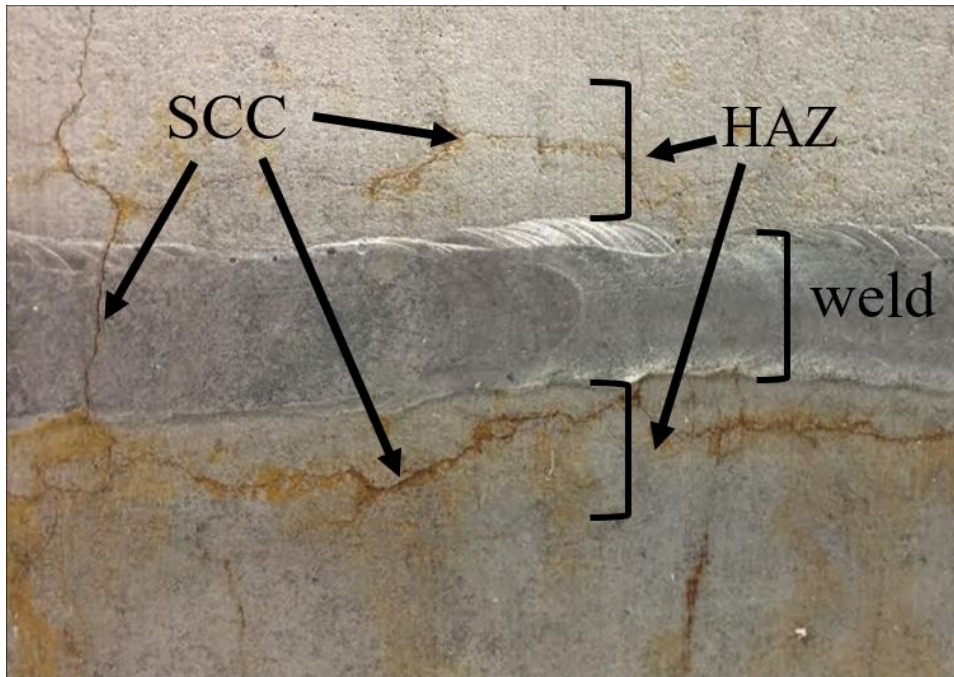


FIG. 2.1. An image of 304L stainless steel with stress corrosion cracking (SCC) in the heat-affected zone (HAZ) just outside the weld. In this case, SCC has developed in the HAZ and occasionally in the weld.

The chapter first describes the details of TREND processing, including the details of the system used, and experimental specifications. This will be followed by a description of the samples as well as the process for inducing SCC in the HAZ of each sample. Results of nonlinear imaging of cracks will be shown in detail for a representative sample after which the overall nonlinearity

for each sample will be calculated and plotted against the sample's time exposed to the hot MgCl_2 solution.

2.3 Experimental Setup

TR utilizes the impulse response to create a focus of energy at a selected location.^{1,2} In what is called the forward propagation step, an impulse is sent from a source location, reverberates throughout the medium, and the recording at a receiver location is the impulse response. In standard TR, the impulse response is reversed in time and emitted from the original receiver location. In this backward propagation step, the emitted waves constructively interfere to generate a focus of acoustic energy at the original location of the source during the forward step. If reciprocity can be assumed in the medium, the time-reversed impulse response can instead be emitted from the source location during the backward step to generate a focus at the receiver location. This method is termed reciprocal TR and utilizes the convenience of a source emitter that doesn't need to be moved.^{10,11} In applying reciprocal TR to nonlinear detection of damage, a non-contact receiver allows a system to be trained to focus at multiple locations without moving the sources and provides a simple and quick method for imaging nonlinearity.

Here a PSV-400 Polytec (Waldbronn, Germany) scanning laser Doppler vibrometer (SLDV) is used as the noncontact receiver to measure out-of-plane velocity on the sample surface and eight piezoelectric transducers (from APC International located in Mackeyville, PA, material type 850), measuring 19.0 mm in diameter by 12.0 mm in thickness, are used to generate the source signals. In practice, a high-energy impulse is difficult to generate with band-limited piezoelectric transducers. Therefore a linear chirp signal, like that shown in Fig. 2.2(a) (where the frequency content has been altered for visualization purposes), can be utilized as the source signal for the

forward propagation step, and a chirp response, shown in Fig. 2.2(b), is collected at the receiver in lieu of an impulse response.^{57,58} The chirp signal is cross correlated with the chirp response in order to determine the required reversed impulse response (see Fig. 2.2(c)). This can then be sent through the sample from the band-limited transducer to the receiver where a focus of energy is generated, an example of which is shown in Fig. 2.2(d). This chirp method both increases the total energy input to the system during the forward step and recognizes bandwidth limitations of transducers by utilizing a finite bandwidth source signal. The span of frequencies used in the chirp signal defines the fundamental bandwidth. Higher harmonics generated by nonlinear vibration are defined as integer multiples of the fundamental bandwidth.

Samples of SCC in 304L stainless steel are created by exposure to a hot chemical bath.⁵⁹ Thirteen rods of length 12.7 cm (5 in) and diameter 1.59 cm (5/8 in) are cut in half along the length of the rod, then welded back together with a “V-groove” weld using 308 weld material, as shown in Fig. 2.3(a). One of the rods is left untouched while the remaining twelve rods are exposed to a 42% MgCl₂ bath at 80 °C (see Fig. 2.3(b)). One rod is removed from the solution every two days, such that the shortest exposure time is 2 days and the longest is 24 days. An example of one of the rods exposed to MgCl₂ for 14 days is shown in Fig. 2.3(c), although SCC is not visually apparent. Water is added to the solution to maintain a consistent salinity as needed.

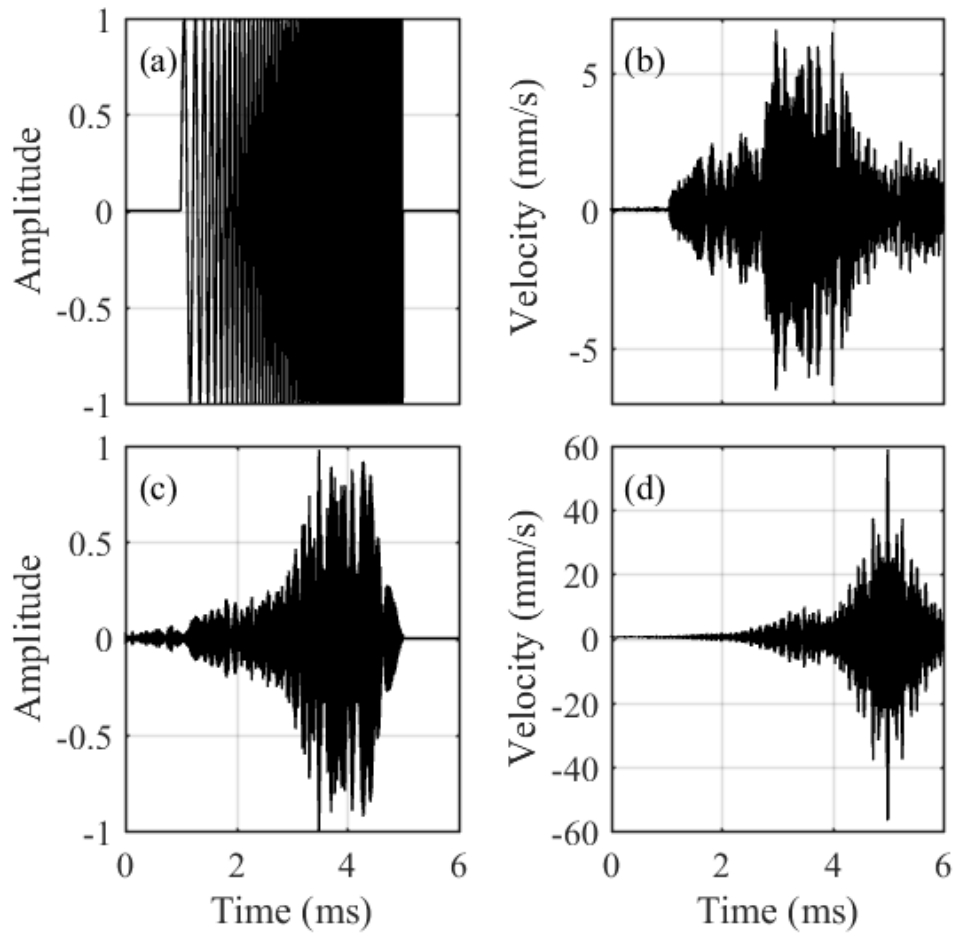


FIG. 2.2 Example signals used in the time reversal process for the given experiments. (a) Normalized chirp signal used as the initial source excitation (the frequencies shown are intentionally decreased for visualization purposes). (b) Normalized chirp response, measured at the receiver location. (c) Normalized reversed impulse response, generated by a cross correlation of (a) and (b). (d) Focal signal generated at the receiver location.

One at a time, a rod is epoxied to the top of a steel disk of diameter 20.2 cm (8 in) and height 2.5 cm (1 in) which is elevated by three rubber mounts 2 cm (0.79 in) above an optical table. To the underside of the steel disk are epoxied the eight piezoelectric transducers. Because nonlinearity can be difficult to detect without sufficiently high amplitude excitation, TR focusing from each of the eight transducers are simultaneously superposed to create a focus at a single location. Placing the eight transducers on the rod itself is both inefficient given the curved rod

surface, and can physically block access to a cracked location. Therefore, the energy from the transducers is transmitted through the disk and into the rod. The disk creates a chaotic cavity to increase diffuse reverberation in the impulse responses.^{60,61,62} The epoxy bond between the disk and rod is an average of 0.79 mm in thickness and care is taken to make the bond both consistent between rods and level such that the disk and rod do not have direct contact in order to avoid contact nonlinearities. The bond is given 36 hours to cure before testing takes place. An image of a rod epoxied to the disk is shown in Fig. 2.4.

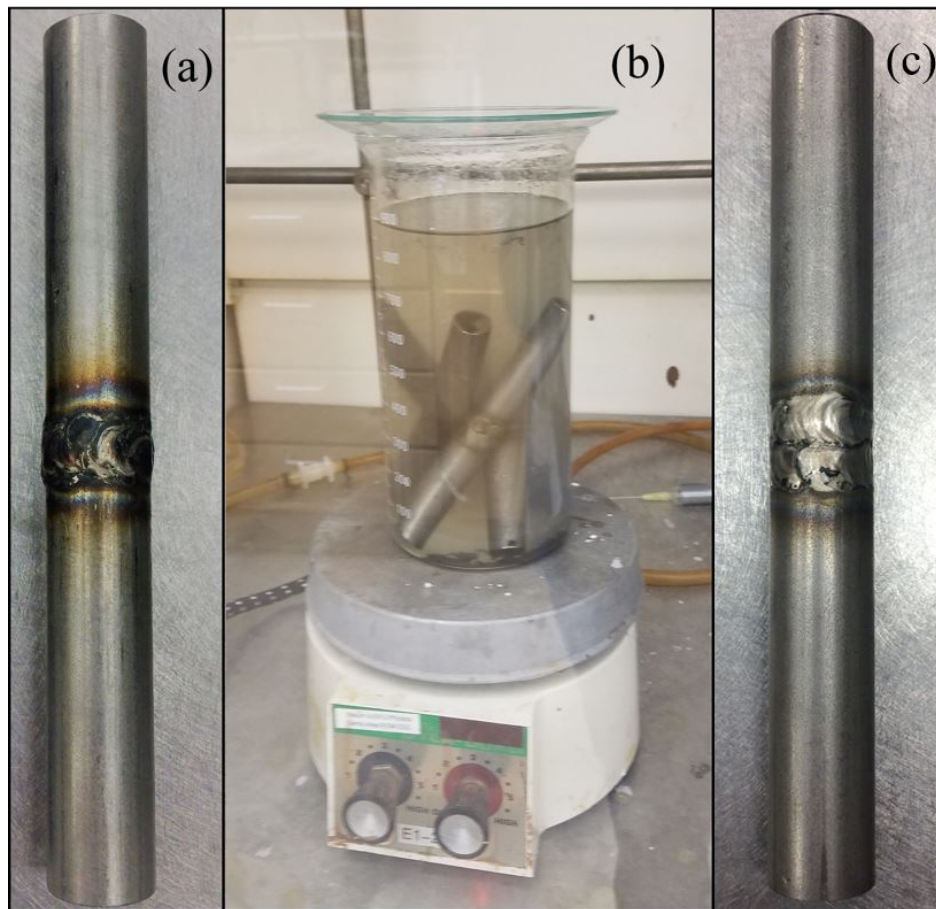


FIG. 2.3. Photographs of the progression of rods from welded to damaged. (a) Undamaged 12.7 mm long, welded rod. The heat-affected zone (HAZ) is evident in the discoloration. (b) Rods in the 42% solution of hot magnesium chloride (MgCl_2). (c) Damaged rod after 14 days exposure in the solution. The MgCl_2 bath removes much of the HAZ discoloration.

The nature of NDE of samples implies that the exact extent of any damage in the samples is truly unknown. While it is supposed that cracking will occur in the HAZ, the HAZ itself is a tenuously defined region, and damage could exist anywhere along the circumference of the rod. Thus a 50 mm scan is conducted along four lines of scan points with each line spaced apart by 90° angles around the rod. Between each measurement along a given scan line on a rod, the rod setup is rotated by 90° . The SLDV is positioned to provide very close to normal incidence sensing of surface vibration (along the length of the rod) throughout the scan.

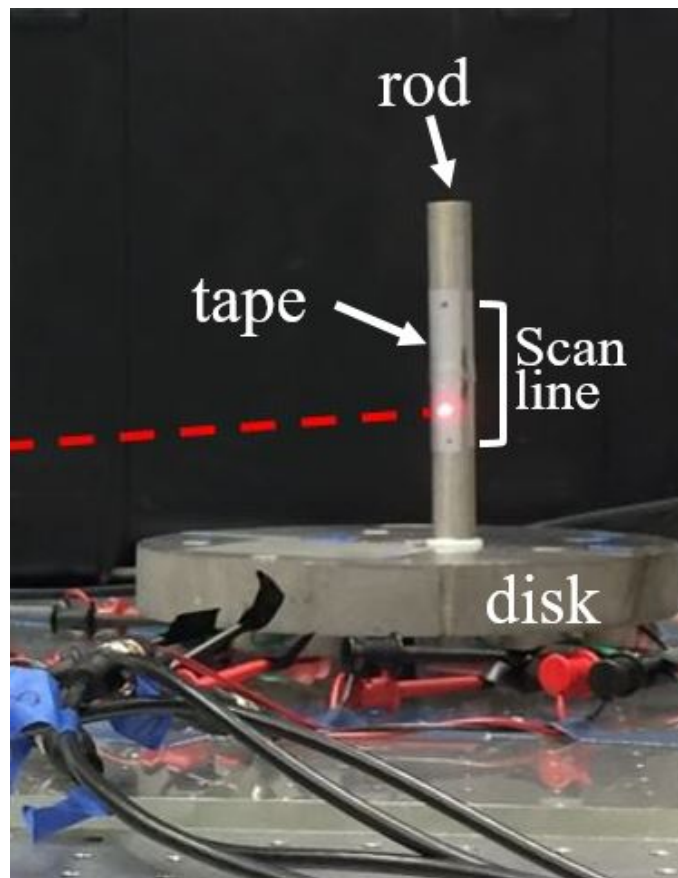


FIG. 2.4. Photograph of the steel disk chaotic cavity with 8 piezoelectric transducers epoxied to the underside. A rod under test is epoxied to the top of the disk and the laser light (drawn in to visualize it) is coming from the direction of the dashed red line. The silver colored region on the rod is retro-reflective tape used to decrease optical noise. The scan line spans the line between the two dots drawn on the tape.

2.4 Results

Two example focal signals are shown in Fig. 2.5. Both of these signals come from the same rod exposed to $MgCl_2$ for 12 days and both are within the supposed HAZ, but Fig. 2.5(a) is the focal signal from a location 14.2 mm from the outer edge of the weld and Fig. 2.5(b) is only 2 mm from the weld. The first attribute of note, relative to many other TR experiments is the large temporal side lobes on either side of the peak focus.⁶³ While some applications of TR require a more delta-function like focal signal, this is less important for crack detection.⁶⁴ The high-amplitude side lobes in the focal signal imply that this system is a highly resonant one; in fact spectral analysis suggests there are several modes within the frequency bandwidth used.⁵⁷ The most important quality of TR focusing for nonlinear detection is large amplitude to induce a nonlinear response and allow detection of nonlinear features (i.e. harmonics). Figure 2.6 shows the spatial distribution of the instantaneous velocity along the rod at the moment of a TR focus on an unexposed rod. The 'x' symbol indicates the location of the focus as well as its amplitude at the focal-time. Examination of this figure indicates an average wavelength of 26 mm. Using the central excitation frequency of 100 kHz, the wave speed is calculated as 2800 m/s, a value less than the shear wave speed in steel. Though TR inherently utilizes all types of waves present in a system, it is instructive to note that this wave speed suggests that Rayleigh waves comprise the bulk of the energy used to generate a focus. The noisy results between 59 mm and 64 mm are likely the result of speckle noise, when the reflected laser light is not strongly detected by the SLDV.

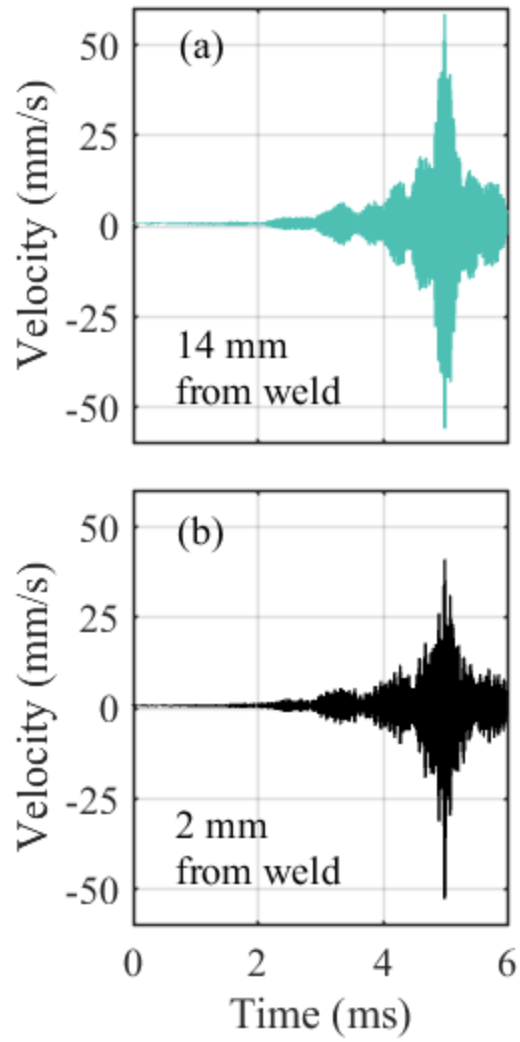


FIG. 2.5. Time-domain focal signals from two scan points on the rod exposed to magnesium chloride for 12 days. (a) Focal signal 14.2 mm from the weld. (b) Focal signal 2 mm from the weld.

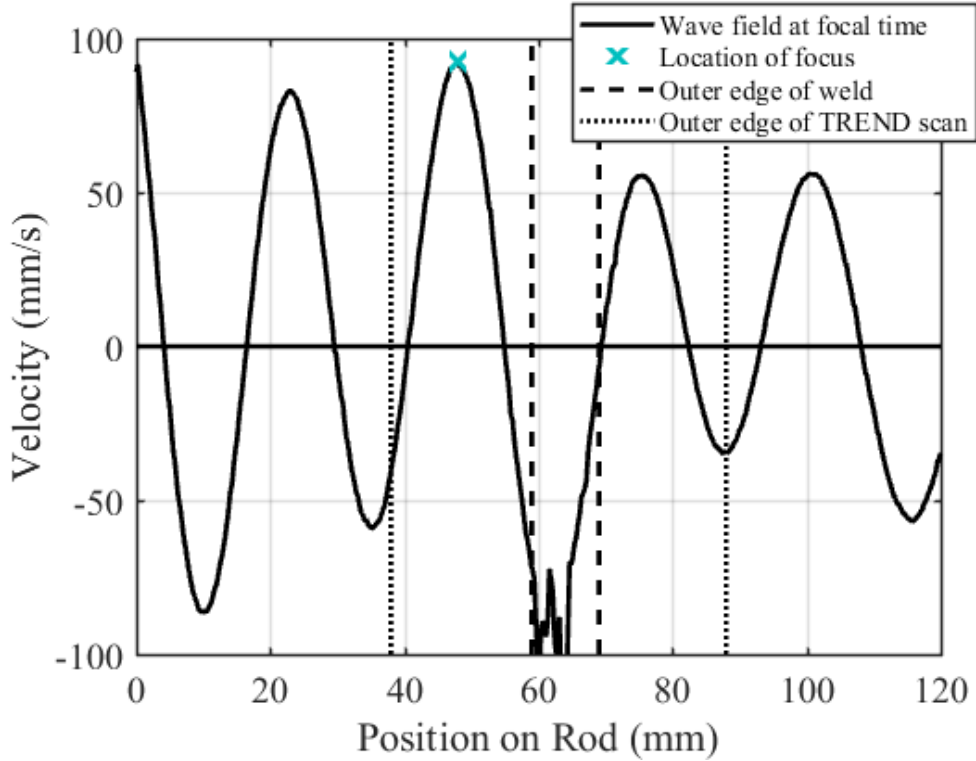


FIG. 2.6. Instantaneous velocity along the length of rod at the moment of time reversal focusing on an unexposed rod. The focus is generated at the location marked by the 'x'.

To quantify any potential nonlinearity in the focal signals due to the presence of damage, the Fourier transforms of the signals in Fig. 2.5 are shown in Fig. 2.7 and labeled with their distance from the outer edge of the weld. In order to compare the two signals on the same amplitude scale, the unnormalized spectra, $G(f)$, are scaled according to the Euclidean norm of the values contained within the fundamental bandwidth, such that what is displayed in Fig. 2.7 is

$$\|G(f)\| = \frac{G(f)}{\sqrt{\sum_{75kHz}^{125kHz} G^2(f)}}. \quad (2.1)$$

The fundamental bandwidth, outlined with vertical dash-dot lines in Fig. 2.7, is the same span of frequencies used for the chirp in the forward propagation step, 75 kHz to 125 kHz. By scaling the

spectra according to the norm of the fundamental bandwidth (the Euclidean norm), differences in focal amplitudes between spectra are removed, allowing any differences in higher harmonic content to be compared directly. The second harmonic, 150 kHz to 250 kHz, is outlined in dashed vertical lines in Fig. 2.7 and comprises the region most likely to indicate the presence of nonlinearity introduced by crack motion. Other harmonics were examined but were determined to be buried in the noise floor. If the localized focus of energy excites SCC, the crack will produce harmonics of the fundamental. The higher the amplitude of the spectra in the second harmonic relative to the fundamental amplitude, the larger extent of SCC is expected.⁷ In Fig. 2.7, the two signals have approximately the same amplitude within the fundamental bandwidth, as expected given the applied scaling, although both have multiple peaks due to the resonances of the sample and source transducer. However, within the second harmonic, the amplitudes for the spectrum corresponding to the location 2 mm from the weld is distinctly higher in amplitude than in the spectrum for the 14.2 mm distance from the weld, indicating a higher severity of damage. This result is expected given that SCC is more likely to form immediately adjacent to the boundary of the weld, nevertheless, both positions are within the HAZ and an examination of the entire spatial region is necessary to see the impact of a variety of differences in the second harmonic amplitude.

In order to compare nonlinearity across the entirety of a scan, the amplitude in the second harmonic is reduced to a single number. This is accomplished by calculating the scaled nonlinearity,

$$\zeta(x, \theta) = \sum_{150kHz}^{250kHz} \|G(x, \theta, f)\|^2, \quad (2.2)$$

where the spectral amplitudes within the scaled second harmonic bandwidth are squared and summed for each scan point, x , and at the rotation angle, θ . The higher the scaled nonlinearity, the more likely SCC has developed at location (x, θ) . The scaling of the focal spectra and comparison

of relative amplitudes of the second harmonic is similar in nature to the frequency domain scaling subtraction method,^{7,38} but the scaling used here is based on the fundamental bandwidth of each spatial scan location rather than comparing a high-amplitude focal spectrum to a low-amplitude focal spectrum.

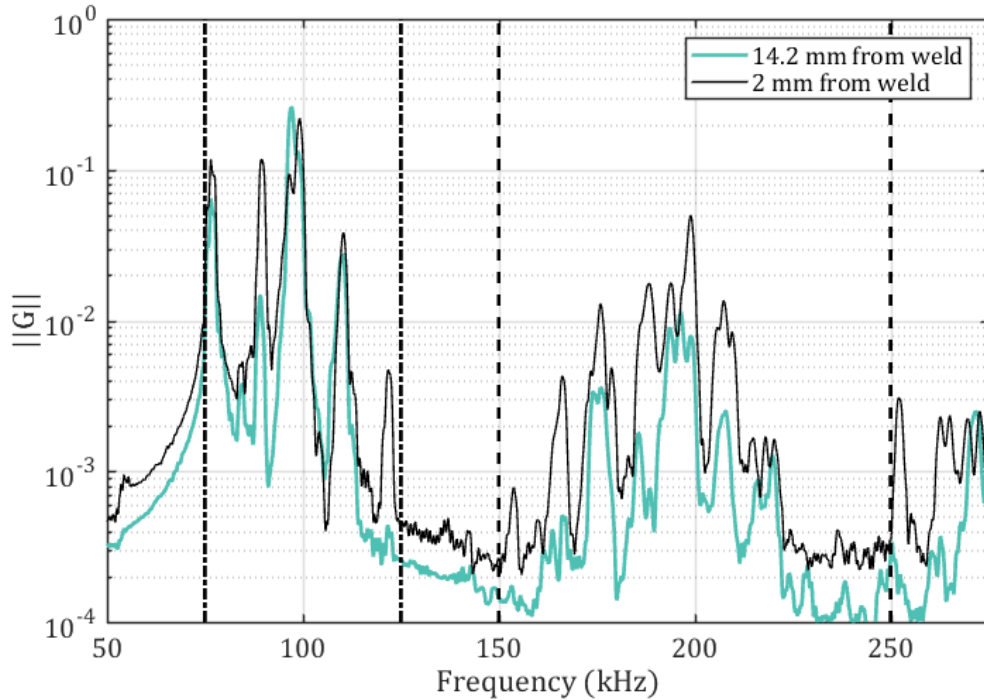


FIG. 2.7. Spectra of the focal signals displayed in Fig. 2.5. Amplitude scaling to the Euclidean norm of the spectra within the fundamental bandwidth is applied, shown mathematically in Eq. (2.1). The fundamental bandwidth is outlined by the vertical dash-dot lines. The second harmonic is outlined by the vertical dashed lines.

Scaled nonlinearity, $\zeta(x, \theta)$, results are shown in Fig. 2.8 for the rod exposed to MgCl_2 for 12 days. The four plots in Fig. 2.8 indicate the results from each of the four θ angles scanned on the rod, where Figs. 2.8(a) and (c) and also Figs. 2.8(b) and (d) show scans on opposite sides of the rod, respectively. The horizontal axis shows the scan position, x , in millimeters with distances relative to the top of the rod (the end not epoxied to the disk). The vertical axis displays the

amplitude of $\zeta(x, \theta)$ and the vertical dashed lines indicate the location of the outer edges of the weld, at $x = 57$ and 68 mm. As anticipated, more nonlinearity exists either at or just outside the edge of the weld for all four angles. The highest amplitudes exist in Fig. 2.8(d), with the peak at 70 mm serving as the example signal in Fig. 2.5(b) and example spectrum in Fig. 2.7. While each of the four scans at each θ have clear peaks at the weld's edge, they also have distinct increases in nonlinearity elsewhere along the scan, as far as 15 mm ($x = 41$ mm) from the edge of the weld (see Fig. 2.8(a)) and even within the weld itself (Fig. 2.8(b)). The fact that SCC is likeliest to form just outside the weld does not restrict its growth to that region alone. In fact, it is impossible to nondestructively verify where tensioned grain boundaries or residual stresses exist, or even how far the HAZ extends from the edge of the weld. SCC can form in any location given the right conditions, so while the largest peaks in nonlinearity are expected to exist at the weld boundary, it is not surprising that other regions show peaks as well. Additionally, the weld region was defined for one rotation angle θ and the weld is assumed to be span the same positions for other θ .

Because the results depicted in Fig 2.8(a)-(d) all illustrate peaks in $\zeta(x, \theta)$ just adjacent to the weld, it could be thought that what is detected is not nonlinearity from SCC at all, but merely odd behavior due to the edge of the weld. However, the data for the rod that was not exposed to the MgCl_2 solution is also shown in each of these figures, and no spikes are observed at the edges of the welds in that sample. When the data for the unexposed rod is inspected more closely, some features exist at levels of $\zeta = 10^{-5}$. These features are inconsistent spikes indicative of noise and occur at random locations on the rod, both near and far from the weld. Therefore, we assert that the nonlinearity detected in the exposed rods is due to SCC, and not the weld boundary.

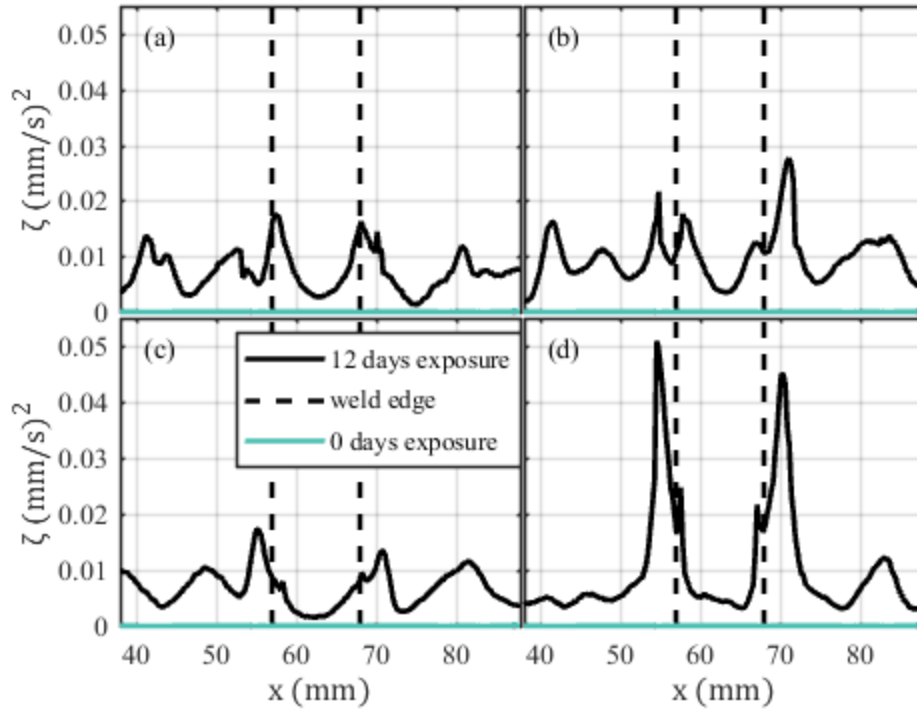


FIG. 2.8. The scaled nonlinearity, $\zeta(x, \theta)$, in the second harmonic bandwidth, versus scan position, x (mm). Vertical dashed lines indicate the approximate outer edge of the weld. Data shown in black are from the rod exposed to the magnesium chloride bath for 12 days, while the curves in teal are for the rod exposed for zero days. Data are from a 200 point scan at (a) 0° , (b) 90° , (c) 180° , and (d) 270° .

NDE techniques may utilize both linear and nonlinear metrics to detect damage. One might expect that severely damaged locations (open cracks) would possess high peak focal amplitude, as the excited crack is more freely able to vibrate at an open crack boundary than within a homogeneous medium. Thus one might expect the fundamental bandwidth to have higher amplitudes and the peak focal amplitude would be higher. In the research shown here, the two focal signals shown in Fig. 2.5 indicated that the rods not only constitute a resonant system, but that high focal amplitude did not correspond to the location where SCC is likely to exist, since the damaged location yielded a lower peak focal amplitude. Figure 2.9 illustrates the resonance characteristics of the rod more clearly by showing the peak focal amplitude, A_p , in mm/s of each

independently generated focal signal on the left vertical axis plotted against x , and $\zeta(x, \theta)$ from the same data set on the right axis, also plotted versus x . The scan data are the same as that shown in Fig. 2.8(d). The peak focal amplitude ranges from 54 to 76 mm/s, and oscillates with an average peak to peak distance of 28 mm, a distance within 2 mm of the wavelength determined from the plot in Fig. 2.6. Notably, the peak focal amplitude is highest where $\zeta(x, \theta)$ is not. There is some indication that damage has an impact on focal amplitude, such as the matching peaks at $x = 54.6$, 57.6, and 67.2 mm. However, these minor peaks in focal amplitude are more likely to look like false detections than cracks if one were basing crack detection solely on the peak focal amplitude, when comparing those minor peaks to the large amplitude gains at $x = 48$, 62, and 76 mm. While an increase in peak focal amplitude may be a valuable linear indicator of damage for some varieties of cracking, it is apparently not sufficient for SCC in a resonant system, and could lead to erroneous results. This result indicates the importance of NDE imaging based on nonlinearities generated by cracking. In addition, given the wavelength of 26 mm, the defects should only be detected if they are larger than the half-wavelength diffraction limit of 13 mm. However, nonlinear cracking features appear to be discernable in regions as small as 5 mm. Though beyond the scope of this thesis, this could be the result of the diffraction limit of the second harmonic used, approximately 6 mm.

Of the 12 rods exposed to MgCl_2 , 10 showed evidence of nonlinearity in the HAZ, especially adjacent to the weld. The two that did not were only exposed for 2 days and 4 days. In order to compare the total damage in the rods, all of the localized and scaled nonlinearity ($\zeta(x, \theta)$) like that shown in Fig. 2.8 must be quantified for each rod. Because each focal spectra is scaled to the amplitude of its fundamental bandwidth, differences in focal amplitude (which is dominated by the fundamental frequency bandwidth) between the rods has no impact and only the relative

height of the second harmonic, the scaled nonlinearity, is used as a damage indicator. The entire length of the scan is used to quantify a total nonlinearity for each rod because, as was evident in Fig. 2.8, not all spikes in $\zeta(x, \theta)$ occur adjacent to the weld, and all nonlinearity should be accounted for. To determine the total nonlinearity, Z , for each rod, the $\zeta(x, \theta)$ values for each of the 200-point scans are averaged. The four values at each angle θ are then averaged to determine one value of total nonlinearity for each rod, shown in Eq. (2.3),

$$Z = \sqrt{\frac{1}{4 \times 200} \left(\sum_{n=1}^{200} \zeta(n, 0^\circ) + \sum_{n=1}^{200} \zeta(n, 90^\circ) + \sum_{n=1}^{200} \zeta(n, 180^\circ) + \sum_{n=1}^{200} \zeta(n, 270^\circ) \right)}. \quad (2.3)$$

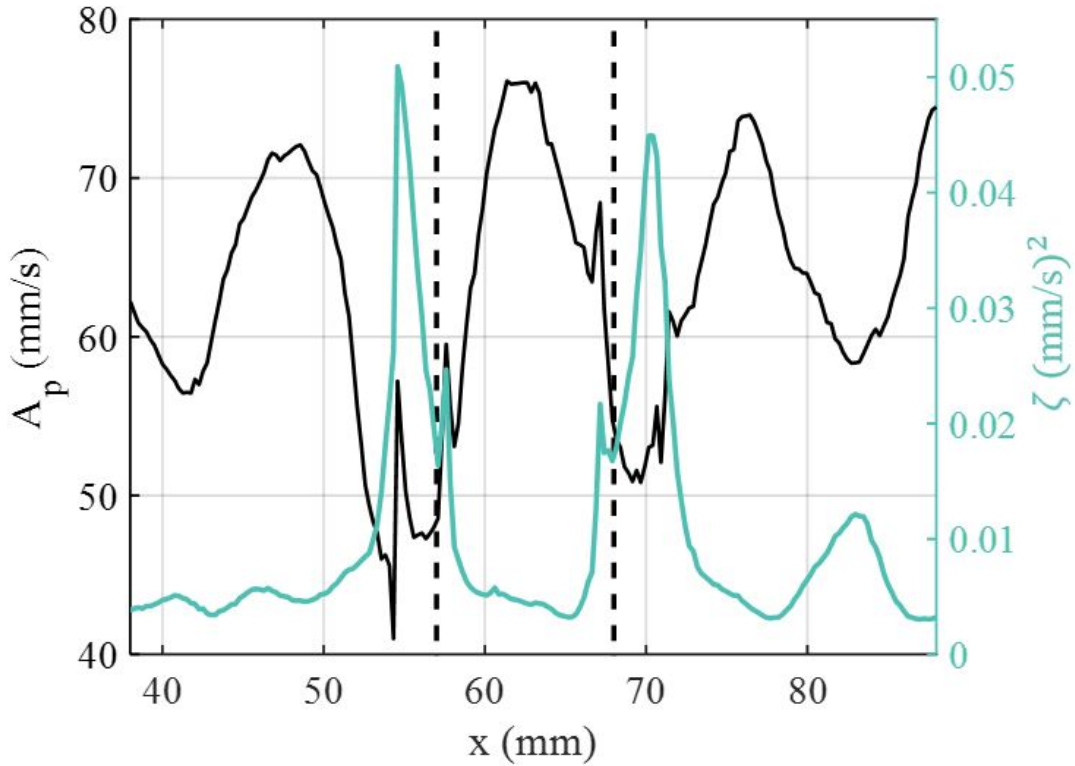


FIG. 2.9. Left axis: peak focal amplitude, A_p , versus scan position, x . Right axis: scaled nonlinearity, $\zeta(x, \theta)$, versus scan position. The outer edges of the weld are indicated by the vertical dashed lines.

Z is plotted versus the amount of time each rod is exposed to the hot MgCl_2 solution in Fig. 2.10. The rods exposed for 0 to 4 days have total nonlinearity values that are very low and essentially negligible. For the rods exposed from 6 to 24 days, various amounts of nonlinearity are detectable and there is an overall increase in Z with exposure time. Notable exceptions to this trend are the rods exposed for 16 and 20 days which show surprisingly low Z given their exposure time. However, because welding is not an exact process, it is not known whether these rods had very little residual stress compared to their peers in the regions examined. It is also possible that the four angles examined on these rods simply missed whatever SCC was present within the rods. A larger set of samples would need to be studied to determine the expected amount of variance in this trend of Z versus exposure time. The data is erratic particularly from the sample exposed for 14 days to the sample exposed for 20 days. However, the general increase in Z with exposure time suggests that TREND can be used to track SCC progression over time on similar samples and need not be a measurement system limited to measurements on a single sample. Given this result, TREND could likely be utilized on storage casks to determine the extent of SCC growth. However, the nonlinearity observed over the short exposure times used here would not be expected to translate to actual casks because the corrosive environment for storage casks is not nearly as severe.

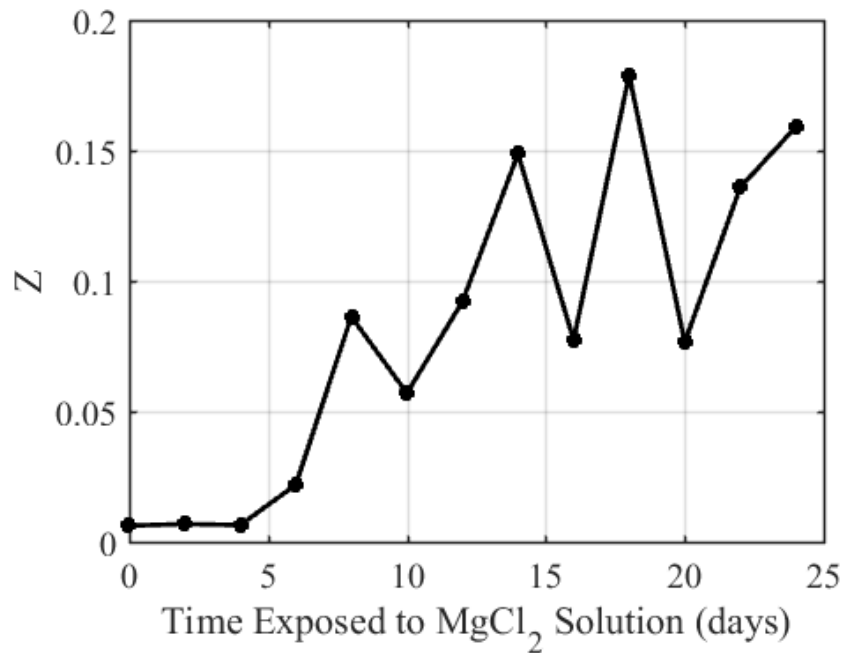


FIG. 2.10. Total nonlinearity, Z , measured in each rod versus the amount of time the rod was exposed to the hot solution of magnesium chloride (MgCl_2).

2.5 Conclusion

Thirteen stainless steel rods were cut in half and welded back together and exposed to a solution of hot magnesium chloride for varying amounts of time. Using TREND, each of the rods was scanned, placing a high-amplitude focus of energy at each scan location, and the nonlinear content in the second harmonic was quantified in the scaled focal signals. It was found that the focal signals of scan points adjacent to the outer edge of the weld overall contained more nonlinearity, an expected result given the propensity of these regions to SCC being located within the heat-affected zone. Additionally, the maxima of the focal signals, a linear imaging quantity, at each scan location could not be used to identify locations with stress corrosion cracking (SCC). A value for total nonlinearity was quantified for each rod and it was found that, in general, the longer a rod was exposed to the hot solution of magnesium chloride, the more nonlinearity was detected.

Thus this chapter has illustrated that SCC around welds can not only be detected using the Time Reversed Elastic Nonlinearity Diagnostic (TREND) but the nonlinear signature measured with TREND increases with the expected amount of SCC from longer exposure to corrosive environments.

Chapter 3: A comparison of impulse response modification techniques for time reversal with application to crack detection

3.1 Abstract

Time reversal (TR) focusing used for nonlinear detection of cracks relies on the ability of the TR process to provide spatially-localized, high-amplitude excitation. The high amplitude improves the ability to detect nonlinear features that are a signature of the motion of closed cracks. It follows that a higher peak focal amplitude, than what can be generated with the traditional TR process, will improve the detection capability. Modifying the time-reversed impulse response to increase the amplitude of later arrivals in the impulse response, while maintaining the phase information of all arrivals, increases the overall focal signal amplitude. A variety of existing techniques for increasing amplitude are discussed, and decay compensation TR, a technique wherein amplitude is increased according to the inverse of the amplitude envelope of the impulse response decay, is identified as the best modification technique for nonlinear crack detection. This is due to the large increase in focal signal amplitude in conjunction with a minor introduction of harmonic content, a larger drawback in two other methods studied, one-bit TR and clipping TR. A final study employs both decay compensation TR and traditional TR focusing on a rod with stress corrosion cracking and compares the merits of each in detecting nonlinearity from cracks in a real system.

3.2 Introduction

The time reversal (TR) process utilizes the impulse response of a system, between a source and a receiver, to generate both a spatial and temporal focus of energy at a chosen location.¹ The impulse response is reversed in time and then emitted by the source (reciprocal TR²) with the low-amplitude vibrations emitted first and the high-amplitude vibrations last. The timing of the emitted waves is determined by the reversed impulse response (RIR). For a time-invariant system, each of the emitted waves travels along the paths traversed during the impulse response measurement and the timing is such that energy from each emission arrives simultaneously at the receiver location, creating a constructive focusing of energy that is generally impulsive in nature.

The high-amplitude TR focus of energy has been utilized for nondestructive evaluation (NDE) (i.e. crack localization) since the early 1990s, for example with Chakroun *et al.* using TR to locate scatterers in a solid sample submerged in a fluid.^{13,26,27} In 2001, Guyer first proposed using TR for nonlinear imaging of cracks³⁵ and Ulrich *et al.* demonstrated this experimentally a few years later by locating a surficial crack in a doped glass sample.⁴ Studies since then have used TR to find nonlinearity in various types of surface cracks,^{6,7,38,42} near-surficial cracks and delaminations,^{3,39} and even buried cracks.^{3,40} The detection of cracks using nonlinear methods is rooted in the premise that cracks will generate nonlinear frequency mixing when excited with sufficient amplitude.^{65,66} It has been shown that nonlinear methods detect damage sooner than their linear counterparts.⁴⁴ TR focusing at a damaged location results in the generation of higher harmonic frequency content. Thus, nonlinear detection methods require a high signal-to-noise ratio (SNR) such that higher-order harmonics are not buried in the noise floor.⁶⁷ While TR focusing inherently generates high-amplitude energy focusing, traditional TR signal processing may not be the optimal technique for nonlinear detection of cracks in otherwise isotropic media.

Modifications to traditional TR processing have been studied in a variety of contexts. One-bit TR was developed by Derode *et al.* as a method of increasing the amplitude of TR focusing, a technique later explored for use in lithotripsy.^{68,69} Others have used similar techniques wherein the instantaneous amplitude of the impulse response as time progresses is increased to compensate for the natural decay from geometric spreading losses and propagation losses in attenuating media, thereby increasing the SNR of an impulse response in strongly attenuating media.^{21,70,71} Deconvolution TR, or inverse filtering, was introduced as a means of compensating for resonances in the impulse response to optimize the impulsive nature of a TR focus of energy.^{64,72} Studies have examined the reliance of focal amplitude on the length of the initial pulse (i.e. the bandwidth).^{73,74,75} Physical system adjustments have sought to increase SNR through other means such as the introduction of a chaotic cavity^{61,62,76,77} or the use of an acoustic metamaterial-based filter.⁷⁸ Recently Willardson *et al.* published experimental research manipulating TR processing in order to maximize focal amplitude of audible sound in a reverberation chamber.⁷¹

The work by Willardson *et al.* experimentally compared five different techniques that adjust the RIR to ultimately determine which provided the highest peak focal amplitude. The study was conducted in a reverberation chamber using a loudspeaker and a microphone, constituting a wide bandwidth system, and examined various attributes of the focal signals, including peak focal amplitude and temporal quality. While this study was valuable for a thorough understanding of TR in air, the study may not contribute information relevant to crack detection in a solid with a fairly resonant system, as is common for NDE experiments. The current chapter includes frequency analysis of higher harmonic generation and an evaluation of the spatial quality of the TR focusing, something that Willardson *et al.* did not explore.

While previous research has successfully developed modifications of RIR signal processing techniques based on specific targeted outcomes, a comparison of each of these modification techniques with application to NDE has not been done, nor have the impacts of these techniques on the introduction of harmonic frequency content been quantified (many of these techniques are inherently nonlinear processes). Typical solutions for generating the necessarily high SNR in focal signals used in crack detection can require the use of many generation channels or signal amplification beyond the linear limits of the system. The ideal solution to maximize SNR would maintain the physical system but optimize available amplification through the processing of the RIR(s) to increase excitation amplitude at the focus without unduly introducing noise at higher harmonic frequencies or undermining the benefits of using TR for nonlinear crack detection (i.e. spatially compressed focusing).

The objective here is to determine the TR signal processing technique that delivers the largest peak focal amplitude in conjunction with the best temporal quality, a spatially confined focus, and low higher harmonic generation. The purpose of this chapter is to experimentally compare five different TR signal processing techniques: deconvolution TR, one-bit TR, clipping TR, decay compensation TR, and as a benchmark, traditional TR, to determine the processing technique best suited for detection of cracks using nonlinear analyses. In this study, it is found that decay compensation TR is the optimal choice for the highest focal amplitude coupled with low higher harmonic generation. It is then shown that decay compensation TR is less susceptible to noise and false detections than traditional TR in the detection of cracks.

The remainder of the chapter first describes the experimental setup followed by a description of each of the TR techniques explored. This is followed by a description of the analysis metrics used to compare the methods, peak focal amplitude, temporal quality, spatial quality, and

fundamental to higher harmonic ratios. The results are presented for all the TR techniques tested, with some techniques tested with different applied thresholds. Finally, a study is presented that compares the use of traditional and decay compensation TR to find stress corrosion cracking in a steel rod.

3.3 Time Reversal and Experimental Setup

The TR process consists of two steps, a forward step and a backward step. The forward step consists of finding impulse responses from one or more sources to one or more receivers. Typically an impulse is broadcast from each source and the response is recorded with each receiver to obtain the impulse response(s). In the backward step of the traditional TR process, each impulse response is simply reversed in time and emitted from the receiver. In a variation called reciprocal TR, the RIRs are broadcast from the original source locations, generating a focus of energy at the receiver location(s).²

For the experiments described in this chapter, a different method is utilized to obtain the impulse responses. First, the broadcast of a true impulsive signal is difficult, from a practical standpoint, for finite-bandwidth transducers. These emissions typically generate low amplitude waves, meaning the SNR of the impulse response is poor. Instead a finite-bandwidth, linear chirp signal is used as the source signal instead, an example of which is shown in Fig. 3.1(a). The chirp signal broadcast, being band limited, is efficiently broadcast from transducers and therefore it affords a higher SNR recording than the recording of the response to an impulsive broadcast. The chirp response is recorded by the receiver and is then cross correlated with the original chirp signal as an approximate means to obtain the impulse response (see Figs. 3.1(b)- (c)).^{57,58} The impulse response is then reversed in time (Fig. 3.1(d)) and is broadcast from the same source as the chirp

signal (reciprocal TR). The TR focus, shown in Fig. 3.1(e), occurs at the receiver. This allows the source transducers to be bonded in place and a focus of energy may be generated wherever the receiver is placed.

The experimental setup, depicted in Fig. 3.2, is comprised of a steel disk measuring 20.2 cm (8 in) in diameter and 2.5 cm (1 in) in thickness, which is elevated by 3 rubber stoppers 2 cm (0.8 in) above an optical table. A piezoelectric transducer (from APC International located in Mackeyville, PA), material type 850, with diameter 19 mm and thickness 9.5 mm is epoxied to one side of the disk, and operates as the source in both the forward and backward propagation steps. The steel disk is placed with the piezoelectric facing downward toward the table. A PSV-400 Polytec (Waldbronn, Germany) Scanning Laser Doppler Vibrometer (SLDV), a noncontact and mobile receiver, is mounted approximately 1 m directly above the disk with the laser aimed at a patch of retroreflective tape on top of the steel disk. The forward propagation step uses a burst chirp broadcast from the Polytec generator with an amplitude of 0.5 V that is amplified by a Tabor (Nesher, Israel) 9400 high-voltage amplifier, with a 50 times gain, and is input to the piezoelectric transducer. To utilize the piezoelectric transducer efficiently, a chirp bandwidth of 75-125 kHz is chosen, centered on the transducer's primary radial resonance frequency, and is broadcast for the first half of a 51.2 ms period. A sampling frequency of 1280 kHz, with $N = 65536$ sample points, and a laser sensitivity of 25 mm/s/V is used. It was found that 30 averages sufficiently reduced noise in the system allowing these settings to be used for both the forward and backward propagation steps. After the impulse response is measured it is normalized and reversed in time. Any additional signal processing techniques, such as one-bit or clipping TR, are then implemented and the resultant signal is broadcast into the steel disk, creating a focus at the location where the SLDV measured the impulse response.

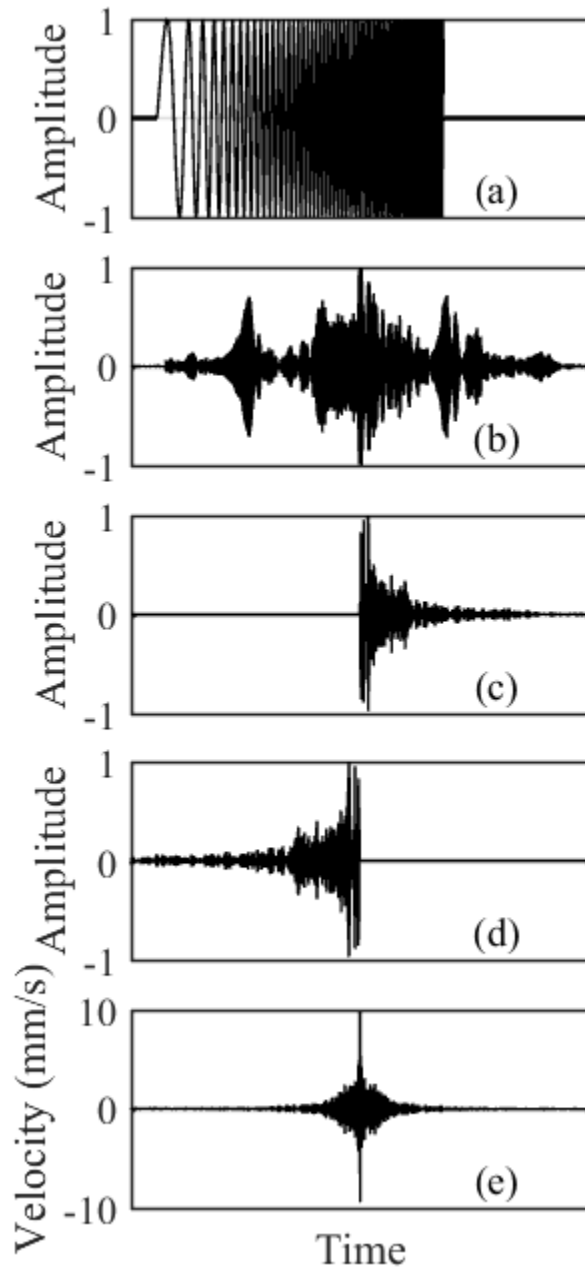


FIG. 3.1. Example signals used in the time reversal process. Except for (e), the amplitudes are normalized and are in arbitrary units. (a) Source chirp (with frequencies altered for visualization), (b) chirp response, (c) impulse response, (d) reversed impulse response, (e) focal signal.

In an additional experiment, a focus is generated at a single location on the steel disk for each of the signal processing techniques and the wave field is scanned with the SLDV. This gives

a spatial map of the velocity at and around the focal location, allowing the spatial extent of the focus to be quantified. For these spatial scans, a region of the steel disk 72 mm x 60 mm in size is covered with retro-reflective tape and a scan grid of 51 points x 43 points is defined, giving a spatial resolution in each dimension of approximately 1.4 mm. A focus is generated at scan position (37, 33.5) mm and the focus is repeated at this location as the SLDV measures the velocity at each scan position.

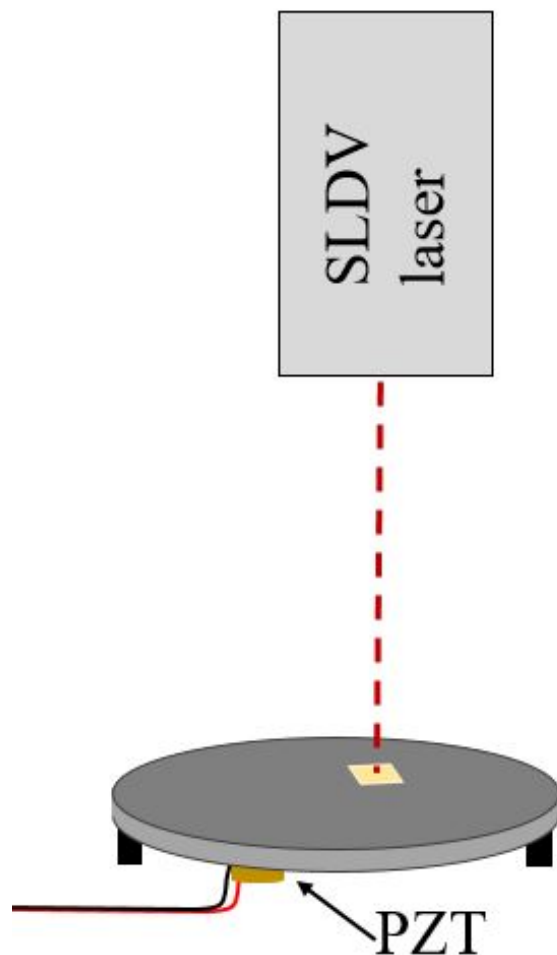


FIG. 3.2. Experimental setup with scanning laser Doppler vibrometer (SLDV) pointed at a steel disk. The steel disk has a piezoelectric transducer (PZT) epoxied to the bottom.

3.4 Time Reversal Signal Processing Modification Techniques

Deconvolution TR, or inverse filtering, is the first technique optimized to apply to the impulse response. Deconvolution TR inverts the spectrum of the impulse response such that when the resulting RIR is broadcast, the system resonances and antiresonances are compensated for in the backward propagation, yielding a focal signal with nearly a flat frequency response. In practice, deconvolution TR takes the spectrum of the impulse response, $R(\omega)^*$, where the $*$ symbol denotes a complex conjugation, and normalizes it by its squared magnitude plus a scaling factor, γ , multiplied by the mean of the squared magnitude, as shown in Eq. (3.1),

$$R_{\text{deconv}} = \frac{R(\omega)^*}{|R(\omega)|^2 + \gamma \text{mean}(|R(\omega)|^2)}. \quad (3.1)$$

The term $\gamma \text{mean}(|R(\omega)|^2)$ is a regularization term used to keep the deconvolution TR operation finite, a process described in more detail by Anderson *et al.*⁶⁴ Optimization of γ for reduction of the energy on either side of the peak focusing (termed side lobes⁶³) followed the process described by Willardson *et al.*⁷¹ and determined an optimal γ value of 0.9, which was also the value reported by Anderson *et al.* for TR focusing of waves in solid media.⁶⁴ As γ approaches infinity, the deconvolution TR process returns a traditional RIR because the γ term dominates in the denominator of Eq. (3.1) and after normalization, Eq. (3.1) returns $R(\omega)^*$. As γ approaches zero, the impulse response begins to look more like an impulse, effectively eliminating the reverberation in the impulse response. The modified RIR, after the deconvolution TR operation and with $\gamma = 0.9$ is shown in Fig. 3.3(b).

The one-bit TR technique alters the amplitude of the normalized RIR, $r(-t)$, according to the relationship of the instantaneous amplitude compared to a user-defined threshold (see Fig. 3.3(c)). The threshold is applied at a positive value T_{OB} and at a negative value $-T_{OB}$. At time

sample t_i , if $|r(-t_i)| \geq T_{OB}$, then $r(-t_i) \stackrel{\text{def}}{=} \text{sign}(r(-t_i)) \cdot T_{OB}$. In other words, any signal above or below the positive or negative threshold, respectively, is set equal to the threshold (or the negative threshold) which is 0.2 in Fig. 3.3(d). If $|r(-t_i)| < T_{OB}$, then $r(-t_i) \stackrel{\text{def}}{=} 0$. The quantity $r(-t)$ is then normalized and the resulting modified impulse response is comprised of +1, -1, and 0 values, hence the name one-bit TR (see Fig. 3.3(e)). The purpose of one-bit TR is to amplify low amplitude reflections in the impulse response and zero-out information with a poor SNR, but maintain the phase information of the non-zero signal. The threshold can be set anywhere from zero to one, thereby defining the acceptable SNR.

Clipping TR, a fairly new technique, is very similar to one-bit TR apart from one key difference.²¹ A threshold, T_{CP} , is applied to the impulse response, just as with one-bit TR, and if $|r(-t_i)| \geq T_{CP}$, then $r(-t_i) \stackrel{\text{def}}{=} \text{sign}(r(-t_i)) \cdot T_{CP}$. However, any signal below the threshold is not set equal to zero as with one-bit TR processing and instead is unmodified (see Figs. 3.3(f)-(g) where threshold is 0.2). When this resulting signal is normalized, any “clipped” signal is set to one and all of the signal that was below the threshold is amplified relative to the original normalized impulse response (see Fig. 3.3(h)). Like one-bit TR, clipping TR amplifies later reflections, but it also amplifies all low-level signal in the recorded impulse response, potentially amplifying background noise.

Decay compensation TR attempts to compensate for the exponential decay of the impulse response.^{70,71} As explained by Willardson *et al.*, the envelope of the RIR is obtained through a Hilbert transform operation, after which the envelope is smoothed through the use of a moving average filter (see Fig. 3.3(i)). The envelope is inverted and normalized and then multiplied by the original, normalized RIR, point by point, creating a signal with approximately the same amplitude over all time (see Fig. 3.3(j)). Because this can amplify unwanted noise, a threshold is applied with

respect to the decay curve such that if the instantaneous value of the decay curve is below the threshold, the modified signal retains the values of the original, normalized, RIR. An example signal after the decay compensation TR processing is shown in Fig. 3.3(k) with an applied threshold of 0.06.

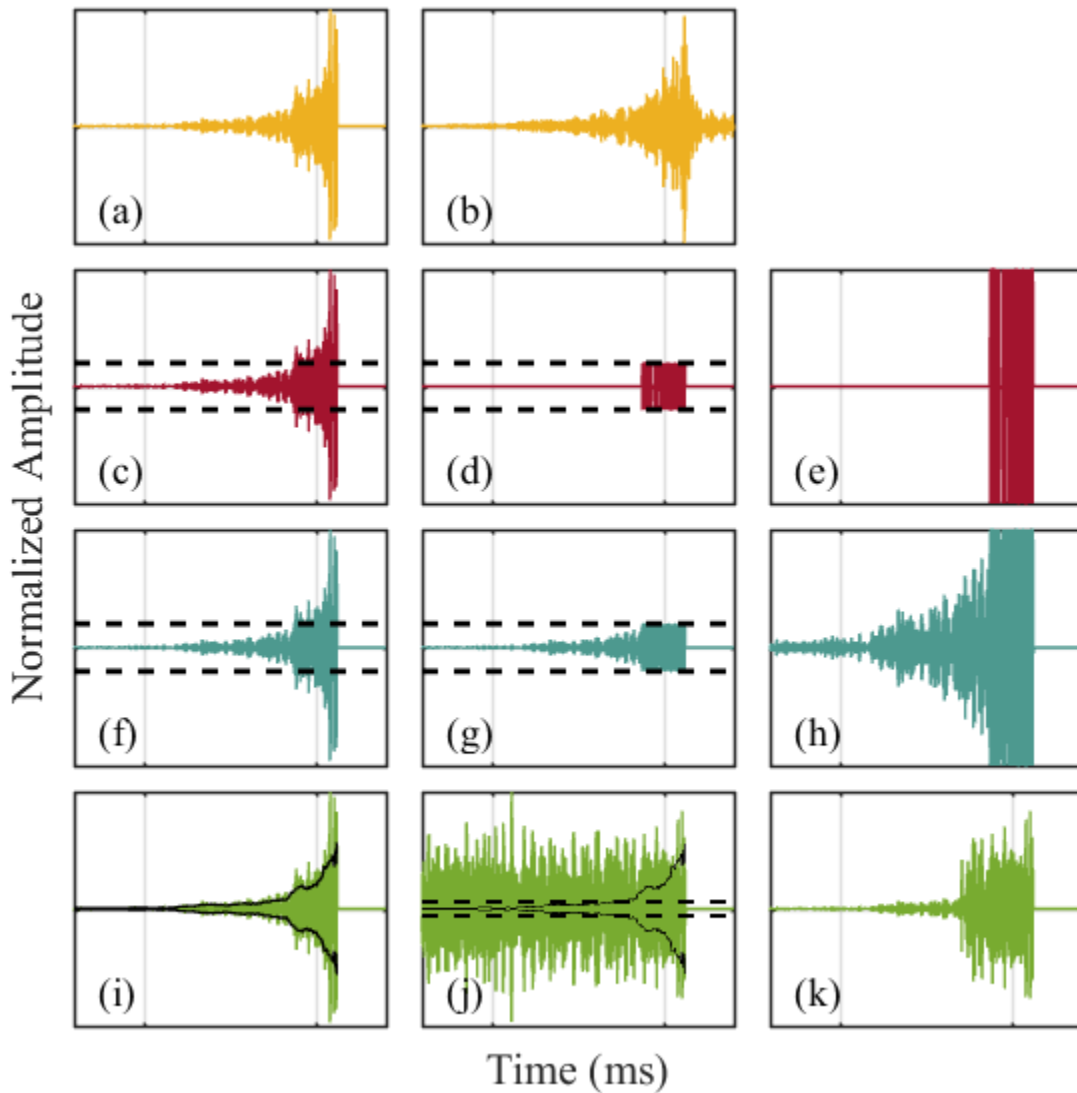


FIG. 3.3. Impulse response modification techniques with each starting with a traditional RIR, (a)-(b) deconvolution TR, (c)-(e) one-bit TR with a threshold of 0.2, indicated by the dashed black lines, (f)-(h) clipping TR with a threshold of 0.2, (i)-(k) decay compensation TR with a threshold of 0.06.

3.5 Focal Signal Analysis Metrics

Four primary metrics are used to quantify the relative merits of the focal signals generated by each of these impulse response modification techniques. The processing methods of deconvolution, one-bit, clipping, and decay compensation TR each result in changing more than just peak focal amplitude and can often result in significant drawbacks along with their benefits. By applying quantitative measures to the focal signal, some of these drawbacks are identified, especially as related to adjustments in the threshold value used in each case. The first metric is the value of the peak amplitude in the time domain waveform at the location of the focus (the focal signal), called the peak focal amplitude, A_p . The second metric, called temporal quality, ξ_t , is a ratio of the instantaneous energy contained in A_p to the average energy in the entire focal signal, $A(x_0, y_0, t)$, of number of time samples N , at the focal location (x_0, y_0) ,

$$\xi_t = \sqrt{\frac{[A_p]^2}{\frac{1}{N} \sum_{n=1}^N [A(x_0, y_0, n)]^2}}. \quad (3.2)$$

A square root operation is used to express the ratio of these energy quantities as a ratio of amplitudes. While variations in the result for Eq. (3.2) can be obtained by using different time windows of the signal, for this study, the entire 51.2 ms signal was used. ξ_t illuminates characteristics of the focal signal otherwise only gleaned from a visual examination of time waveforms, such as the amplitude of the side lobes compared to A_p .

Spatial quality, ξ_s , the third metric, defines a ratio of the energy in the peak focal amplitude, A_p , which occurs at the focal location, to the average energy of the spatial locations that surround it at the time of the focus, t_0 ,

$$\xi_s = \sqrt{\frac{[A_p]^2}{\frac{1}{M_x M_y} \sum_{m_x=1}^{M_x} \sum_{m_y=1}^{M_y} [A(m_x, m_y, t_0)]^2}}, \quad (3.3)$$

where M_x and M_y are the number of spatial locations sampled in the x and y directions, respectively.²¹ The velocity at each point, $A(m_x, m_y, t)$, is measured as the TR process is repeated while the SLDV records the velocity at $M_x \times M_y$ spatial points both at and surrounding the focal location. At t_0 , ξ_s represents how significant the peak amplitude is to the rest of the amplitude over the entire scan area. Given in conjunction with ξ_s are values for the full-width-half-maximum (FWHM) values for the spatial extent of the focusing. The FWHM is determined from two cross sectional plots of the instantaneous squared velocity along the x and y axes in the spatial map of the focusing to determine the full width of the focus at half the maximum amplitude.

The fourth metric examines the harmonic content of the spectrum of the focal signal (the focal spectrum) by quantifying a ratio of the energy contained in the fundamental frequency bandwidth (75-125 kHz), to the second (150-250 kHz) or third (225-375 kHz) harmonic frequency bandwidth. Because the chirp of the forward propagation step has a finite bandwidth, the frequency content of the focal spectrum for traditional TR should be limited to the fundamental bandwidth. Any second or third harmonics of the fundamental bandwidth that occur can only be a result of nonlinearity in the system, whether that is the physical system or any nonlinear signal processing. Mathematically, the fundamental-to-second harmonic ratio, R_{12} , is

$$R_{12} = 10 \log_{10} \left(\frac{\frac{1}{N_1} \sum_{f_0}^{f_1} |F|^2}{\frac{1}{N_2} \sum_{2f_0}^{2f_1} |F|^2} \right). \quad (3.4)$$

The absolute value of the square of the focal spectrum, $|F|^2$, is summed across the values between $f_0 = 75$ kHz and $f_1 = 125$ kHz, the fundamental bandwidth, then scaled by the number of points

within that bandwidth, N_1 . This quantity is divided by a similar term wherein $|F|^2$ has been summed across the values between $2f_0$ and $2f_1$, the second harmonic, and divided by N_2 , the number of frequency points in the second harmonic. The fundamental-to-third harmonic ratio, R_{13} , is defined similarly,

$$R_{13} = 10 \log_{10} \left(\frac{\frac{1}{N_1} \sum_{f_0}^{f_1} |F|^2}{\frac{1}{N_3} \sum_{3f_0}^{3f_1} |F|^2} \right). \quad (3.5)$$

3.6 Results

In examining the focal signals, many of the benefits and drawbacks of these impulse response modification techniques are made manifest. Figure 3.4 shows five example focal signals. Each were measured at the same focal location using the same source chirp signal and thus start out with the same impulse response signal, but this impulse response was then processed with the five different signal processing modification techniques described in Section 3.4. Figure 3.4(a) shows the focal signal generated using an unmodified impulse response, or traditional TR, where an impulse response is only flipped in time and broadcast to generate a focal signal. This focal signal has the expected symmetrical side lobes with a $A_p = 10$ mm/s and $\xi_t = 34.1$, and is the baseline against which all of the other focal signals are compared. The focal signal shown in Fig. 3.4(b) uses deconvolution TR and one may observe that, relative to traditional TR, the energy in the side lobes are reduced in the focal signal (shown in Fig. 3.4(b)) resulting in a signal that more closely approximates a delta function. This is confirmed by the ξ_t which equals 60 for deconvolution TR, however, this benefit is obtained at the expense of a reduction in A_p to 5mm/s, a factor of two relative to traditional TR. A one-bit TR focal signal is shown in Fig. 3.4(c) with a

$A_p = 30$ mm/s. This focal signal employed a threshold value of 0.02 to amplify the impulse response, which increases the A_p but also dramatically increases the amplitude of the side lobes prior to the focus, resulting in a non-symmetrical focal signal with $\xi_t = 24.2$. Even more non-symmetric side lobe amplitudes are evident in the clipping TR focal signal in Fig. 3.4(d) where $\xi_t = 22.2$. This focal signal also employs a threshold of 0.02 but is able to reach a $A_p = 32$ mm/s. The focal signal displayed in Fig. 3.4(e) is generated with decay compensation TR also at a threshold of 0.02. The $A_p = 27$ mm/s here is not quite as high as that shown in Figure 3.4(c) and (d), but the heavily asymmetric side lobes are just as evident, as indicated by $\xi_t = 22.5$.

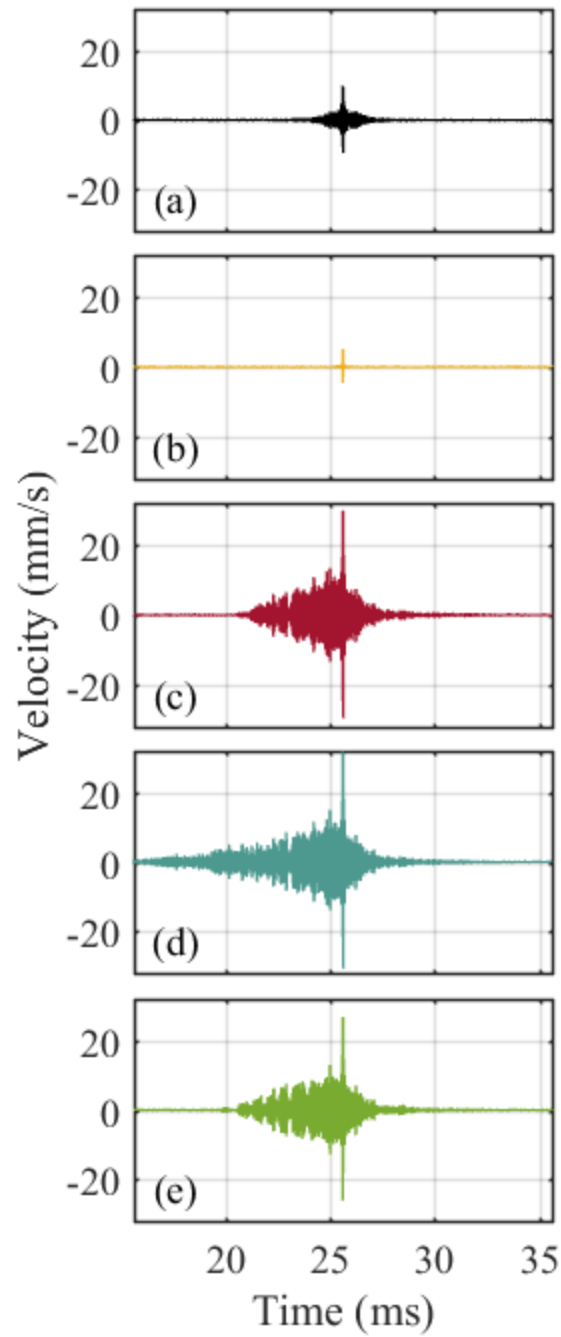


FIG. 3.4. Measured focus signals using (a) traditional, (b) deconvolution, (c) one-bit, (d) clipping, and (e) decay compensation TR. One-bit, clipping, and decay compensation TR all use a threshold value of 0.02.

3.6.1 Peak Focal Amplitude

As explained previously, the threshold used in the modification techniques of one-bit, clipping, and decay compensation TR can be defined as any number between zero and one, where a lower number ultimately boosts low amplitude arrivals later in the impulse response relative to the higher amplitude arrivals earlier in the impulse response. This sends more energy overall into the medium, upon normalization of the reversed signal, which is then broadcast in the backward propagation step. Figure 3.5 reports the A_p measured from all five processing techniques versus the threshold applied. The A_p of traditional TR and deconvolution TR are plotted with a threshold value of one because they do not use a threshold in their processing but are worth comparing to. At the lowest thresholds shown, between 10^{-4} and 10^{-3} , the A_p of one-bit, clipping, and decay compensation TR all plateau at around 29 mm/s. At these thresholds, all of the coherent signal has been amplified during the impulse response processing and thus no further gains in A_p are possible. Though not shown, focal signals were actually obtained with thresholds as low as 10^{-12} and it was found that A_p did not increase beyond the 28-30 mm/s region. In the vicinity of a threshold value of 0.01, one-bit and clipping TR provide a maximal A_p . These maxima are likely a balance between amplifying late arrivals in the impulse response and amplifying background noise in the impulse response. Any noise that is amplified generates destructive interference while any amplified late reflections will constructively interfere in the TR focusing. On the contrary, the A_p of decay compensation TR is optimal only at the lowest threshold values and converges to traditional TR at a threshold of one. One-bit and clipping TR are maximized at thresholds of 0.007 and 0.02 respectively with clipping TR reaching the highest overall peak focal amplitude of 31 mm/s. Both methods achieve lower A_p as the threshold is increased with clipping TR being equivalent to traditional TR at the limiting value of one and the A_p for one-bit TR going to zero.

Clipping TR merges with traditional TR and one-bit TR does not at a threshold of one because these techniques treat the signal below the threshold differently. One-bit TR zeros out the signal below the threshold while clipping TR leaves it intact meaning that a threshold of one would leave one-bit TR with an impulse response of mostly zeros with a single sample value set to one. The resulting TR focal signal is not a focus at all but merely a low amplitude impulse response. Clipping TR would return a traditional focal signal for a threshold of one. Decay compensation TR merges with traditional TR at a threshold of one for reasons similar to clipping TR.

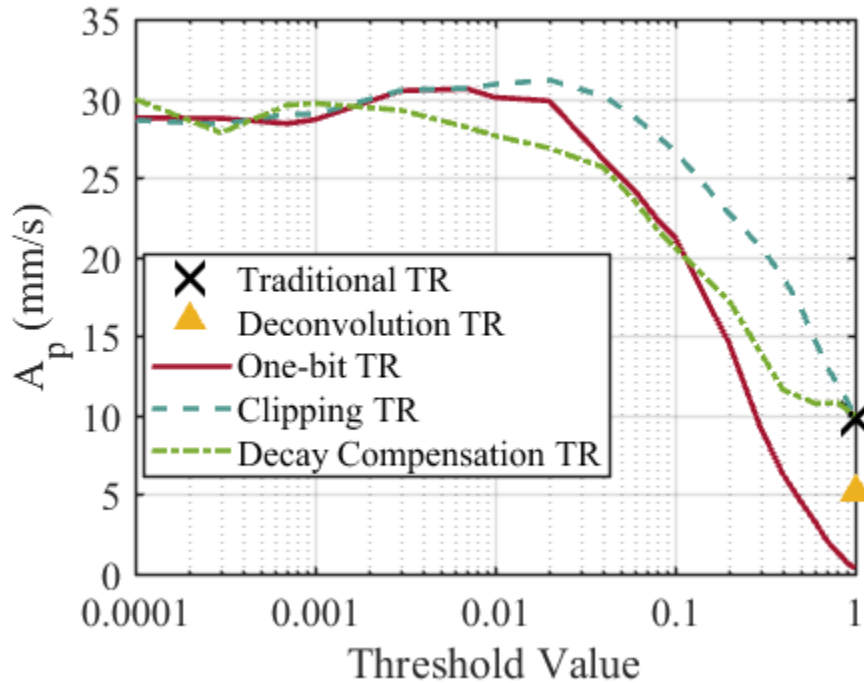


FIG. 3.5. Peak focal amplitude, A_p , vs threshold applied obtained from time reversal (TR) focal signals with various TR processing techniques applied. Traditional TR and deconvolution TR do not use a threshold and so are plotted at a threshold of one.

3.6.2 Temporal Quality

ξ_t was calculated for the focal signals obtained with a range of thresholds and is a second instructive way to study the impact of threshold for each method. The curves displayed in Fig. 3.6 show an overall increase in ξ_t with an increasing threshold, reaching an approximate maximum at a threshold value of one when the curves merge with traditional TR. This indicates that, aside from deconvolution TR, traditional TR has the lowest amplitude side lobes and therefore the cleanest focal signal. The application of a threshold for one-bit, clipping, and decay compensation TR techniques results in an increase in the amplitude of side lobes in exchange for a gain in A_p . The notable exception is one-bit TR, which never collapses with traditional TR, as described in the previous paragraph, but instead drops sharply in ξ_t over thresholds from 0.3 to 1. The overarching trade-off presented by the threshold analysis is that a lower threshold results in higher A_p with a decrease in ξ_t . A high threshold results in a high ξ_t but lower A_p . The application of the TR processing is then what should determine whether maximal A_p or maximal ξ_t is more important. For crack detection in NDE, high A_p , whatever the processing used to obtain it, is assumed to be ideal for the excitation of nonlinear vibrations of a crack. While high ξ_t produces very clean signals, which is important for communications applications for example,¹² the accompanying low A_p likely makes it unsuitable for crack detection, and thus it will not be further explored. With this in mind the optimal threshold value for one-bit, clipping, and decay compensation TR techniques is suggested to be 0.02 to yield a high A_p while maintaining a reasonably high ξ_t .

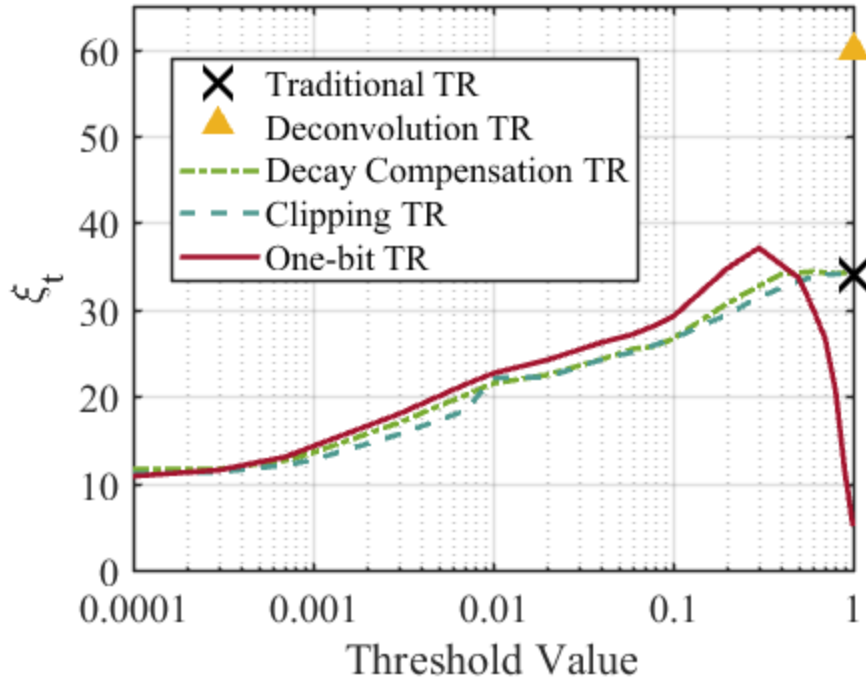


FIG. 3.6. Temporal quality, ξ_t , vs threshold applied obtained from time reversal (TR) focal signals with various TR processing techniques applied. Traditional TR and deconvolution TR are plotted at a threshold value of one.

3.6.3 Spatial Quality

ξ_s was calculated according to Eq. (3.3) using the spatial scans collected for each of the five signal processing techniques. Table 3.1 shows the results of this analysis where one-bit, clipping, and decay compensation TR are generated with thresholds of 0.02. In the first data column, ξ_s for decay compensation TR gives the highest value of 4.6, indicating that decay compensation has the most energy in its peak focal value relative to the energy in the field around it. Each of the modification techniques yields a higher ξ_s than the value obtained for traditional TR. It is interesting that one-bit TR, clipping TR, and decay compensation TR all yield higher ξ_s values since the side lobes for each of these techniques are higher than obtained with traditional TR as observed in Fig. 3.6.

The FWHM is smaller for all techniques relative to traditional TR. This is not surprising for deconvolution TR since the purpose of this technique is to temporally and spatially compress the focus. The FWHMs for one-bit, clipping, and decay compensation TR are smaller than traditional TR, a somewhat surprising result, but helpful in this case since it shows that they do not increase the spatial extent of the focus. A larger focal size could decrease the resolution with which cracks can be detected, making crack detection less reliable overall. However since this is not the case for any of the modification techniques shown here, the benefits to crack detection of a spatially compressed TR focus remain intact.

TABLE 3.1. Spatial quality and full-width-half-max (FWHM) of the spatial scans taken of a focal signal for each time reversal (TR) signal processing technique. A threshold of 0.02 was used for one-bit, clipping, and decay compensation TR techniques.

Technique	ξ_s	FWHM (mm)
Traditional TR	3.5	13.6
Deconvolution TR	3.9	12.6
One-bit TR	4.4	12.3
Clipping TR	4.3	12.8
Decay Compensation TR	4.6	12.5

3.6.4 Harmonic Generation

Because one-bit, clipping, and decay compensation TR utilize nonlinear processing of the RIR, an examination of the spectral content of the focal signals is vital. Nonlinear frequency content generated by the impulse response modification techniques effectively raises the noise floor in harmonic frequency bands, thereby decreasing the ability to detect harmonic generation in a focal signal. Focal spectra of the focal signals measured using one-bit, clipping, and decay compensation TR, are shown in Figs. 3.7(b)-(d), respectively. The threshold used for all three

methods is 0.02, the same as the focal signals shown in Fig. 3.4, and is the optimal threshold value as determined in the previous sections. The focal spectrum created using traditional TR is helpful for comparison and is given in Fig. 3.7(a). In each plot in Fig. 3.7, the fundamental bandwidth is defined as the frequency content between the two solid vertical lines (75-125 kHz), the second harmonic bandwidth is between the two dashed vertical lines (150-250 kHz), and the third harmonic bandwidth is between the two dash-dot vertical lines (225-375 kHz). With these bandwidths defined, the amplitudes in each bandwidth may be compared. The fundamental bandwidth amplitude is clearly the lowest in traditional TR and the highest for clipping TR, which is expected given their peak focal amplitudes. For the second and third harmonics, this is not true. Traditional TR appears to contain only uncorrelated background noise in the harmonic bandwidths, increasing somewhat with frequency above 300 kHz. Both clipping and one-bit TR spectra exhibit a marked increase in harmonic amplitudes, especially for the third harmonic. In fact, both clipping and one-bit TR exhibit increases in the fifth harmonic amplitudes as well. Decay compensation TR does exhibit an increase in harmonic content, but this introduction of higher frequency content decreases as frequency increases (until 425 kHz) and the levels of the harmonic amplitudes are at least half as high as in clipping and one-bit TR. All three techniques are nonlinear processes but clearly the other two are more nonlinear than decay compensation TR.

On closer examination of the higher frequency spectra of clipping and one-bit TR, the marked increases in harmonic amplitudes centered about 300 and 500 kHz represent odd harmonics of the fundamental peak centered about 100 kHz. This is because the two techniques essentially create square waves, which have prominent odd harmonics. Decay compensation TR does not alter the waveform structure as dramatically; so while decay compensation TR does generate some increase in harmonic amplitudes, it is not nearly as prominent as the increases

introduced by clipping and one-bit TR.

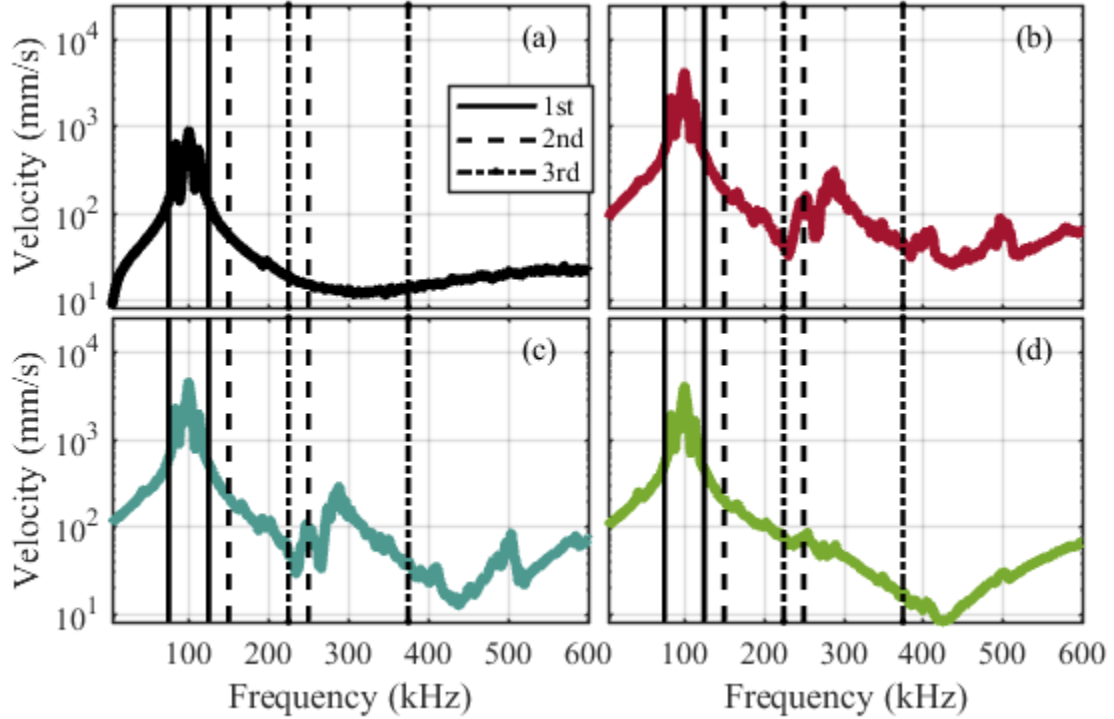


FIG. 3.7. The focal spectra measured with (a) traditional time reversal (TR), (b) one-bit TR, (c) clipping TR, (d) decay compensation TR. (b)-(d) use a threshold of 0.02 for the impulse response modification. The region between the solid vertical lines is the fundamental bandwidth (75-125 kHz). The region between the dashed lines is the second harmonic (150-250 kHz), and the region between the dash-dot lines is the third harmonic (225-375 kHz).

To better quantify the harmonic content, ratios between the first harmonic and the second or third harmonic bandwidths can be calculated using Eqs. (3.4) and (3.5). The results of these calculations are shown in Table 3.2. The best case scenario for a harmonic ratio is traditional TR, which only has background noise at the harmonic frequencies and so has the largest ratios of $R_{12} = 37$ dB and $R_{13} = 34$ dB. The next best is decay compensation TR, which has a lower $R_{12} = 35$ dB, but an equal $R_{13} = 34$ dB. It is clear in Fig. 3.7 that the amplitude of the third harmonic is higher for decay compensation TR than for traditional TR, but the fundamental amplitude also is

markedly higher for decay compensation TR than for traditional TR. The ratios for clipping and one-bit TR are lower, especially for R_{13} , for the reasons identified in the previous paragraph. It should be remembered that when a crack vibrates it does so nonlinearly and thus a higher amplitude excitation raises the harmonic frequency amplitudes by more than any increase in the fundamental frequency amplitude. Thus while these modification techniques have lower fundamental to higher harmonic amplitude ratios, they each should be able to induce a larger nonlinear response of a crack.

TABLE 3.2. Harmonic ratios: the ratio of the energy in the fundamental bandwidth to the energy in a higher harmonic, shown below for the second harmonic, R_{12} , and the third harmonic, R_{13} for each of the amplitude-increasing modification techniques and traditional time reversal (TR).

Technique	R_{12} (dB)	R_{13} (dB)
Traditional TR	37	34
One-bit TR	30	24
Clipping TR	33	26
Decay Compensation TR	35	34

3.7 Nonlinear Detection of SCC Using Decay Compensation TR

Because decay compensation TR has shown to provide higher A_p , without a significant decrease in R_{12} and R_{13} , a preliminary study was conducted for nonlinear TR crack detection using decay compensation TR as the means of excitation to detect stress corrosion cracking (SCC). SCC is known to develop in steel in the Heat-Affected-Zone surrounding welds that are exposed to harsh environments.⁴⁶ To obtain a sample with SCC, a 304L steel rod, 12.7 cm (5 in) in length and 1.59 cm (5/8 in) in diameter, is cut in half and welded back together. The sample is then exposed to a 42% magnesium chloride bath at a temperature of 80°C for 16 days, following

recommendations of Jackson *et al.*⁵⁹ After exposure the rod is epoxied to the top of the disk used in the previous study and to the bottom of the disk are epoxied eight piezoelectric transducers (APC, material type 850) with diameter 19 mm and thickness 12 mm. The piezoelectric transducers are connected to two 4-channel, 50x gain, Tabor 9400 amplifiers that in turn are connected to a National Instruments (Austin, Texas) PXI-7852R 8-channel generator card. A SLDV, externally controlled by custom LabVIEW-based software, is directed to scan 200 points along a 50 mm length of the rod (0.25 mm spacing between scan points), extending roughly 20 mm to either side of the edge of the weld. For each scan point, each of the eight generation channels, in turn, emits a 2 V, 75-125 kHz chirp signal and each of the chirp responses are measured at the current scan point with the SLDV. Eight RIRs are calculated, using either traditional TR or decay compensation TR, and are simultaneously emitted from the piezoelectric transducers at 0.25 V and then again at 1.5 V. A TR focus of energy is generated by each transducer and the simultaneous emission of all 8 transducers ensures that these foci superpose at the scan location. The SLDV has a sensitivity of 25 mm/s/V and the signal is acquired with a National Instruments PXIe-5122 Digitizer with 14-bit resolution.

At each scan location, it is possible to calculate the nonlinearity present in the focal signal recorded at that location by obtaining the cumulative amplitude of the second harmonic, E_2 , where

$$E_2 = \sum_{150kHz}^{250kHz} |F|^2. \quad (3.5)$$

E_2 is plotted versus the location of the scan point in Fig. 3.8(a)-(b) to determine where along the rod nonlinearity from the second harmonic was highest and therefore SCC is more likely to exist. The detection ability of decay compensation TR can be directly compared to that of traditional TR, point by point, in Fig. 3.8 with E_2 versus distance normalized by the peak value detected with each technique. Because the foci measured using decay compensation TR are an average of two times

higher than those measured using traditional TR, the second harmonic of decay compensation TR is also higher at every scan point and thus normalization better compares the peaks in nonlinearity to the supposed background nonlinearity levels at locations where SCC is not expected.

Given the propensity to damage formation in the heat-affected-zone, second harmonic nonlinearity is expected to increase in the assumed Heat-Affected-Zone regions spanning 9-19 mm and 30-40 mm on either side of the weld. Two vertical dashed lines at 19 mm and 30 mm give the approximate location of the outer edge of the weld, meaning the material between 19-30 mm is comprised of the weld itself. In Fig. 3.8(a), where a 0.25 V excitation was used, the most notable distinction between the two techniques is that traditional TR presents higher values of normalized nonlinearity than decay compensation TR at various locations. Both techniques detect a strong feature at 34 mm in the expected region just outside of the weld. The peak at 34 mm was chosen as the normalization constant because the amplitude was consistently high across several scan points. At 8 mm a large peak is evident in the traditional TR data nearly of the same amplitude as the feature at 34 mm. The decay compensation TR data on the other hand does not exhibit as large an amplitude feature at 8 mm as at 34 mm. The seemingly random peaks in the traditional TR data at 2, 12, 24, 27, 38, 39, 47, 48, and 50 mm are at individual scan points, calling these features into question. The decay compensation TR data is smoother from scan point to scan point. Other than the main peak at 34 mm and the small one at 8 mm, the nonlinearity in the decay compensation TR data oscillates at low levels indicative of consistent background nonlinearity.

Figure 3.8(b) shows the same scan taken at an excitation amplitude of 1.5 V. The decay compensation TR data looks essentially the same, though a bit more smooth, suggesting that the amplitude of the 0.25 V measurement was sufficiently above the noise floor to result in reliable measurements. The data of traditional TR in Fig. 3.8(b) is drastically different, with all of the

seemingly random peaks removed and even the gradual rises at 8 mm and 27 mm significantly reduced. With the increase in excitation amplitude, the traditional TR result nearly merges with the decay compensation TR measurement. This indicates that decay compensation TR is not only able to measure nonlinearity from SCC as well as traditional TR, but is also more reliable at lower excitation levels where traditional TR struggles. Additionally, false detections of features at 8 mm and 27 mm in the traditional TR data are not present at either excitation level for decay compensation TR.

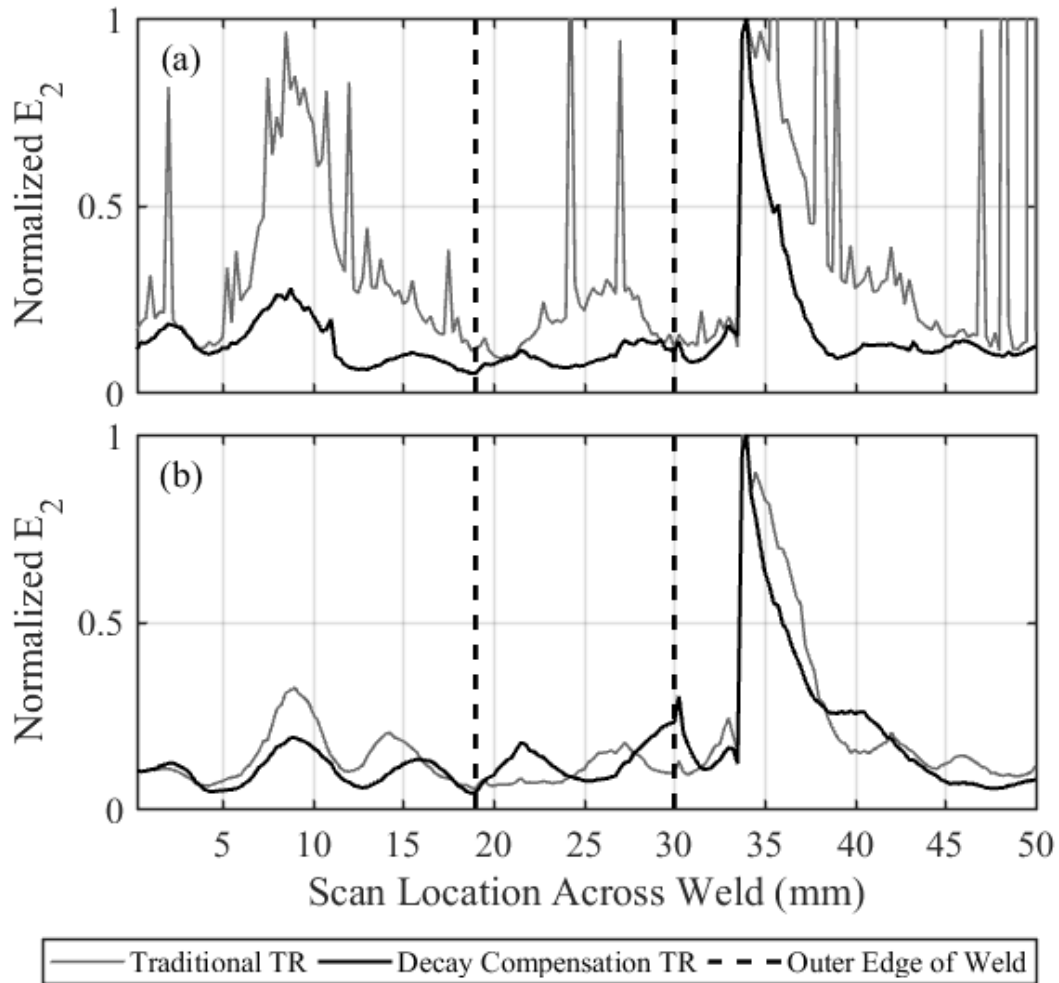


FIG. 3.8. Normalized nonlinearity contained in the second harmonic of a focal signal, shown as E_2 on the vertical axis, generated at each of 200 scan locations along a rod with stress corrosion cracking. Traditional time reversal (TR) (gray) and decay compensation TR (black) were used to excite TR foci at each location. Figure 3.8(a) shows the results when the focal signals were excited with an amplitude of 0.25 V. Figure 3.8(b) shows the results at an excitation amplitude of 1.5 V. While ultimately unknown, stress corrosion cracking is likely to occur in the region just outside the weld on the rod, called the Heat-Affected-Zone.

3.8 Conclusion

Time reversal (TR) focusing used for the purpose of exciting nonlinearity in cracks has the potential to suffer from a low signal to noise ratio (SNR) and therefore false detections if only traditional TR techniques are utilized. Modifications to the reversed impulse response, wherein

later reflections are amplified relative to early reflections, ultimately increases the peak focal amplitude, but often at the expense of lowering the temporal quality of the focal signal, and increasing higher-order harmonics, a problem for nonlinear crack detection that relies on higher-order harmonics to sense cracks. Four techniques were studied relative to traditional TR, deconvolution, one-bit, clipping, and decay compensation TR. One-bit, clipping, and decay compensation TR were able to realize focal amplitudes 3 times higher than traditional TR. Deconvolution TR had a temporal quality much higher than any other technique, but with a focal amplitude that was much lower. Only decay compensation TR significantly increased peak focal amplitude without a drastic increase in higher harmonic content as well. In addition, spatial focus quality and the width of the focusing was found to be slightly better for the 4 modification techniques than for traditional TR. In the study of TR optimization in a reverberation chamber, Willardson *et al.* found results similar to these, but with clipping TR able to reach amplitudes over 4 times higher than traditional TR at a threshold value of 0.03.

Decay compensation TR was utilized to locate regions of high nonlinearity on a rod with stress corrosion cracking. These were then compared to results from the same test conducted using traditional TR. It was determined that because of decay compensation TR's higher SNR in its focal signals, it was able to more cleanly detect nonlinearity compared to traditional TR. In addition, when the experiment was repeated at higher excitation amplitudes, the random spikes in nonlinearity and a couple of false detections measured at the low excitation level with traditional TR disappeared and the data tended to converge to the data found with decay compensation TR.

Chapter 4: Conclusion

The physical implementation of the time reversal (TR) process, especially reciprocal TR, provides the means for localizing and characterizing defects using ultrasonic nondestructive evaluation (NDE) of a sample without moving the excitation sources. Reciprocal TR is able to use the measured impulse response of a sample to generate a focus of high energy at the location of the measurement of the impulse response, far from the actual source of acoustic energy. When the high amplitude focus is generated and measured at a cracked location, the physical interaction of crack surfaces creates nonlinear signatures discernible in the focal signal, thus allowing the crack to be identified nondestructively. However, this process can be problematic, especially when the focal amplitude is insufficient for excitation of crack nonlinearities. The research described in this thesis has provided two distinct contributions to the field of TR NDE. The first is the use of TR measurements to identify the location of stress corrosion cracking (SCC) as well as verifying the increase in nonlinearity in samples assumed to possess more SCC. The second contribution experimentally optimizes TR processing and introduces the decay compensation signal processing technique as a means to increase the amplitude of TR focusing without compromising the ability to detect nonlinearities using TREND, providing a technique that is less susceptible to noise and false detections.

SCC has been known to develop in steel canisters holding spent nuclear fuel, especially near welds that have been exposed to harsh temperature and chloridic conditions. To approximate the SCC in these canisters, welded steel rods were exposed to a magnesium chloride solution for sequentially increasing amounts of time, generating rods with a range of SCC. The rods were tested using the Time Reversed Elastic Nonlinearity Diagnostic (TREND), which placed an individual TR focus at each of the 800 points scanned per rod. The focal signals were analyzed for nonlinear

content and it was determined that overall nonlinearity increased in the region adjacent to the weld, as anticipated. A total amount of nonlinearity per rod was calculated and it was discovered that, in general, the amount of total nonlinearity increased for rods that had been exposed to the hot magnesium chloride for longer times. This finding implies that TREND need not be limited to relative measurements on a single sample but it can also be used to monitor SCC development over time on a variety of samples.

Successful NDE requires a high SNR such that the analysis of collected data is clear and undeniable. The TR focus is high amplitude by nature, but could still be insufficient to excite nonlinear signatures sufficiently for damage detection. To optimize the SNR of the TR focus, five impulse response modification techniques were quantitatively compared according to peak focal amplitude, temporal quality, spatial quality, and harmonic content, in order to determine the one technique most suitable for crack detection. Of the five techniques, traditional, deconvolution, one-bit, clipping, and decay compensation TR, it was determined that decay compensation had the highest focal amplitude while still maintaining low harmonic content. To verify its efficacy for crack detection, decay compensation was compared to traditional TR by employing both to detect SCC in a rod using TREND. It was found that decay compensation was able to successfully detect damage while raising the SNR, making TREND more reliable when it is used in conjunction with decay compensation TR. In fact, a false positive detection of SCC found with traditional TR was determined to be false by comparing to the results using decay compensation and to the use of traditional TR at higher amplitude.

4.1 Future Work

Ongoing research for both contributions will be interrelated. Additional samples may be exposed to hot magnesium chloride baths. This may include a larger number of samples to determine a better idea of the variability expected in this damage inducing process as mentioned in Section 2.3 or the repeated exposure of individual samples with measurements made between exposures. The latter will determine how SCC nonlinearity changes as the same welded region is exposed for longer amounts of time, thus accounting for any inconsistencies among samples in the current research due to weld differences. Decay compensation has been implemented into the TREND software and may be employed to scan samples in conjunction with or instead of traditional TR. As the characteristics of the samples are revealed, they will be compared to those in this thesis.

There is a plan to image the rods tested in this thesis at the Advanced Photon Source (APS) user facility at Argonne National Laboratory. This work will be carried out by collaborators at North Carolina State University who are part of the Integrated Research Project (IRP) that is funded by the U.S. Nuclear Energy Department, of which BYU is receiving a subcontract through Los Alamos National Laboratory to fund the work carried out in this thesis. This imaging may be done on only some of the samples tested here. It is anticipated that this imaging will give us a better idea of the actual amount of SCC in the samples and this comparison could be written up for a paper. Additionally, a destructive evaluation of the samples may be carried out by cutting the samples into slices and x-ray imaging each slice.

Bibliography

- ¹ M. Fink, "Time reversed acoustics," *Phys. Today* **50**, 34-40 (1997).
- ² B. E. Anderson, M. Griffa, C. Larmat, T. J. Ulrich, and P. A. Johnson, "Time reversal," *Acoust. Today* **4**(1), 5-16 (2008).
- ³ B. E. Anderson, M. Griffa, T. J. Ulrich, P.-Y. Le Bas, R. A. Guyer, and P. A. Johnson, "Crack localization and characterization in solid media using time reversal techniques," *Am. Rock Mech. Assoc.*, #10-154 (2010).
- ⁴ T. J. Ulrich, P. A. Johnson, and A. Sutin, "Imaging nonlinear scatterers applying the time reversal mirror," *J. Acoust. Soc. Am.* **119**(3), 1514-1518 (2006).
- ⁵ B. E. Anderson, M. Griffa, P.-Y. Le Bas, T. J. Ulrich, and P. A. Johnson, "Experimental implementation of reverse time migration for nondestructive evaluation applications," *J. Acoust. Soc. Am.* **129**(1), EL8-EL14 (2011).
- ⁶ T. J. Ulrich, P. A. Johnson, and R. A. Guyer, "Interaction dynamics of elastic waves with a complex nonlinear scatterer through the use of a time reversal mirror," *Phys. Rev. Lett.* **98**, 104301 (2007).
- ⁷ B. E. Anderson, L. Pieczonka, M. C. Remillieux, T. J. Ulrich, and P.-Y. Le Bas, "Stress corrosion crack depth investigation using the time reversed elastic nonlinearity diagnostic," *J. Acoust. Soc. Am.* **141**(1), EL76-EL81 (2017).
- ⁸ B. van Genneren, B. Zybach, and J. Dual, "How to induce dynamic fracture by focusing flexural waves," *Proc. Mtgs. Acoust.* **32**, 045025 (2017).
- ⁹ J.-L. Thomas, F. Wu, and M. Fink, "Time reversal mirror applied to lithotripsy," *Ultrason. Imag* **18**, 106-121 (1996).
- ¹⁰ A. Parvulescu, "Signal detection in a multipath medium by M.E.S.S. processing," *J. Acoust. Soc. Am.* **33**(11), 1674 (1961).

- ¹¹ A. Parvulescu and C. S. Clay, "Reproducibility of signal transmission in the ocean," *Radio Elec. Eng.* **29**, 223-228 (1965).
- ¹² B. E. Anderson, T. J. Ulrich, P.-Y. Le Bas, and J. A. Ten Cate, "Three-dimensional time reversal communications in elastic media," *J. Acoust. Soc. Am.* **139**(2), EL25-EL30 (2016).
- ¹³ N. Chakroun, M. Fink, and F. Wu, "Ultrasonic non destructive testing with time reversal mirrors," *Proc. IEEE Ultrason. Symp.*, Tucson, **2**, 809-814 (1992).
- ¹⁴ C. Larmat, J.-P. Montagner, M. Fink, Y. Capdeville, A. Tourin, and E. Clevede, "Time-reversal imaging of seismic sources and applications to the great Sumatra earthquake," *Geophys. Res. Lett.* **33**(19), L19312 (2006).
- ¹⁵ C. Larmat, J. Tromp, Q. Liu, and J.-P. Montagner, "Time-Reversal location of glacial earthquakes," *J. Geophys. Res.* **113**(B9), B09314 (2008).
- ¹⁶ C. Larmat, R. A. Guyer, and P. A. Johnson, "Tremor source location using time-reversal: selecting the appropriate imaging field," *Geophys. Res. Lett.* **36**(22), L22304 (2009).
- ¹⁷ R. Ernst and J. Dual, "Acoustic emission localization in beams based on time reversed dispersion," *Ultrason.* **54**(6), 1522-1533 (2014).
- ¹⁸ G. K. Kocur, E. H. Saenger, C. U. Grosse, and T. Vogel, "Time reverse modeling of acoustic emissions in a reinforced concrete beam," *Ultrason.* **65**, 96-104 (2016).
- ¹⁹ R. K. Ing and N. Quieffin, "In solid localization of finger impacts using acoustic time-reversal process," *Appl. Phys. Lett.* **87**(20), 204104 (2005).
- ²⁰ D. Vigoureux and J.-L. Guyader, "A simplified Time Reversal method used to localize vibrations sources in a complex structure," *Appl. Acoust.* **73**(5), 491-496 (2012).
- ²¹ C. Heaton, B. E. Anderson, and S. M. Young, "Time reversal focusing of elastic waves in plates for educational demonstration purposes," *J. Acoust. Soc. Am.* **141**(2), 1084-1092 (2017).
- ²² M. Scalerandi, A. S. Gliozzi, C. L. E. Bruno, D. Masera, and P. Bocca, "A scaling method to enhance detection of a nonlinear elastic response," *Appl. Phys. Lett.* **92**(10), 101912 (2008).

- ²³ M. Scalerandi, A. S. Gliozzi, C. L. E. Bruno, and K. Van Den Abeele, "Nonlinear acoustic time reversal imaging using the scaling subtraction method," *J. Physics D: Appl. Phys.* **41**(21), 215404 (2008).
- ²⁴ A. Sutin, P. Johnson, and J. TenCate, "Development of nonlinear time reverse acoustics (NLTRA) for application to crack detection in solids," In *Proceedings of the 5th World Congress on Ultrasonics, Paris, France*, 121-124 (2003).
- ²⁵ A. M. Sutin, J. A. TenCate, and P. A. Johnson, "Single-channel time reversal in elastic solids," *J. Acoust. Soc. Am.* **116**(5), 2779-2784 (2004).
- ²⁶ N. Chakroun, M. Fink, and F. Wu, "Time reversal processing in ultrasonic nondestructive testing," *IEEE Trans. Ultrason. Ferroelectr. Freq. Control* **42**, 1087-1098 (1995).
- ²⁷ V. Miette, L. Sandrin, F. Wu, and M. Fink, "Optimisation of time reversal processing in titanium inspections," *IEEE Ultrason. Symp. Proc.*, 643-647 (1996).
- ²⁸ R. K. Ing and M. Fink, "Time recompression of dispersive Lamb wave using a time reversal mirror. Applications to flaw detection in thin plates," *IEEE Ultrason. Symp. Proc.* (San Antonio, USA, Nov. 1996), 659-664 (1996).
- ²⁹ C. Prada and M. Fink, "Separation of interfering acoustic scattered signals using the invariant of the time-reversal operator. Application to Lamb waves characterization," *J. Acoust. Soc. Am.* **104**, 801-807 (1998).
- ³⁰ E. Kerbrat, R. K. Ing, C. Prada, D. Cassereau, and M. Fink, "The DORT method applied to detection and imaging in plates using Lamb waves," *Rev. Prog. Quant. Nondestruct. Eval., AIP Conf. Proc.*, 934-940 (2000).
- ³¹ C. Prada, E. Kerbrat, D. Cassereau, and M. Fink, "Time reversal techniques in ultrasonic nondestructive testing of scattering media," *Inv. Prob.* **18**, 1761-1773 (2002).
- ³² E. Kerbrat, C. Prada, D. Cassereau, and M. Fink, "Ultrasonic nondestructive testing of scattering media using the decomposition of the time reversal operator," *IEEE Trans. Ultrason. Ferroelectr. Freq. Control.* **49**, 1103-1113 (2002).

- ³³ C. Prada, F. Wu, and M. Fink, “The iterative time reversal mirror: A solution to self-focusing in the pulse-echo mode,” *J. Acoust. Soc. Am.* **90**(2), 1119-1129 (1991).
- ³⁴ C. Prada, J-L. Thomas, and M. Fink, “The iterative time reversal process: Analysis of the convergence,” *J. Acoust. Soc. Am.* **97**(1), 62-71 (1995).
- ³⁵ R. Guyer, “Nonlinear tomography and time reversed acoustics,” presented at *The 6th International Workshop on Nonlinear Elasticity in Materials*. Leuven, Belgium (2001).
- ³⁶ P. P. Delsanto, P. A. Johnson, M. Scalerandi, and J. A. TenCate, “LISA simulations of time-reversed acoustic and elastic wave experiments,” *J. Phys. D: Appl. Phys.* **35**(23), 3145-3152 (2002).
- ³⁷ O. Bou Matar, S. Dos Santos, J. Fortineau, T. Goursolle, L. Haumesser, and F. Vander Meulen, “Pseudo spectral simulations of elastic waves propagation in heterogeneous nonlinear hysteretic medium,” In *Proceedings of the 17th International Symposium on Nonlinear Acoustics, State College, PA* 95-98 (2005).
- ³⁸ P.-Y. Le Bas, M. C. Remillieux, L. Pieczonka, J. A. Ten Cate, B. E. Anderson, and T. J. Ulrich, “Damage imaging in a laminated composite plate using an air-coupled time reversal mirror,” *Appl. Phys. Lett.* **107**, 184102 (2015).
- ³⁹ T. J. Ulrich, A. M. Sutin, T. Claytor, P. Papin, P.-Y. Le Bas, and J. A. TenCate, “The time reversed elastic nonlinearity diagnostic applied to evaluation of diffusion bonds,” *Appl. Phys. Lett.* **93**(15), 151914 (2008).
- ⁴⁰ P.-Y. Le Bas, T. J. Ulrich, B. E. Anderson, R. A. Guyer, and P. A. Johnson, “Probing the interior of a solid volume with time reversal and nonlinear elastic wave spectroscopy,” *J. Acoust. Soc. Am.* **130**(4), EL258-EL263 (2011).
- ⁴¹ P. Blanloeuil, L. R. F. Rose, J. A. Guinto, M. Veidt, and C. H. Wang, “Closed crack imaging using time reversal method based on fundamental and second harmonic scattering,” *Wave Motion* **66**, 156-176, (2016).
- ⁴² G. Zumpano and M. Meo, “A new nonlinear elastic time reversal acoustic method for the identification and localisation of stress corrosion cracking in welded plate-like structures—A simulation study,” *Int. J Solids Struct.* **44**(11), 3666-3684, (2007).

- ⁴³ M. C. Remillieux, P.-Y. Le Bas, L. Pieczonka, B. E. Anderson, and T. J. Ulrich, “Estimating the Penetration Depth and Orientation of Stress Corrosion Cracks Using Time-Reversal Acoustics,” *Trans. Am. Nuclear Soc.* **115**, 217-220 (2016).
- ⁴⁴ P. B. Nagy, “Fatigue damage assessment by nonlinear ultrasonic materials characterization,” *Ultrason.* **36**, 375-381 (1998).
- ⁴⁵ T. J. Ulrich, B. E. Anderson, M. C. Remillieux, P. Y. Le Bas, and L. Pieczonka, “Application of nonlinear ultrasonics to inspection of stainless steel for dry storage,” *Tech. rep.* LA-UR-15-27382, Los Alamos National Laboratory (LANL), 2015.
- ⁴⁶ E. Gray, “Coast to coast spent fuel dry storage problems and recommendations,” in Division of Spent Fuel Management Regulatory Conference (Nov. 2015), <http://www.nrc.gov/public-involve/conferencesymposia/dsfm/2015/dsfm-2015-erica-gray.pdf> (Last viewed June 7, 2018).
- ⁴⁷ K. L. Banovac, “Summary of August 5, 2014, public meeting with the nuclear energy institute on chloride induced stress corrosion cracking regulatory issue resolution protocol,” U.S. Nuclear Regulatory Commission Public Meeting (August 2014), <http://pbadupws.nrc.gov/docs/ML1425/ML14258A081.pdf> (Last viewed June 7, 2018).
- ⁴⁸ D. S. Dunn, “Chloride-induced stress corrosion cracking tests and example aging management program,” U.S. Nuclear Regulatory Commission Public Meeting (August 2014), <https://www.nrc.gov/docs/ML1425/ML14258A082.pdf> (Last viewed June 7, 2018).
- ⁴⁹ *Welding Handbook*, edited by A. O’Brien (American Welding Society, Miami, FL, 2011), Vol. 4, pp. 308-313.
- ⁵⁰ A. Bustreo, “All you need to know about the heat-affected zone,” in *The Fabricator* (July 2016), <https://www.thefabricator.com/article/shopmanagement/all-you-need-to-know-about-the-heat-affected-zone> (Last viewed on 6/7/18).
- ⁵¹ *Welding Handbook*, edited by C. L. Jenney and A. O’Brien (American Welding Society, Miami, FL, 2001), Vol. 1, pp. 136.

- ⁵² Y. Ohara, H. Endo, T. Mihara, and K. Yamanaka, "Ultrasonic measurement of closed stress corrosion crack depth using subharmonic phased array," *Japanese J. Appl. Phys.* **48**(7S), 07GD01 (2009).
- ⁵³ A. Ouchi, A. Sugawara, Y. Ohara, and K. Yamanaka, "Subharmonic phase array for crack evaluation using surface acoustic wave," *Japanese J. Appl. Phys.* **54**(7S1), 07HC05 (2015).
- ⁵⁴ J. Riviere, M. Remillieux, Y. Ohara, B. E. Anderson, S. Hauptert, T. J. Ulrich, and P. A. Johnson, "Dynamic Acousto-Elasticity in a Fatigue-Cracked Sample," *J. Nondestruct. Eval.* **33**(2), 216-225 (2014).
- ⁵⁵ Y. Ohara, B. E. Anderson, T. J. Ulrich, P.-Y. Le Bas, P.A. Johnson, and S. Hauptert, "Localization of closed cracks using multi-mode nonlinear resonant ultrasound spectroscopy," *J. Japanese Soc. Nondest. Inspec.* **64**(12), 571-578 (2015).
- ⁵⁶ F. Morlock, L. J. Jacobs, J.-Y. Kim, P. Singh, and J. J. Wall, "Nonlinear ultrasonic assessment of stress corrosion cracking damage in sensitized 304 stainless steel," *AIP Conference Proceedings* **1650**, 1641 (2015).
- ⁵⁷ B. Van Damme, K. Van Den Abeele, Y. Li, and O. Bou Matar, "Time reversed acoustics techniques for elastic imaging in reverberant and nonreverberant media: an experimental study of the chaotic cavity transducer concept," *J. Appl. Phys.*, **109**, 104910 (2011).
- ⁵⁸ B. E. Anderson, M. Clemens, and M. L. Willardson, "The effect of transducer directionality on time reversal focusing," *J. Acoust. Soc. Am.* **142**(1), EL95-EL101 (2017).
- ⁵⁹ B. K. Jackson, D. A. Bosko, M. T. Cronin, J. L. W. Warwick, and J. J. Wall, "Detection of incipient SCC damage in primary loop piping using fiber optic strain gages," *ASME Proc. of Pressure Vessels and Piping*, PVP2014-28979 (2014).
- ⁶⁰ G., Montaldo, D. Palacio, M. Tanter, and M. Fink, "Time reversal kaleidoscope: A smart transducer for three-dimensional ultrasonic imaging," *Appl. Phys. Lett.* **84**(19), 3879-3881 (2004).
- ⁶¹ O. Bou Matar, Y. F. Li, and K. Van Den Abeele, "On the use of a chaotic cavity transducer in nonlinear elastic imaging," *Appl. Phys. Lett.* **95**, 141913 (2009).

- ⁶² S. Delrue, K. Van Den Abeele, and O. Bou Matar, "Simulation study of a chaotic cavity transducer based virtual phased array used for focusing in the bulk of a solid material," *Ultrason.* **67**, 151-159 (2016).
- ⁶³ C. Draeger, J-C. Aime, and M. Fink, "One-channel time reversal in chaotic cavities: Experimental results," *J. Acoust. Soc. Am.* **105**(2), 618-625 (1999).
- ⁶⁴ B. E. Anderson, J. Douma, T. J. Ulrich, and R. Snieder, "Improving spatio-temporal focusing and source reconstruction through deconvolution," *Wave Motion* **52**(9), 151-159 (2015).
- ⁶⁵ R. A. Guyer and P. A. Johnson, "Nonlinear mesoscopic elasticity: Evidence for a new class of materials," *Phys. Today* **52**, 30-35 (1999).
- ⁶⁶ P. A. Johnson, "The new wave in acoustic testing," *Mat. World* **7**, 544-546 (1999).
- ⁶⁷ M. Bentahar, R. El Guerjouma, S. Idijmarene, and M. Scalerandi, "Influence of noise on the threshold for detection of elastic nonlinearity," *J. Appl. Phys.* **113**, 043516 (2013).
- ⁶⁸ A. Derode, A. Tourin, and M. Fink, "Ultrasonic pulse compression with one-bit time reversal through multiple scattering," *J. Appl. Phys.* **85**(9), 6343-6352 (1999).
- ⁶⁹ G. Montaldo, P. Roux, A. Derode, C. Negreira, and M. Fink, "Generation of very high pressure pulses with 1-bit time reversal in a solid waveguide," *J. Acoust. Soc. Am.* **110**(6), 2849-2857 (2001).
- ⁷⁰ A.S. Gliozzi, M. Scalerandi, and P. Antonaci, "One-channel time-reversal acoustics in highly attenuating media," *J. Phys. D: Appl. Phys.* **46**, 135502 (2013).
- ⁷¹ M. L. Willardson, B. E. Anderson, S. M. Young, M. H. Denison, and B. D. Patchett, "Time reversal focusing of high amplitude sound in a reverberation chamber," *J. Acoust. Soc. Am.* **143**(2), 696-705 (2018).
- ⁷² M. Tanter, J.-L. Thomas, and M. Fink, "Time reversal and the inverse filter," *J. Acoust. Soc. Am.*, **108**(1), 223-234 (2000).
- ⁷³ G. Ribay, J. de Rosny, and M. Fink, "Time reversal of noise sources in a reverberation room," *J. Acoust. Soc. Am.*, **117**(5), 2866-28720 (2005).

- ⁷⁴ K. J. Haworth, J. B. Fowlkes, P. L. Carson, and O. D. Kripfgans, “Generalized shot noise model for time-reversal in multiple-scattering media allowing for arbitrary inputs and windowing,” *J. Acoust. Soc. Am.* **125**(5), 3129-3140 (2009).
- ⁷⁵ M. Davy, J. de Rosny, J.-C. Joly, and M. Fink, “Focusing and amplification of electromagnetic waves by time reversal in an leaky reverberation chamber,” *C. R. Physique* **11**, 37-43 (2010).
- ⁷⁶ O. Bou Matar, Y. Li, S. Delrue, and K. Van Den Abeele, “Optimization of chaotic cavity transducers to nonlinear elastic imaging,” *Proceedings of the 10th French Congress on Acoustics*, Lyon, 2010.
- ⁷⁷ J. Robin, M. Tanter, and M. Pernot, “A semi-analytical model of a time reversal cavity for high-amplitude focused ultrasound applications,” *Phys. Med. Biol.* **62**, 7471-7481 (2017).
- ⁷⁸ A. S. Gliozzi, M. Miniaci, F. Bosia, N. M. Pugno, and M. Scalerandi, “Metamaterials-based sensor to detect and locate nonlinear elastic sources,” *Appl. Phys. Lett.* **107**, 161902 (2015).

Appendix A

TREND Instruction Manual

Table of Contents

(No page numbers included for practical reasons. Page numbers and links included in TREND Instruction Manual saved as separate document)

Part1: Cable Setup

Part2: Opening TREND

Part3: Hardware settings

- a) Generator
- b) Digitizer/Acquisition Card
- c) Scanning System
- d) Laser Alignment

Part 4: Signal Generation Settings

Part 5: signal Acquisition Settings

Part 6: Specifying Scan Points

Part 7: TR Process

Part 8: Signal Analysis

Part 9: Acquiring Data

- a) Forward Only, TR Only, Forward + TR
- b) Single Point, Scan, Focus & Scan
- c) Data Collection

Part 10: Saving Data

- a) Automatic save
- b) One-the-fly save
- c) What you get when a single point measurement is saved
- d) What you get when a scan saves data

Part 11: Typical Signals

Part 12: Other things

- a) Other options under File
- b) Nonlinear characteristics of acquisition and generation cards

Part 12: How to load your own scan grid

Part 13: Useful Matlab code developed for TREND

- a) Settings filed turned into a Matlab structure
- b) Read in .dat files from forward and TR steps

Part 1: Cable Setup

Begin by finding the laser control box and switching control to “External.” The laser should be off at this point. This switch enables TREND to control the laser mirrors and therefore move the laser independent of Polytec software.



A cable runs from the laser control box and is wired to the NI DAQmx shown below. The DAQmx then connects to the NI Chassis via USB.



Now you can turn on the laser at the Polytec controls by turning the key clockwise. A BNC cable collects the analog SLDV signal through the Velocity –output connector, pointed out with a red arrow. This BNC cable runs to the NI Chassis and into the acquisition card, ch0.



The live laser video feed comes out of the BNC connection labeled “VIDEO” on the back of the junction box. A red arrow points out this location in the figure below. This is what it looks like with just Polytec software hooked up.



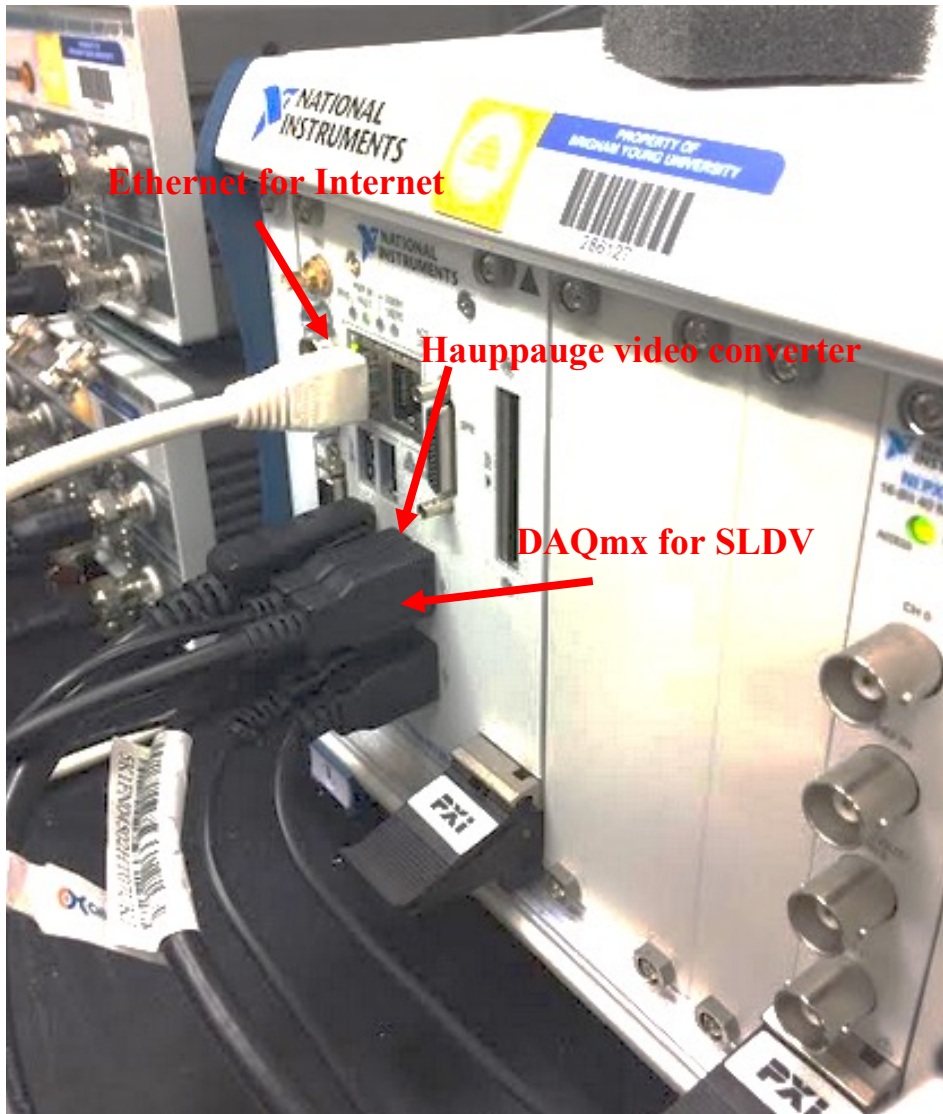
To also send the video feed to TREND, use a BNC T to split off another line. For some reason, splitting the feed like this has the potential to make the video quality much grittier.



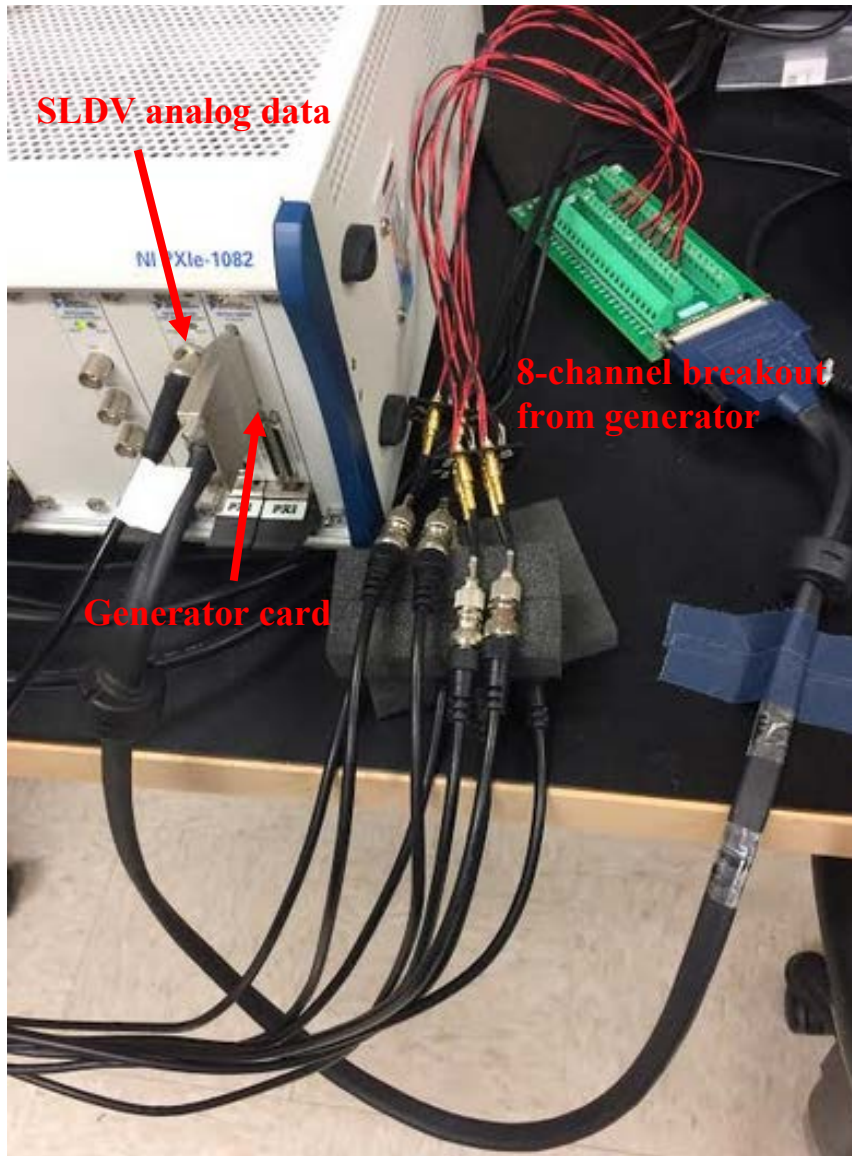
The BNC cable is converted to RCA and attached to this small adaptor, the Hauppauge device that converts the video feed to work with TREND (incidentally, the WinTV software, and a few others, came with this gadget). The Hauppauge device connects to the NI Chassis via USB.



NI Chassis connections, Left side (shown below)



NI Chassis connections, Right side (shown below)



The whole shebang, setup with 8 generation channels hooked to Tabor amplifiers for use with piezoelectrics glued to a solid steel sample. (below)

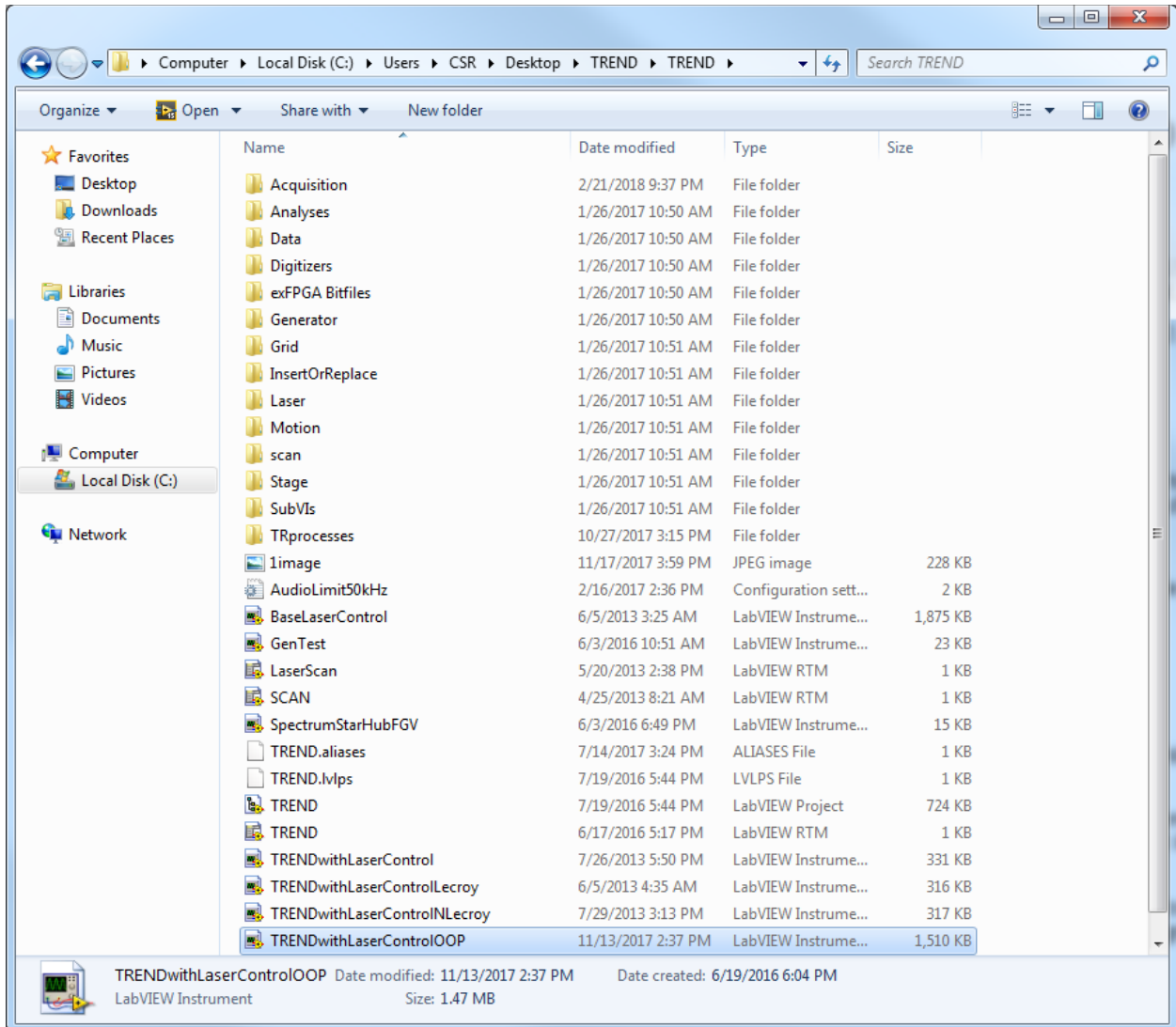


Part 2: Opening TREND

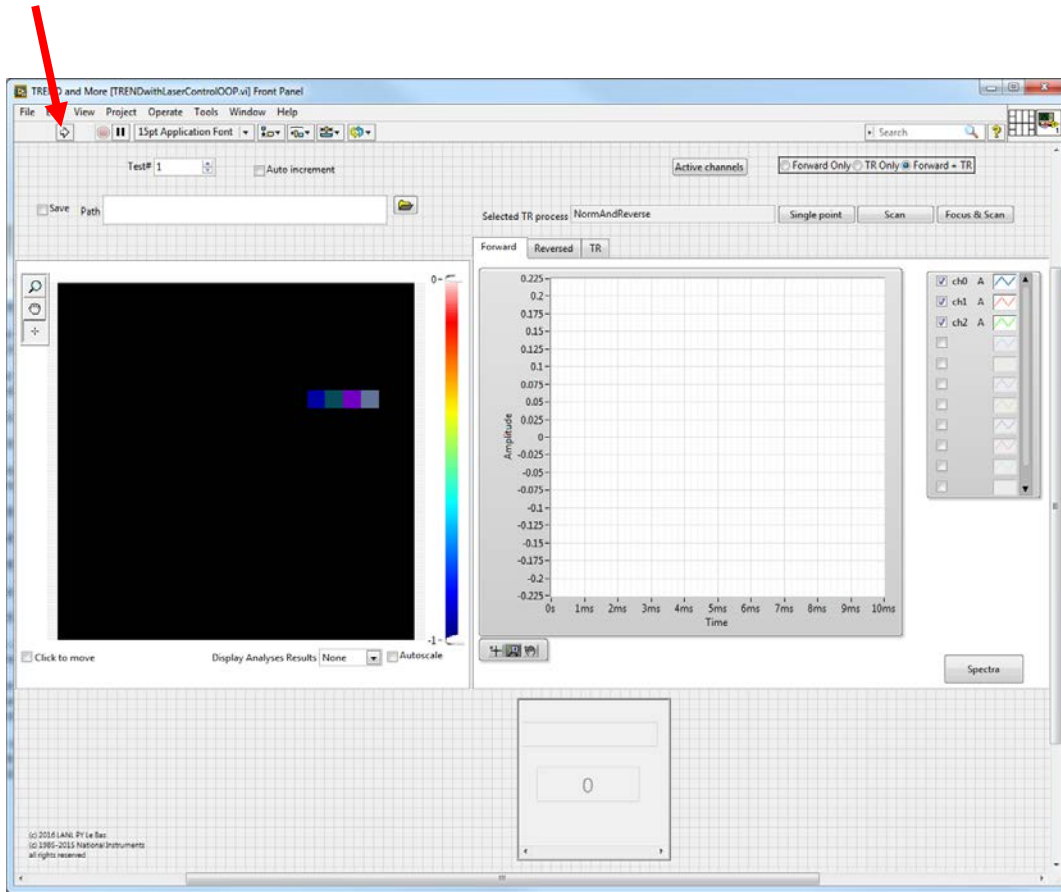
TREND is opened by double-clicking the following icon, hopefully on the desktop.



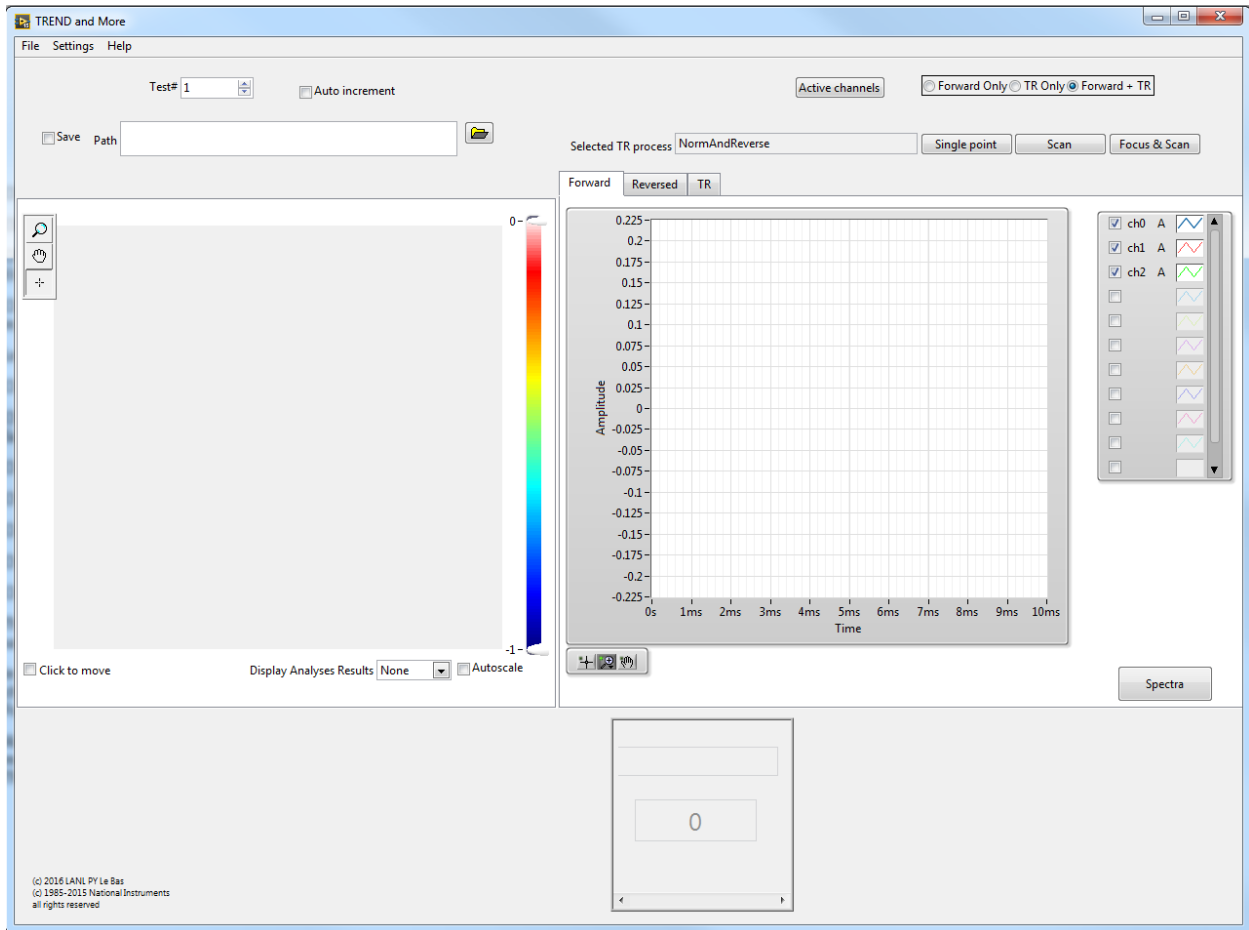
If it's not on the desktop, its root location on the NI Anderson Chassis (shown below) is C:\Users\CSR\Desktop\TREND\TREND\TRENDwithLaserControlOOP (the OOP means out-of-plane) and it can be opened from there.



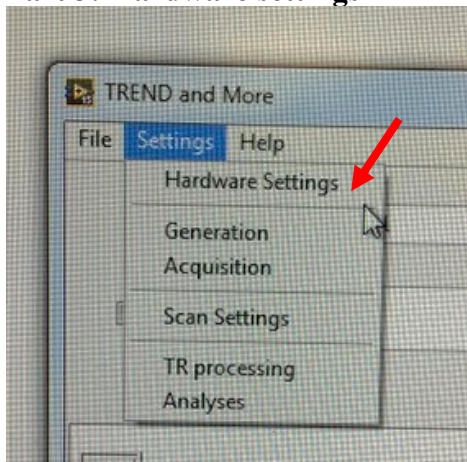
The software opens to a LabVIEW front panel. Click the ‘run’ button to run the vi, indicated by a red arrow in the picture below.



This opens the main TREND interface, shown below.

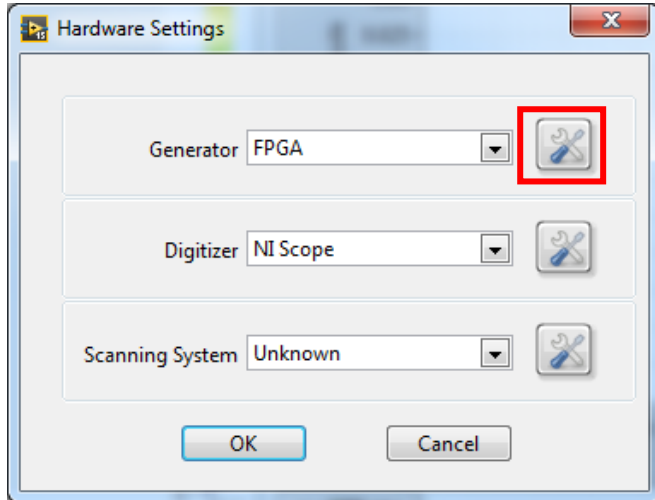


Part 3: Hardware settings

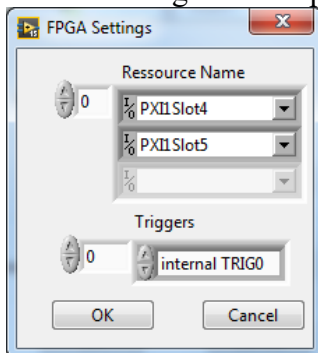


a) Generator

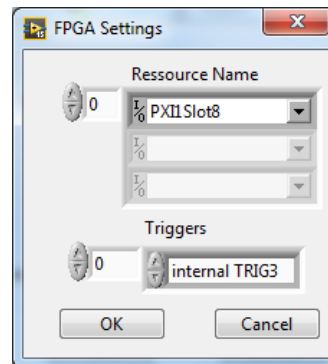
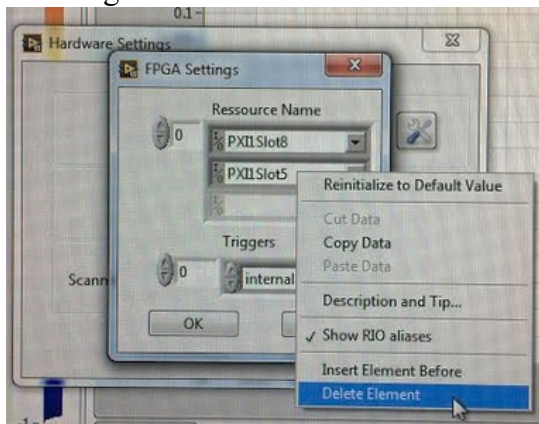
Under the Settings tab in the upper left, click on “Hardware Settings” and the following box will open. Under Generator, FPGA should be chosen (at the moment it’s the only option). Click on the box to the right with a wrench and screwdriver on it (outlined in red in figure below). In the future this button will be referred to as the WS button.



The following box will pop up.



Change the settings to those shown below. The PXI1Slot5 is removed by rt-clicking the box and selecting “Delete Element.”

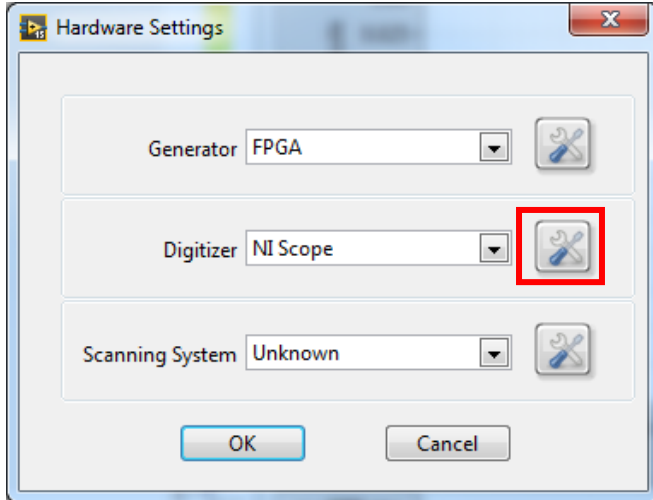


Recommended Settings

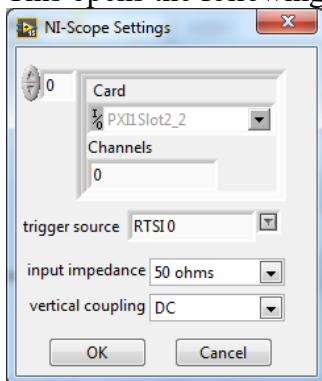
When you click “OK” it is normal for the system to take a few seconds here to get back to the Hardware Settings window.

b) Digitizer/Acquisition Card

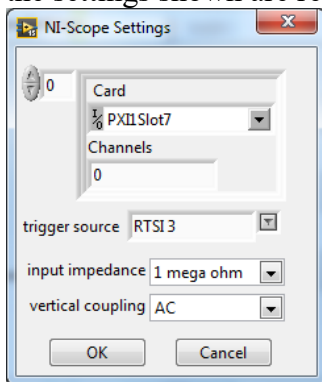
Back on the “Hardware Settings” screen select the Digitizer as “NI-Scope” (again, the only option) and click the WS button.



This opens the following window.



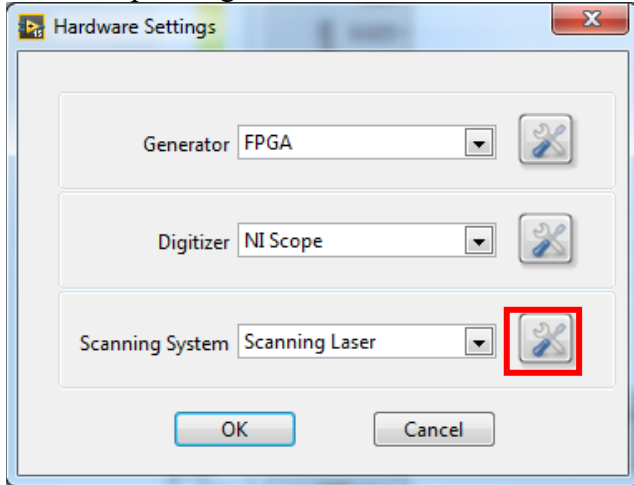
Change the settings to those shown just below. Under trigger source, the RTSI # must be the same as the number used in the FPGA Settings for “Triggers.” If “internal TRIG1” is used in FPGA Settings, “RTSI 1” must be used under trigger source in NI-Scope Settings. Most of the triggers have been tested but “internal TRIG3” and “RTSI 3” have been used extensively during testing. The input impedance and vertical coupling can be 50 ohms and DC, if implemented together, but the settings shown are recommended.



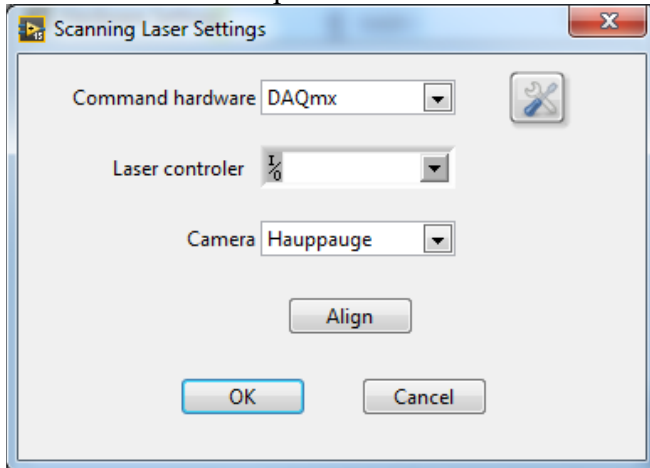
Recommended Settings

c) Scanning System

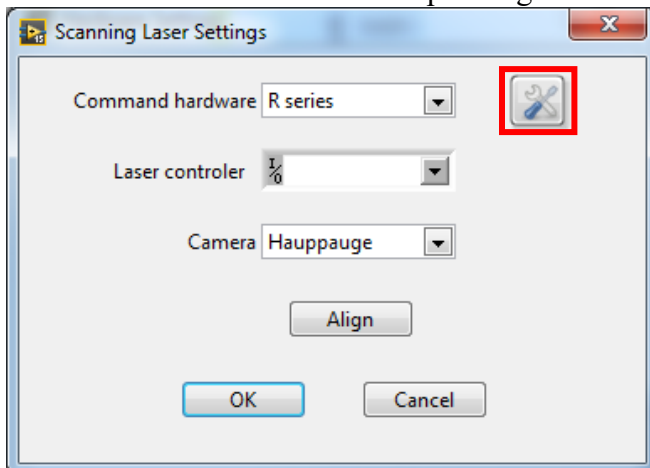
Back on the Hardware Settings window, select “Scanning Laser” under Scanning System and click the corresponding WS button.



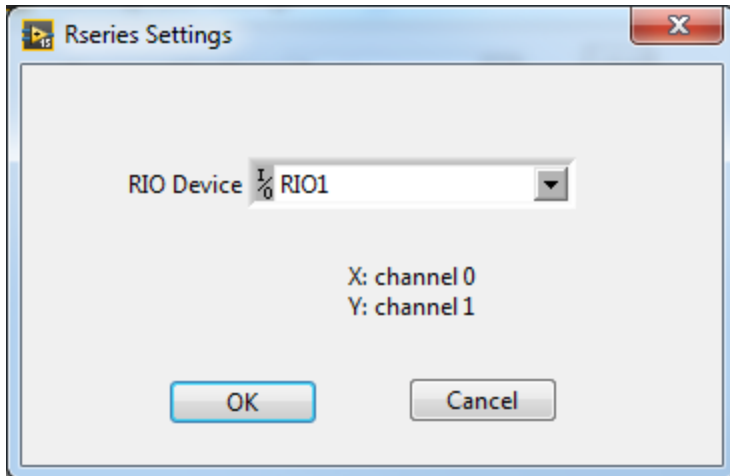
The initial window opened will look like this:



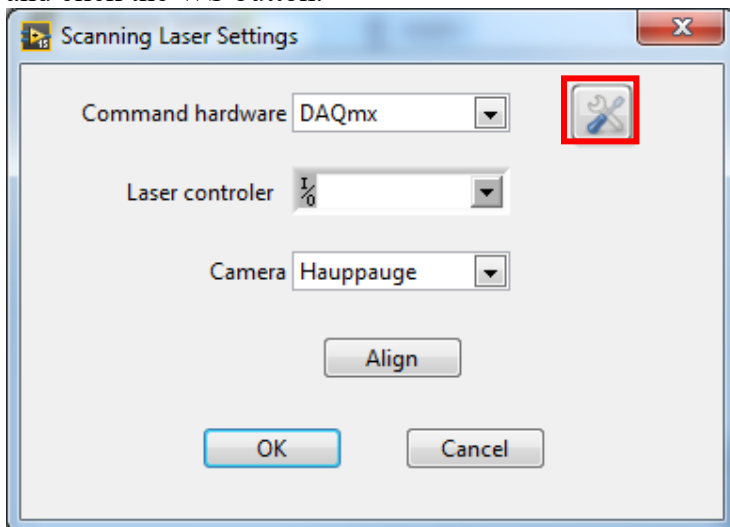
Technically, DAQmx is the Command hardware you want for laser mirror control, but it won't connect to the laser mirrors unless you follow some weird steps. First, change Command hardware to “R series” and click the corresponding WS button.



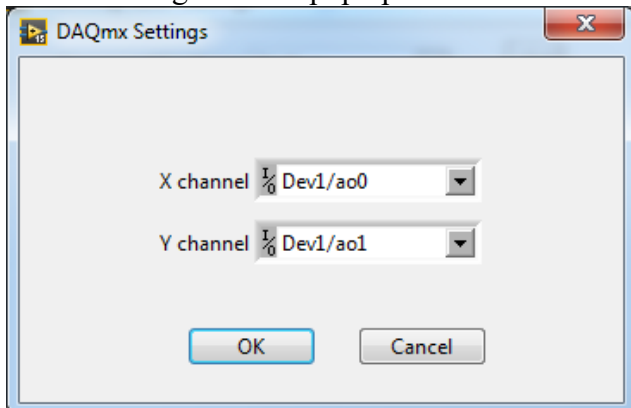
Make sure RIO1 is shown under RIO Device



Select “OK” until you’re back to the Hardware Settings window. Then select the WS button to get you back into the Scanning Laser Settings window. Change Command hardware back to DAQmx and click the WS button.



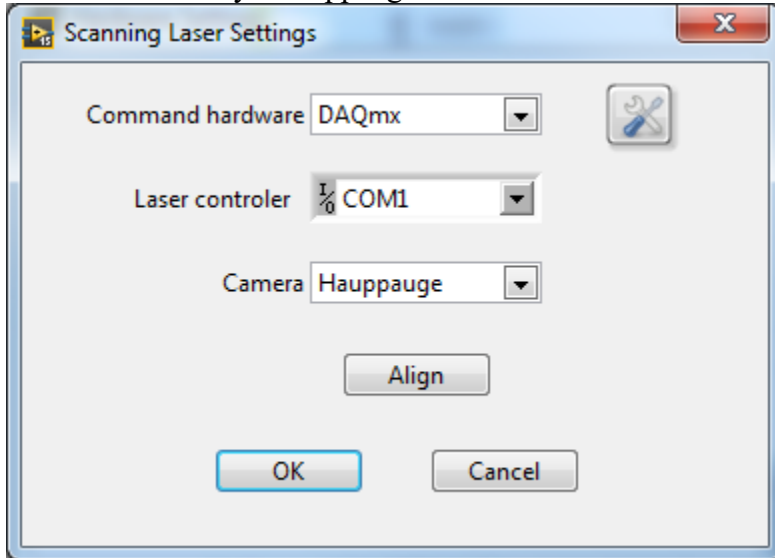
The following box will pop up. Use the down arrows to put in the settings shown.



If you don’t follow this process of selecting “R Series” first, when you try and open the WS button under DAQmx, you will get a message stating that there are no settings for this class and you will be unable to connect TREND to laser motion control.

Back in Scanning Laser Settings, click the down arrow under Laser Controller and set it to “COM1.” When you click this down arrow, it will take a few seconds for any options to come up. You’ll likely get the swirling blue circle and possibly a (Not Responding) message on the top of the dialogue box, but if you wait, everything will show up as expected and you can choose “COM1”

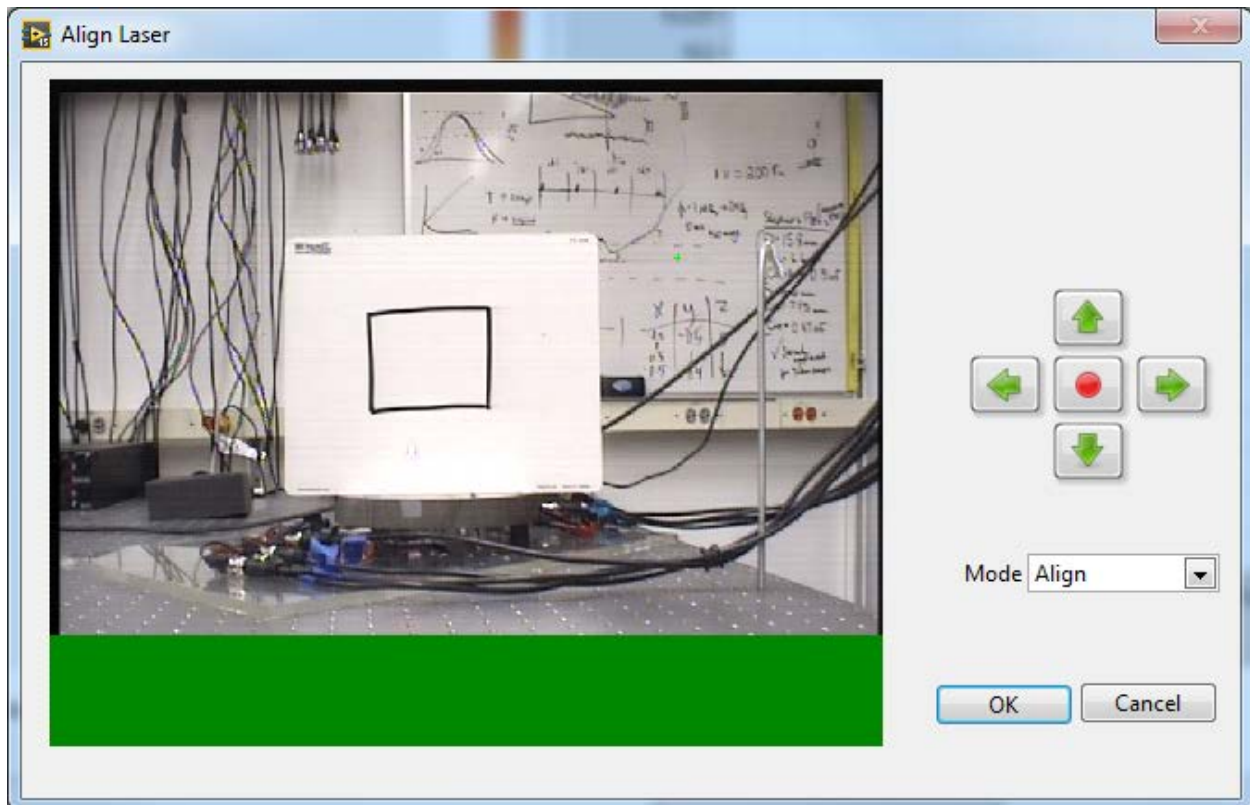
Camera should say “Hauppauge”



Recommended Settings
(after some
manipulation to get
there)

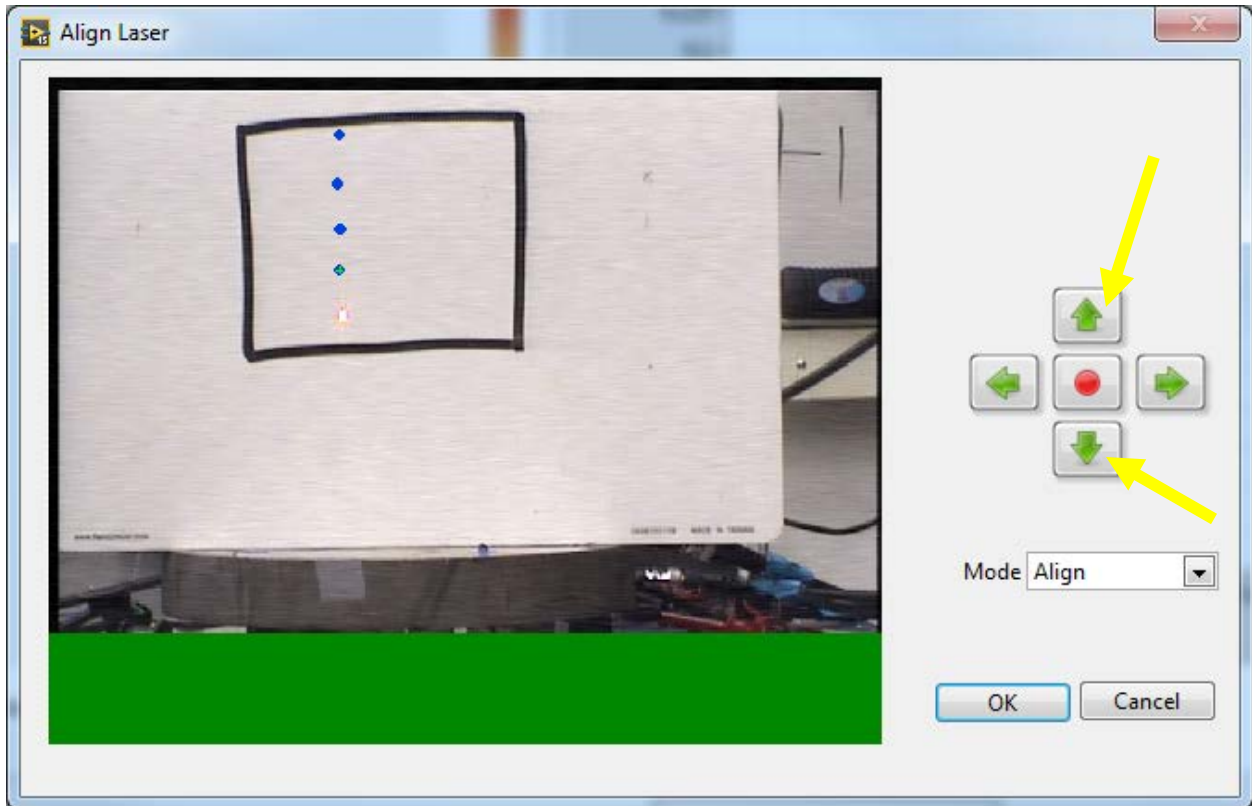
d) Laser Alignment

Click the “Align” button under Scanning Laser Settings (under Hardware Settings) and the following window will pop up. This is typically the first time the camera in the SLDV will send video of the setup to TREND, so don’t worry if it doesn’t show up before this point. If you’re not getting a video feed at all (cause sometimes it shows up in black and white and that’s fine), something in your cabling is off and you need to check all of your connections from the back of the Polytec Junction Box. The white board with a black box drawn on in the picture below is used for demonstration purposes.

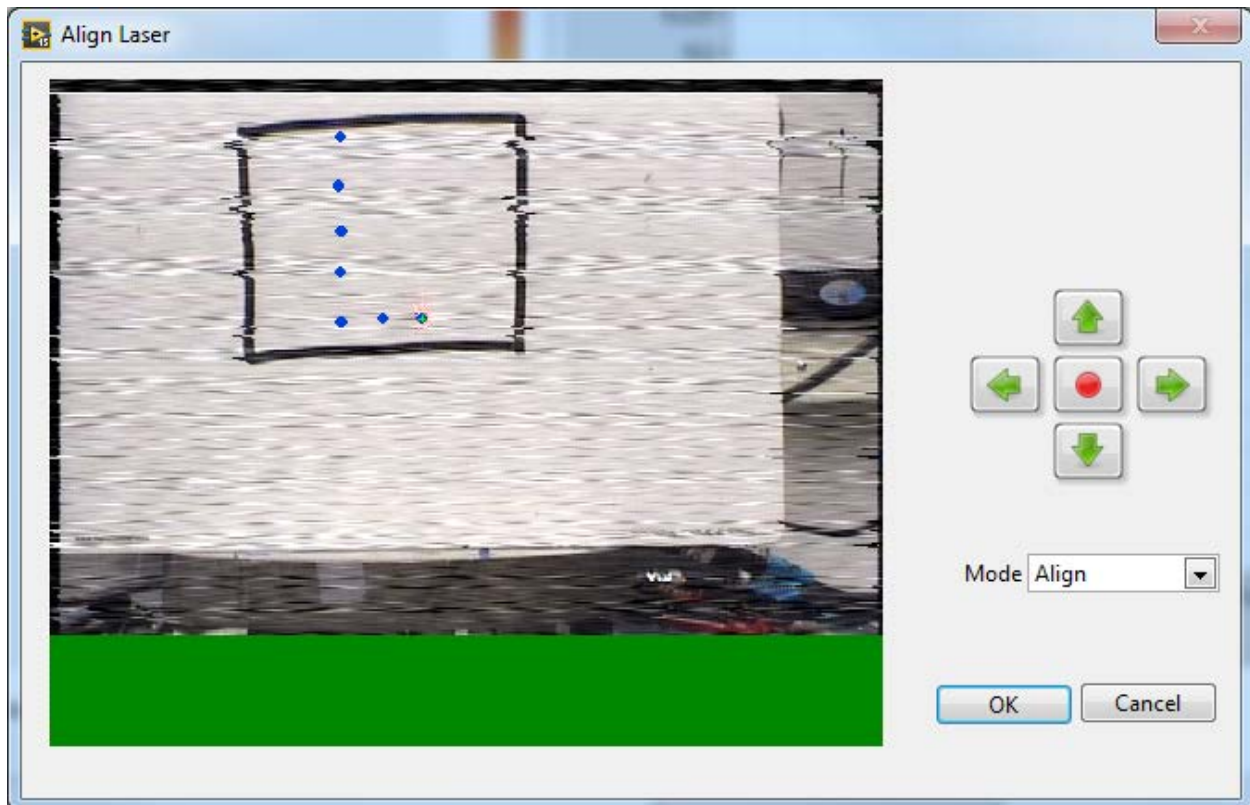


At this point I would suggest going to the Polytec computer and opening the PSV Acquisition software. This allows you to adjust the camera zoom, making the picture tighter around the sample and allowing you to be better able to visually select the laser location.

Using the up and down green arrow buttons to the right of the picture, pointed out with yellow arrows below, adjust the position of the laser on the sample vertically. When you want to align the laser to the sample shown in the picture, click on the picture in the exact position of the laser and a blue marker will show up where you clicked. Move the laser from this position and the blue marker will remain, allowing you to align the laser to another position.

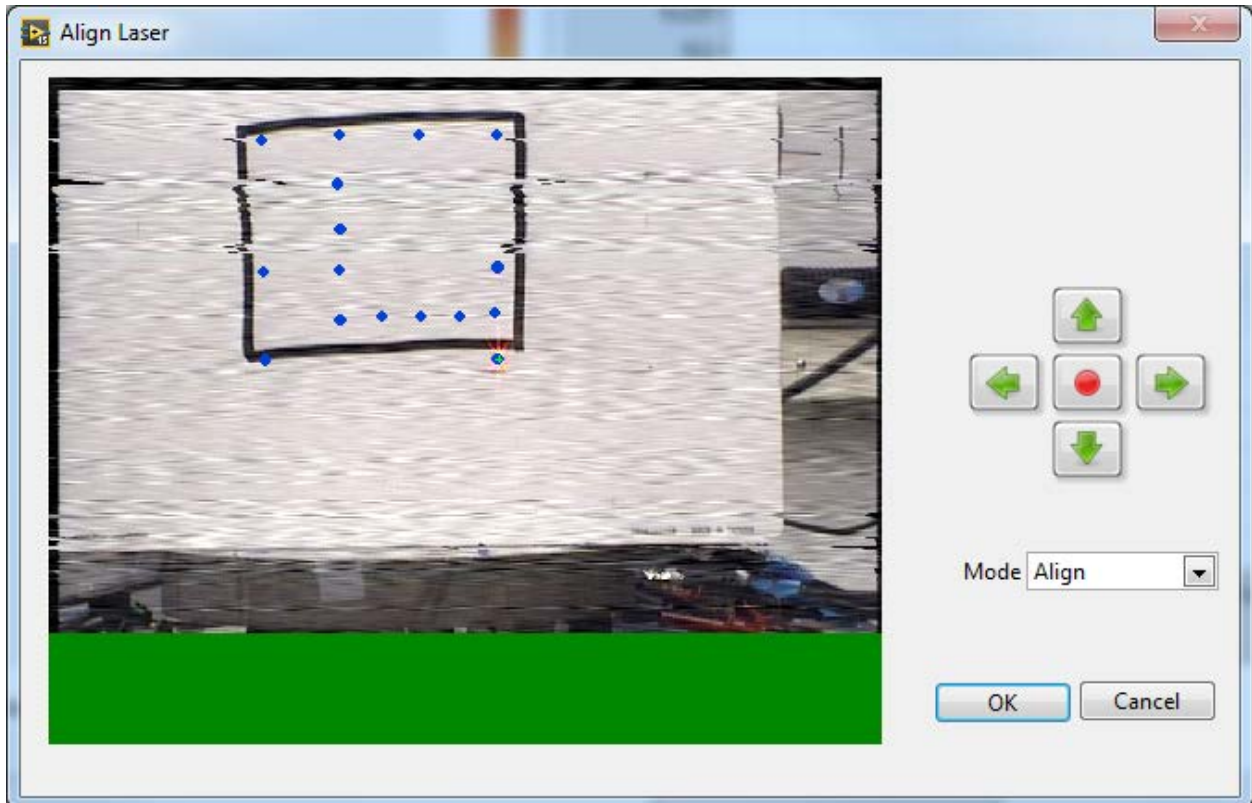


When moving horizontally with the green arrow buttons, the directions are coded incorrectly in the TREND software. The right-hand arrow moves the laser left, and the left-hand arrow moves the laser right. This may or may not be an easy fix by switching the x-direction wires into the DAQmx. Feel free to investigate.



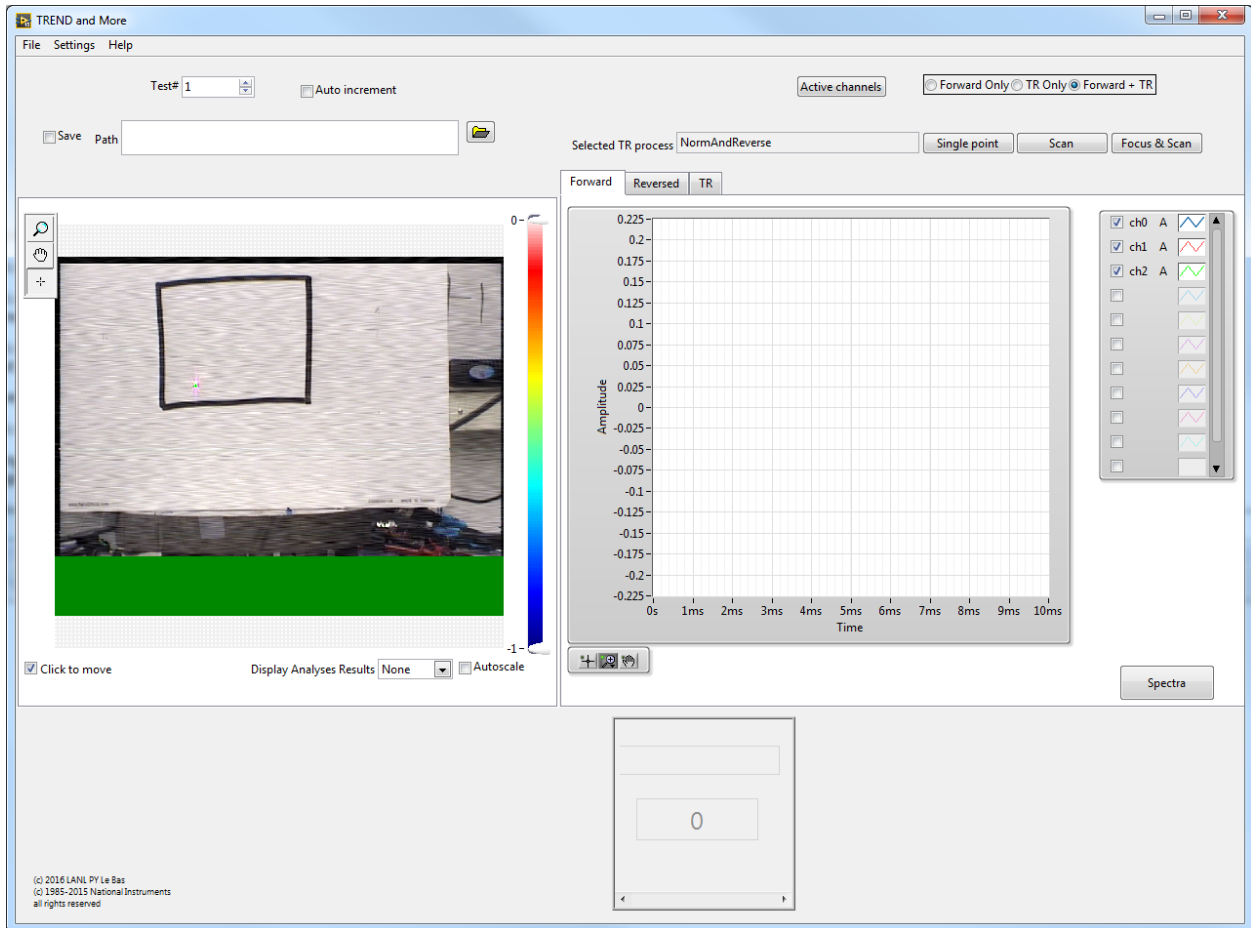
Make a smattering of alignment points across your sample, emphasizing the edges with a few points across the middle region. Flat surfaces are best.

You've probably noticed that in some of these figures, the video feed of the sample has deteriorated and become streaky. This is likely to occur when the optical laser strength is poor (i.e. the surface on which the laser is pointed is not very reflective or the laser focus is large). It is also not uncommon for the video feed to look granulated at all times. There's nothing you can do about this outside of switching out all possible cables, but even this doesn't appear to help much. Also, the green stripe across the bottom is normal and there's nothing you can do about it.

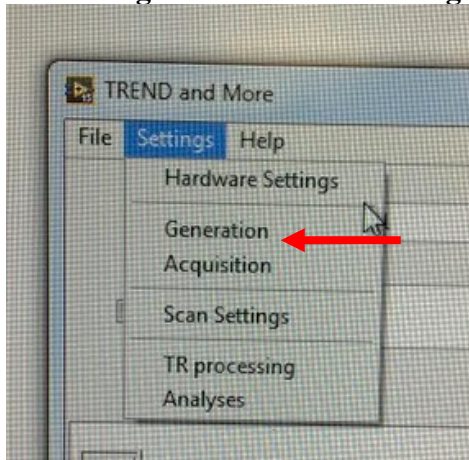


When you have finished aligning, click OK -> OK -> OK to accept all settings and exit Hardware settings.

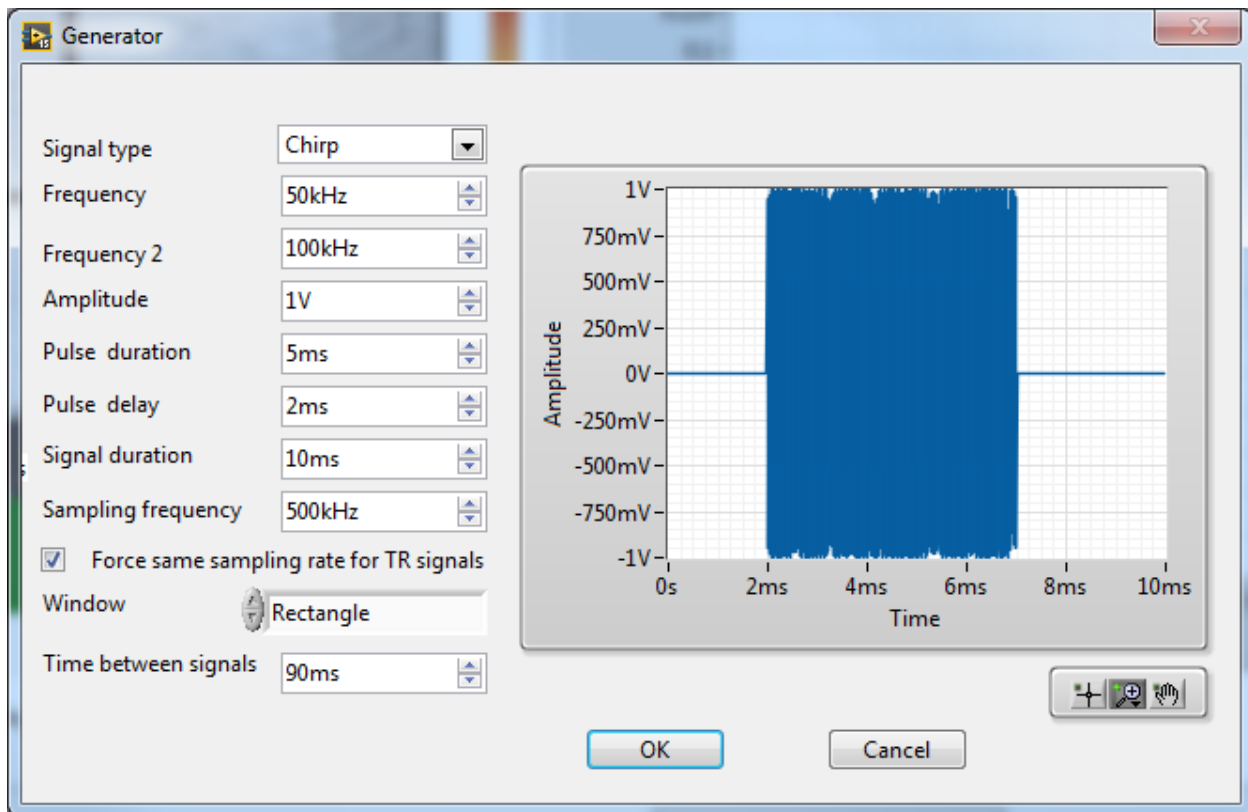
The video feed will now show up on the main TREND screen (shown below).



Part 4: Signal Generation Settings



If you go to Settings -> Generation the following window will appear



There are a whole range of possible signal types. For time reversal using a cross-correlation to compute an impulse response, a chirp is used.

Tip for entering info in these boxes: do not use the up-down arrows. They mess everything up. Just type in the desired values including units (the system will sometimes automatically translate your units. For example, if you type 0.003s it will turn into 3ms)

Frequency defines the chirp beginning frequency and *Frequency 2* defines the chirp end frequency. *Amplitude* is the output voltage at which the signal is generated (If you are using the Tabor amps, the limit is 3.9 V_{pk}. The NI PXI-7852R card limit is 10 V_{pk}). *Pulse duration* and *Pulse delay* are best understood in terms of *Signal duration*. *Signal duration* is the total time-length, or period, of the generated signal as well as the acquired signal. To allow time to collect signal reverberation and decay, the signal acquired must be longer than the chirp. Therefore, *Pulse duration* defines how long the chirp is within the total time of *Signal duration* and *Pulse delay* determines by how much time the chirp is delayed (and therefore how much time is left for signal to be acquired after the chirp is finished).

Pulse delay also determines the timing of the focus when it is generated and acquired. If, as in the above figure, the *Signal duration* is 10 ms and the *Pulse delay* is 2ms, the waves will focus at 8 ms in the acquired signal. If *Pulse delay* is 0 ms, the focus is generated at the very end of the acquisition window.

The generator *Sampling frequency* can only be 500 kHz. We are not sure if this is a limitation of the software or the acquisition card. If a sampling frequency is used other than 500 kHz, a focus isn't generated. Something about the timing is off.

In addition, the 8-channel generator card (NI PXI-7852R) is purported to have an onboard memory limit of 8192 points. This means that the signal generated must be shorter than 8192 points. Because the *Sampling frequency* must be 500 kHz, the longest possible *Signal duration* is 16.3 ms.

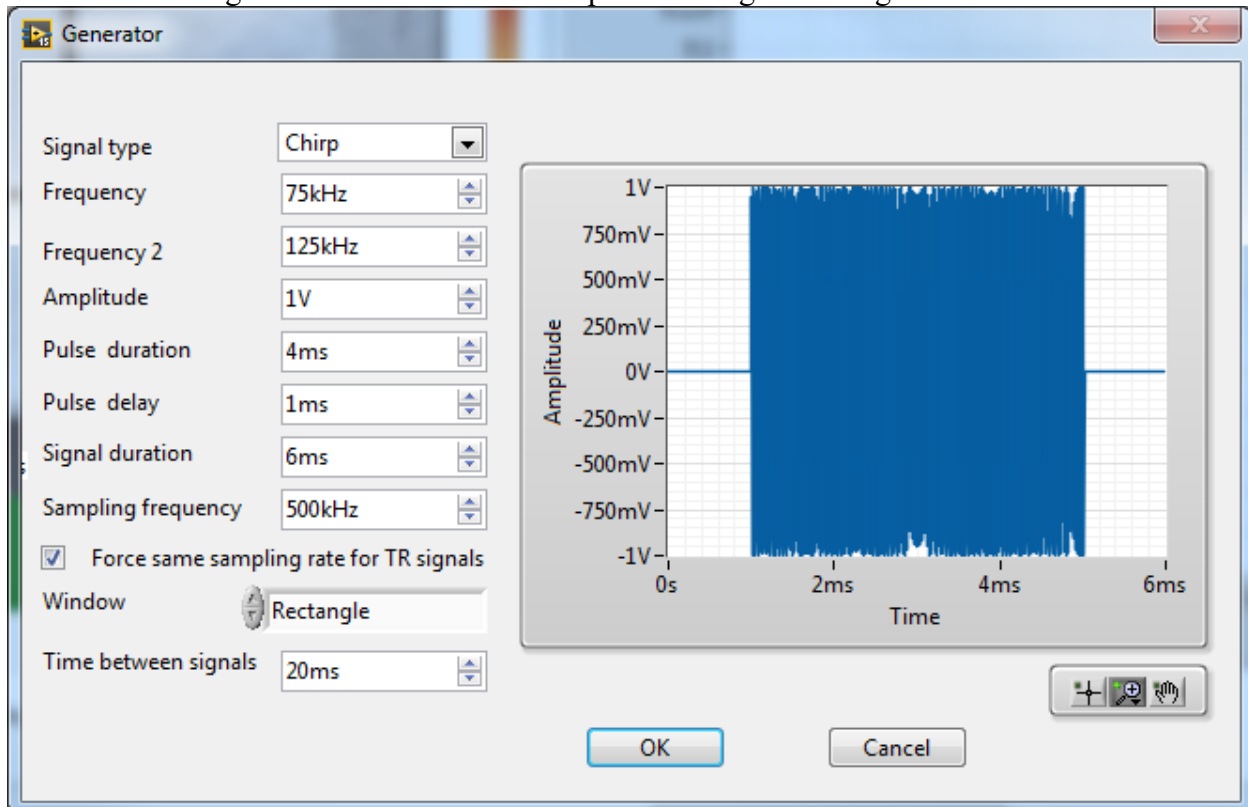
$$T_{max} = 8192 \text{ pts}/500\text{kHz} = 0.0163 \text{ s}.$$

Keep the “Force same sampling rate for TR signals” box checked. This means that when the reversed impulse response is generated, it will be generated with the same sampling frequency of 500 kHz, irrespective of what the chirp response or impulse response was acquired at. This will require either upsampling or downsampling unless the acquisition sampling frequency is also 500 kHz.

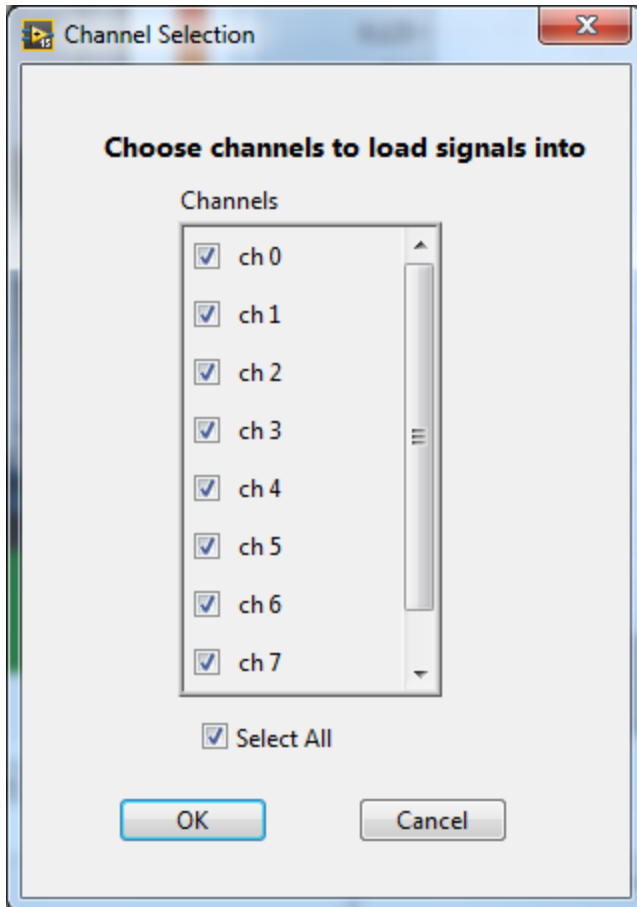
Window needn't be changed unless a different signal type is used.

Time between signals is how long the system waits between every average. This allows any extra reverberation to die down before a new signal is introduced.

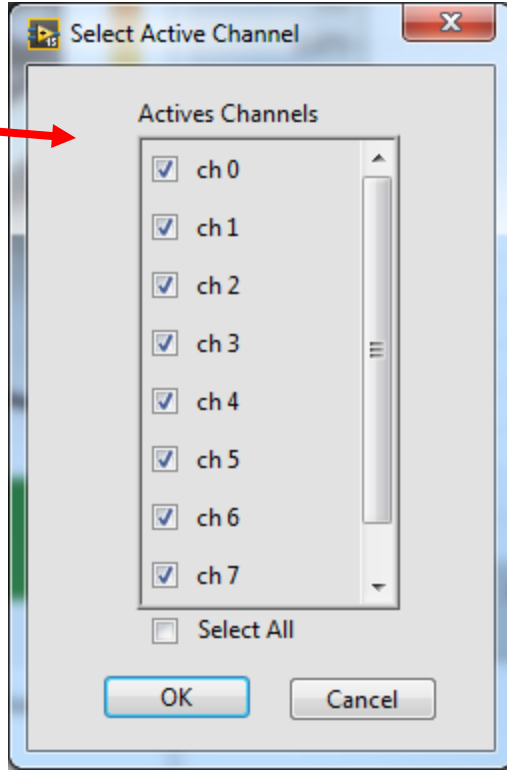
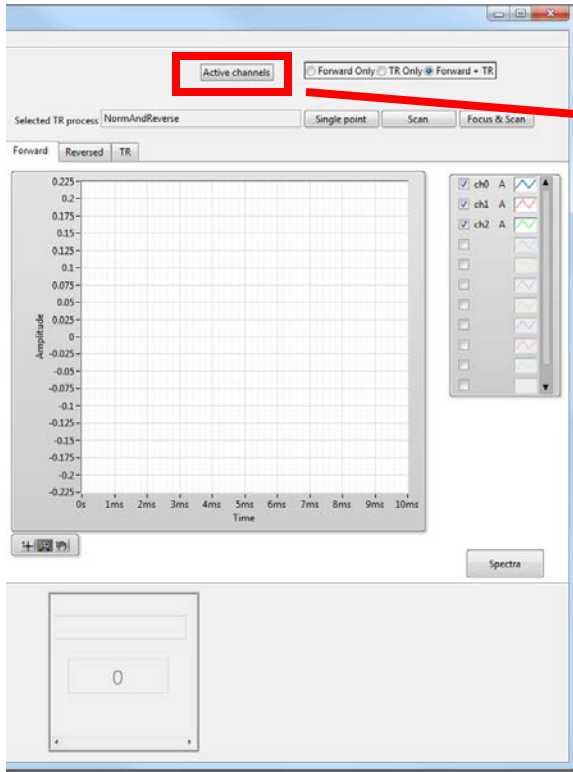
While the Generator settings shown in the figure above are functional as is, they can be adjusted as needed. The figure below shows one example of settings used to great success.



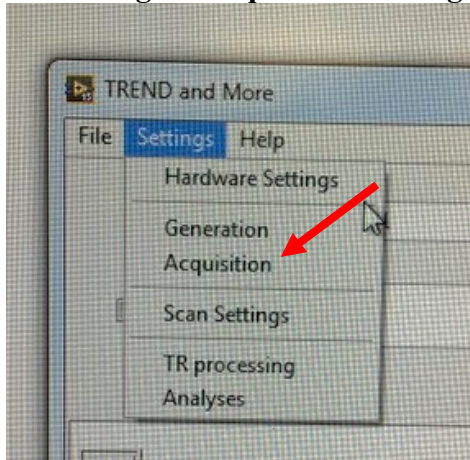
After you hit “OK” on the Generator window, the following box pops up, asking you how many generator channels you are using. You cannot have more than 8 channels (through ch 7).



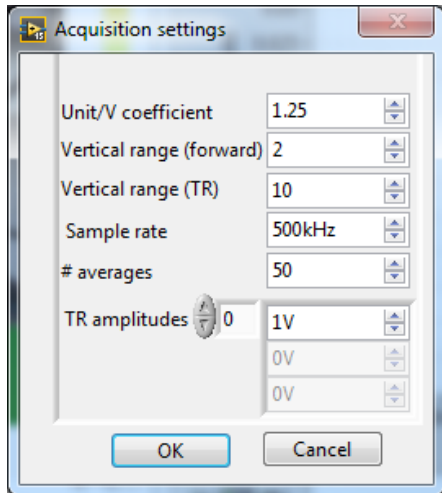
This information must also be specified under the “Active channels” button on the main TREND screen (upper right). When clicked, this button opens the window below showing which generator channels are in use. All 8 channels are active unless otherwise specified in this window. If all 8 channels are left as active but not all of those channels are actually generating a signal, an acquisition slot still exists where the generated signal would have existed and noise is recorded. While this ultimately does not harm the focus, it takes up a lot of unnecessary extra time if not all 8 channels are in use. The “Active channels” feature supersedes the channels specified in the “channel selection” window that pops up after the Generator window. Even if you deselect channels in “channel selection,” they will still be in use unless deselected in “Active channels.”



Part 5: Signal Acquisition Settings



By clicking Settings -> Acquisition the following window will appear. These settings govern how signals are acquired from the constant analog feed from the SLDV.



Tip for entering info in these boxes: do not use the up-down arrows. They mess everything up. Just type in the desired values including units (the system will sometimes automatically translate your units. For example, if you type 0.25V it will turn it into 250mV)

Unit/V coefficient is a factor that scales the acquired signal. We want to collect Volts so set this to 1.

Vertical range (forward) is the dynamic range allowed for the collected forward signal (the chirp). This is specified as roughly a peak-to-peak value in Volts so the 2 V shown really means you can collect amplitudes up to about 1 V_{pk}. Don't rely on it being peak-to-peak though. It could be slightly less or more.

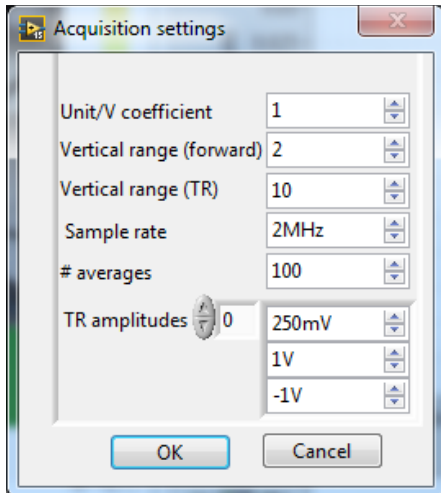
Vertical range (TR) is the dynamic range for the focus signal. Often the focus has a much higher amplitude than the chirp, so a higher voltage limit is required. The value shown here may or may not be roughly peak-to-peak. For example, a 10 V vertical range shown here means the acquisition voltage limit is about 5.5 V. A 15 V vertical range allows data to be collected up to about 11 V. The documented limit of the NI PXIe-5122 Digitizer card is 10 V_{pk}.

Sample rate specifies the acquisition sampling rate. This can be set to any number without the system behaving strangely (different from the generator sampling rate).

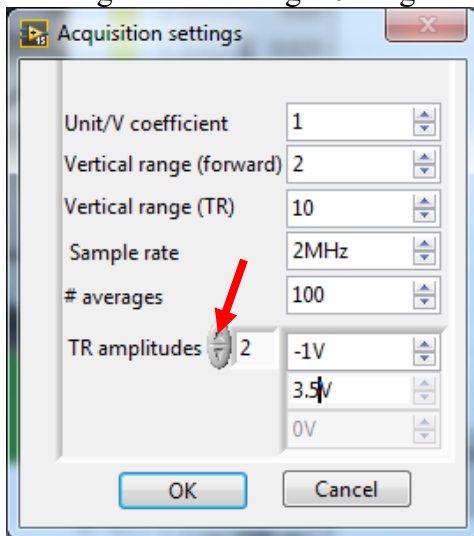
averages is the number of times the generated signal will be emitted and corresponding data acquired, the values of which will be averaged.

TR amplitudes is actually a generator command. After the impulse response is collected, the reversed impulse response must be emitted and this option allows you to emit the reversed impulse response at a variety of voltage levels (emitted/acquired in the order you specify).

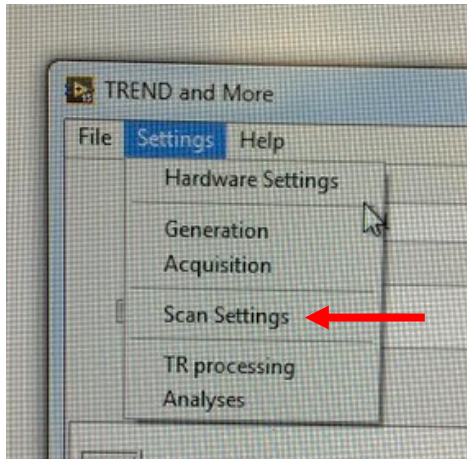
Shown below are some sample settings and 3 TR amplitudes: 0.25V, 1V, and -1V. TREND allows you to set negative voltages, which just switches the emitted signal phase by 180°.



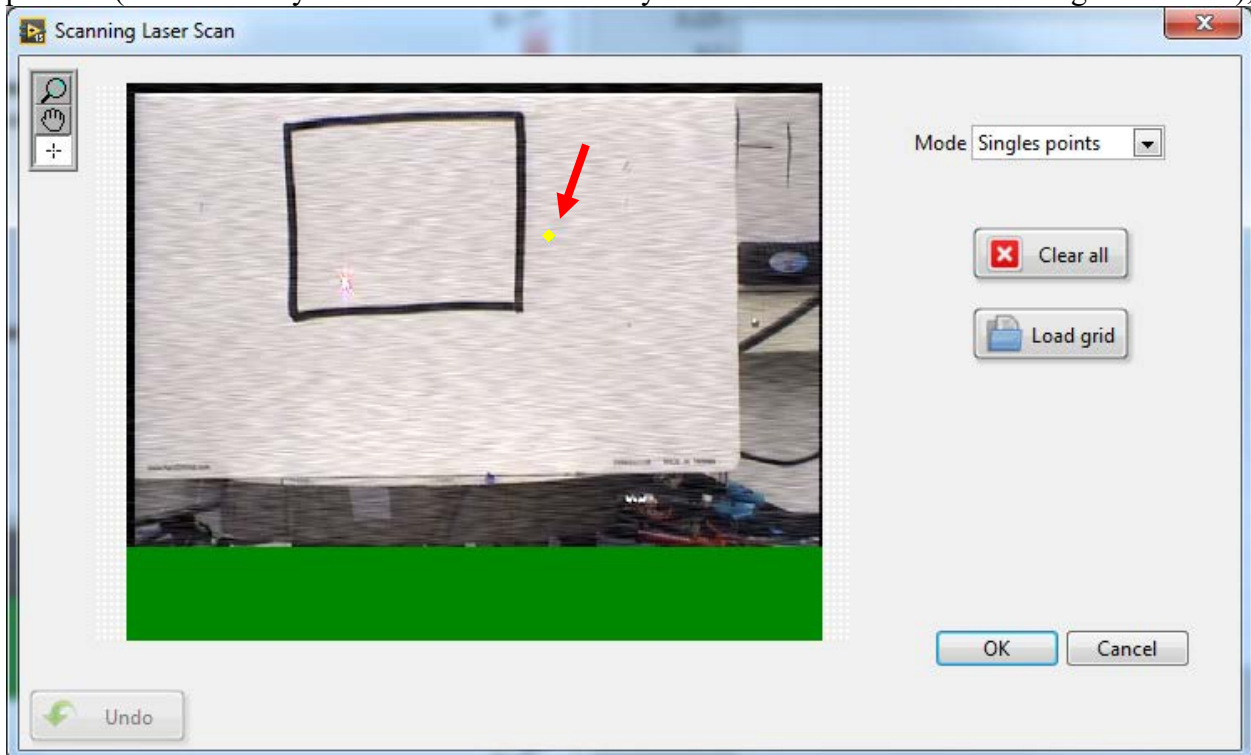
If you click the up arrow next to *TR amplitudes* (pointed out with red arrow in figure below) more voltage input slots are shown. As far as I am aware, there is no limit to the number of voltages you can input. If you wish to remove one of the input voltages, rt-click the box and click “Delete element.” The box must be faded out for it to not be used. Even if it says 0V, time will be spent emitting and collecting a 0V signal if it’s not faded out.



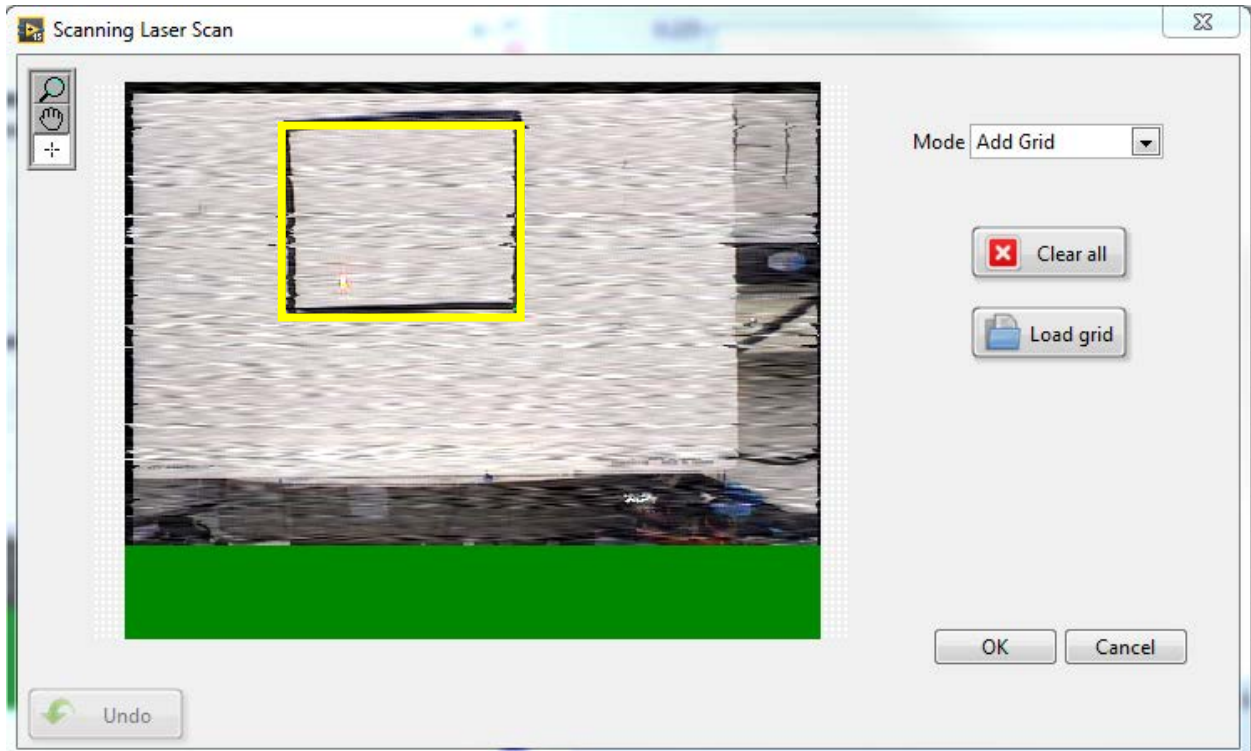
Part 6: Specifying Scan Points



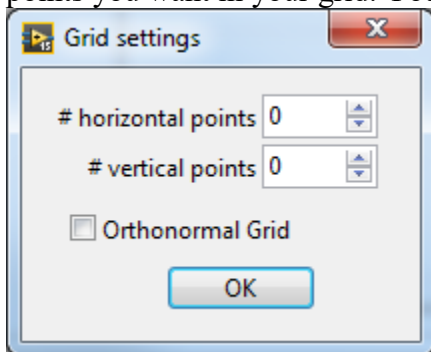
Under Settings -> Scan Settings the following box emerges which allows you to specify which points you want scanned (What is meant by the word “scan” will be discussed in Part 9: Acquiring Data). Scan points can be created two different ways: by clicking on the picture to set individual points (the small yellow dot indicated by the red arrow in the figure below),



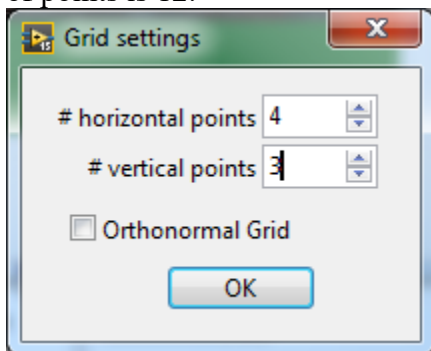
Or by changing the Mode to “Add Grid” and drawing a rectangular box over the region you want to scan (it’s not actually yellow, it’s a black square, but you can’t see that in the picture).



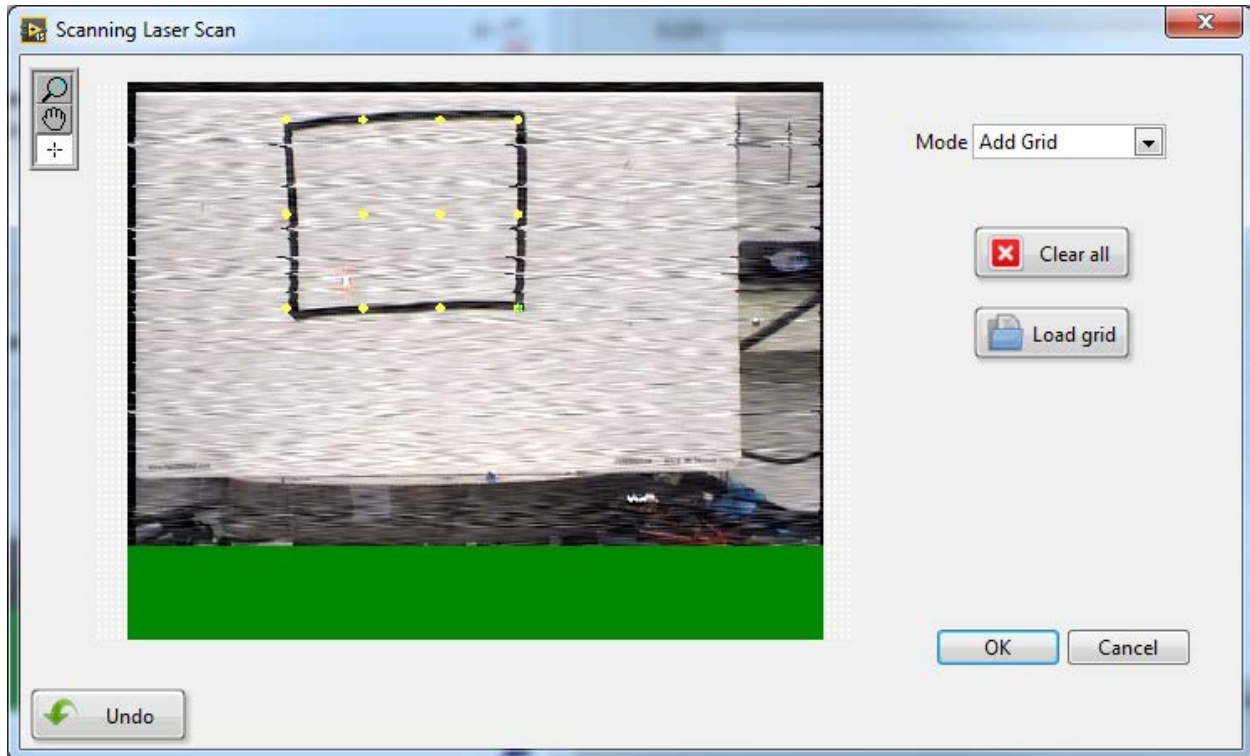
After drawing the rectangular box, the following small window will pop up, asking how many points you want in your grid. You can only specify a rectangular grid.



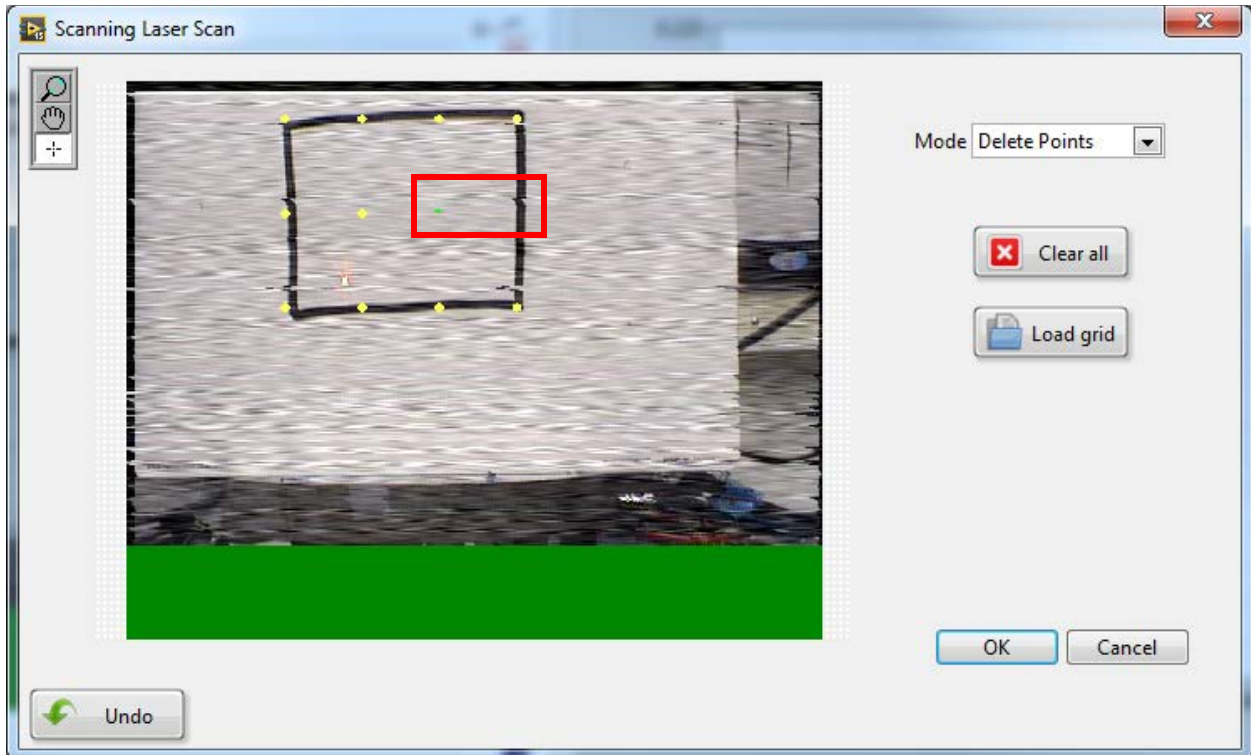
If you select “Orthonormal Grid” the grid region you selected will restructure itself to become a square with the specified number of points per dimension. The total number of scan points is the number of horizontal points times the number of vertical points. In the case below, the total number of points is 12.



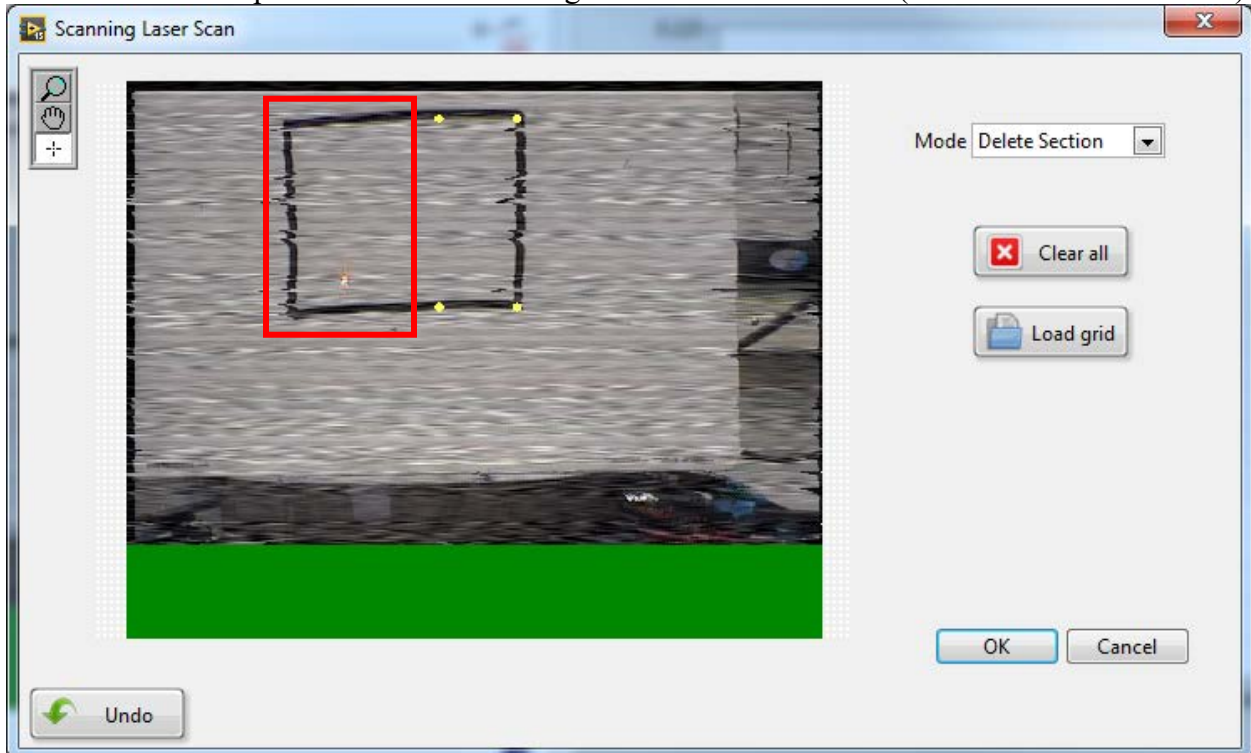
After you specify the number of points, the scan grid is arranged in yellow dots in the rectangle you drew such that points always exist on the perimeter and middle points are spaced evenly in between.



By changing the Mode to “Delete Points” you can click on a single scan point and it will be deleted. Two points have been deleted in the figure below. The region where they existed is outlined in a red box.



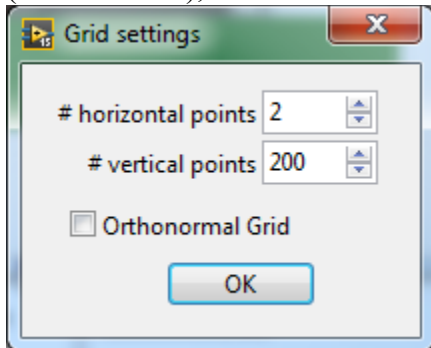
By changing the Mode to “Delete Section” you can draw a box around an entire region of points and all of the points within that region will be deleted (outlined in red below).



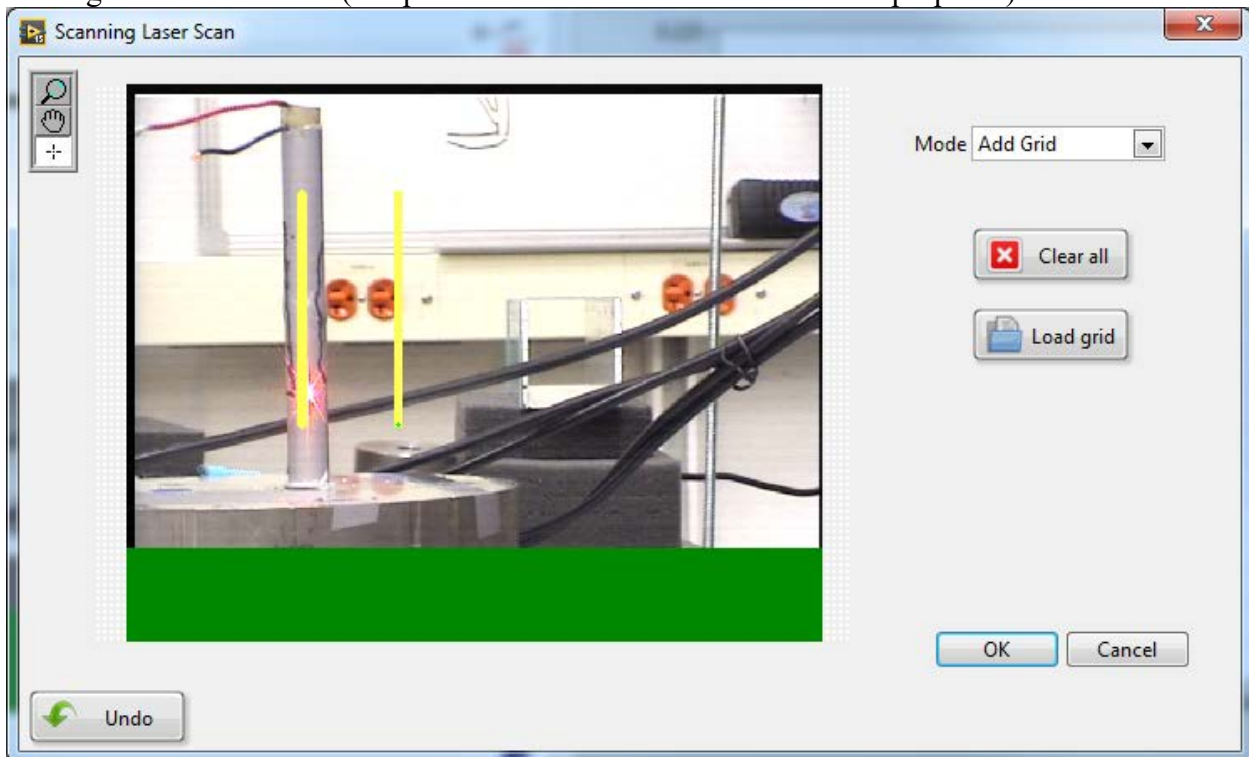
To select the “Clear all” button removes all points in the grid. Selecting “Undo” does exactly what you’d expect (although you might only be allowed 1 undo). How to successfully use the “Load

grid” feature is described in Part 12 of this document because it is a complicated process that involves multiple software features that have yet to be described.

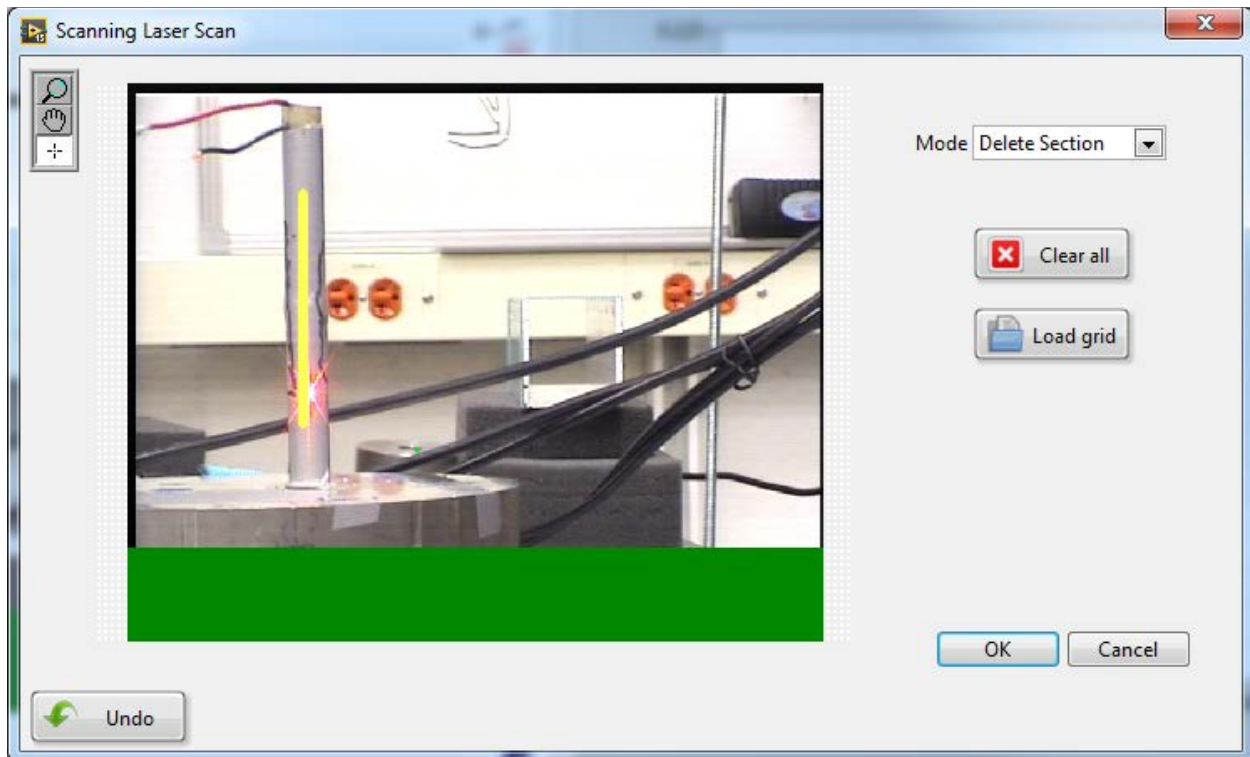
If you are trying to specify a scan line of points, you have to cheat the software. If you put in 1 for either the horizontal or vertical points, no grid will show up. You have to put in 2 in that dimension (shown below),



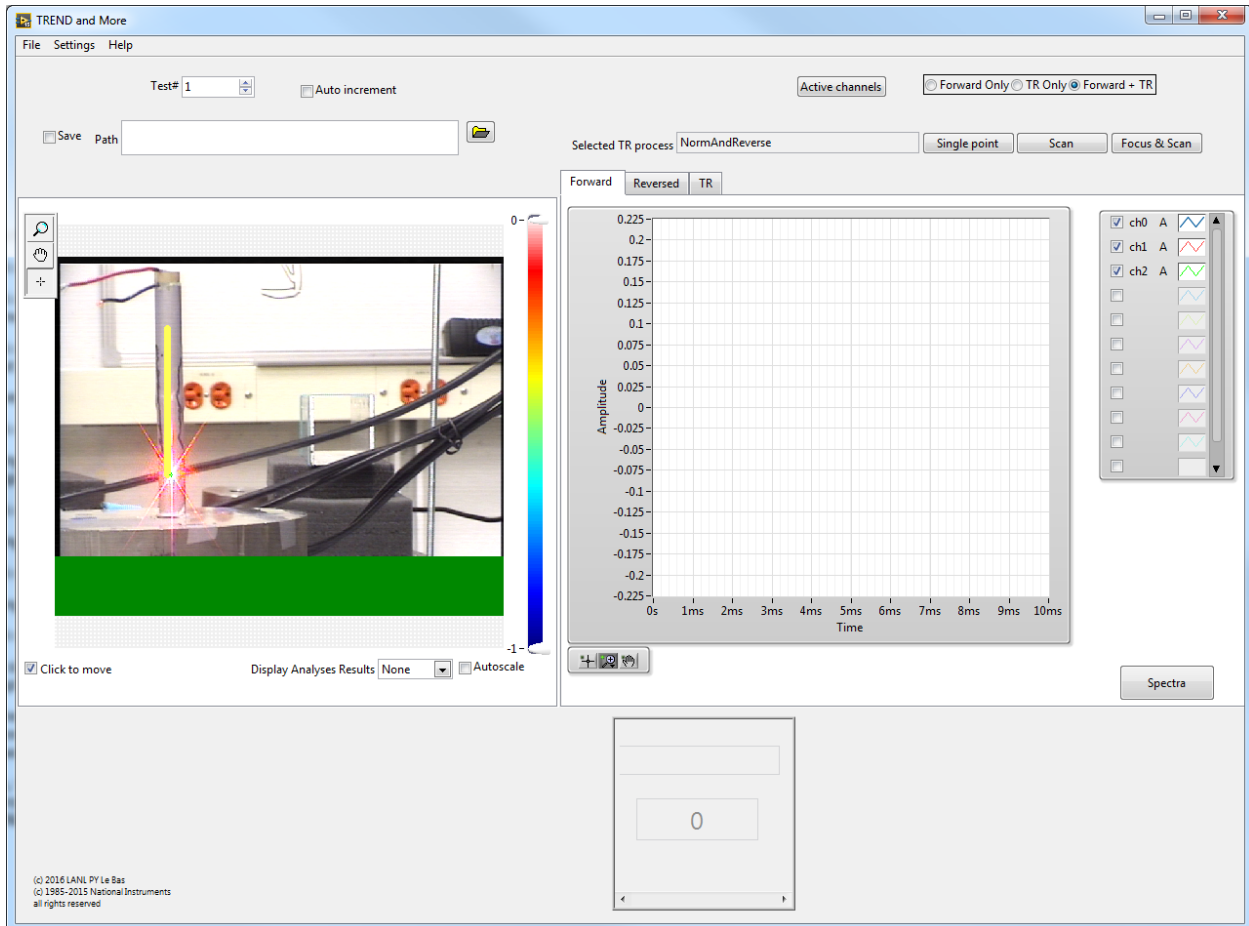
Getting an extra scan line (sample has been switched for educational purposes).



Then the extra scan line must be deleted by using the “Delete Section” Mode.

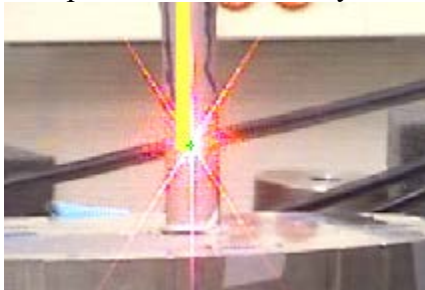


Once you click “OK” and return to the main TREND screen, the grid points will show up on the video feed. And useful tidbit: on the main TREND screen there’s a little box under the video feed with the label “Click to move.” Checking that box allows you to click on the picture and move the laser to where you clicked. This allows you to check how good your alignment actually is. If you only aligned the laser in the vertical direction (like in the case below), it will not move horizontally. Also, you cannot ever click on individual scan points or even the entire grid. That feature simply does not exist. Sorry.

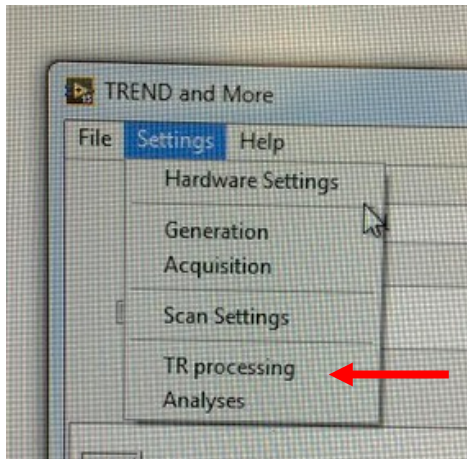


Last word about defining a grid or scan points: The placement of your grid/scan points is only as good as your alignment and visual identification on the video feed. If your alignment is off, the picture of your sample doesn't correspond to where the laser actually goes so your scan points are off. Also, there is nothing tying the scan points to any physical location on the sample, nor is there any spatial scan point resolution defined. If you want a specific spatial resolution, you must know exactly where the scan will start and end on the sample and be able to clearly note those locations in the video feed.

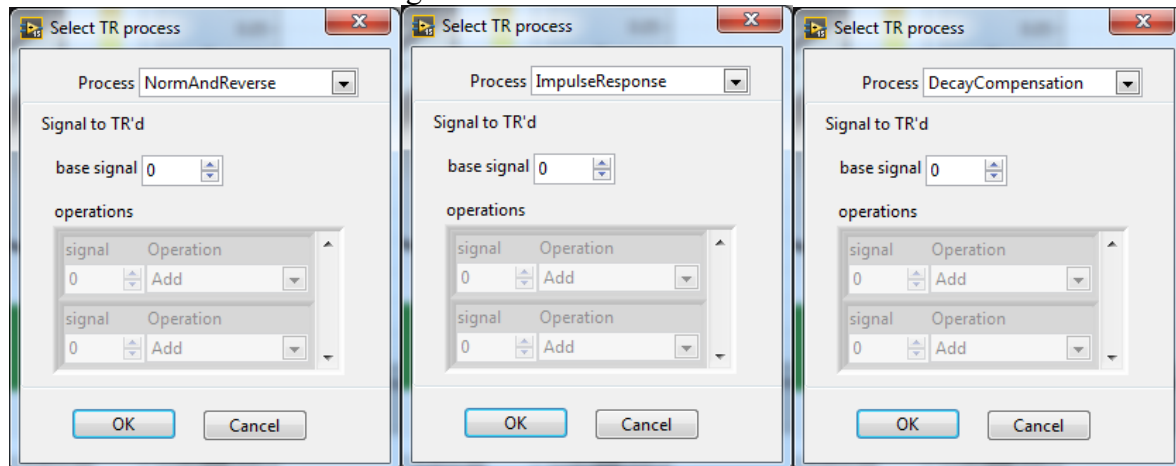
In the picture below, the scan points are vertical, the laser line is vertical relative to the positioning of the laser head, and the bar is approximately vertical, sort-of. This means that the laser point near the bottom of the rod is not exactly on the grid points, but just adjacent to them. The scan points cannot be shifted without redrawing an entire line, and the sample can't be shifted without realigning the laser, so best practice here would be to note on the sample the actual beginning and start points of the scan so you know exactly where the scan was.



Part 7: TR Process



Under Settings -> TR Process you can select which style of time reversal you are implementing, meaning how the impulse response is collected and processed. The automatic setting is “NormAndReverse” which implies that a pulse, NOT a chirp, is generated, and this signal is merely reversed in time and emitted to generate a focus.



“ImpulseResponse” uses a chirp excitation which is then cross-correlated with the chirp response to find the impulse response. The calculated impulse response is reversed and emitted to generate a focus.

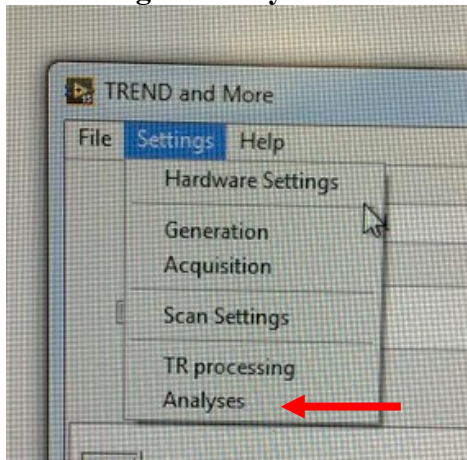
“DecayCompensation” uses a chirp excitation which is then cross-correlated with the chirp response to find the impulse response. The impulse response amplitude is then manipulated (according to the process defined in Sarah M. Young’s Masters Thesis, Chapter 3.4). The threshold hard-coded is 0.02. The Process listed as “DecayCompensation_unofficial” is a version of the Decay Compensation vi that works but was saved for future code manipulation. It can be deleted from the code if desired. The vi’s that define these processes are found in the folder “TR Processes” under the main TREND folder

“Deconvolution” (not shown here) uses a chirp excitation which is then cross-correlated with the chirp response to find the impulse response. An inverse filter is applied before the signal is time-reversed and emitted.

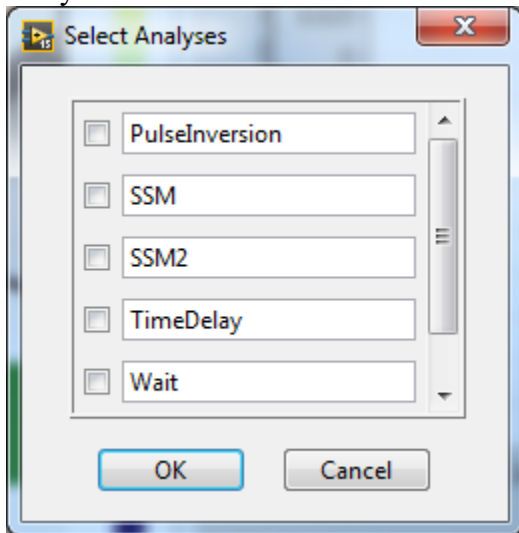
Other Processes include “ImpulseResponseAndFilter” and “NormAndReverseDesample” but it is unknown what they do.

The *Signal to TR'd* section has never been used successfully. Previous blind attempts made the software crash.

Part 8: Signal Analysis

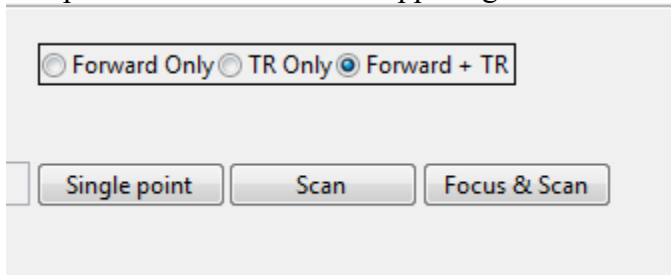


Under Settings is another option called “Analysis.” This opens a window, shown below, with a number of different pre-coded analyses, the results of which can be viewed on the main TREND screen (that’s what the colorbar is for) and saved. However, it is unknown what each of these analyses precisely entails without examining the TREND code in detail. To date, none of these analyses have been utilized in BYU research.



Part 9: Acquiring Data

The picture below shows the upper right corner of the TREND main screen



a) Forward Only, TR Only, Forward + TR

Forward Only: if this option is highlighted only the forward signals will be emitted and their responses collected (chirp or pulse)

TR Only: use of this option requires a forward step to be either loaded from data taken elsewhere or from a previously collected forward step. It will only generate a focus if the forward data was taken at the exact same location.

Forward + TR: this option means a new impulse response will be collected (or 8 impulse responses, depending on the number of active generator channels), and a single focus. This option is automatically selected.

b) Single Point, Scan, Focus & Scan

Single Point: clicking this button starts a data acquisition process where signals are simultaneously generated and acquired. Data will be acquired according to one of the three options selected above. Data will be collected at the location where the laser is pointed. Data collection with this button does not require laser motion control.

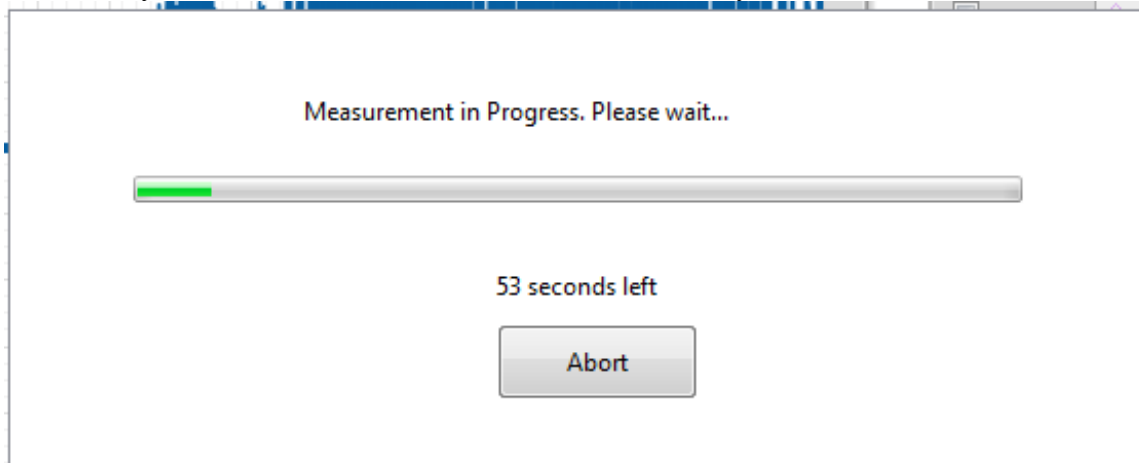
Scan: clicking this button starts a data acquisition process where signals are simultaneously generated and acquired. Scan points must be defined and laser motion control enabled for this to work. At a single scan point, an impulse response (or 8 impulse responses, depending on active channels), is collected, processed and focused. This entire time reversal sequence (collection of impulse response and generation of focus), is repeated at each scan point. The scan starts in the upper left corner and moves right. After completing a row it jumps to the left side of the next row down and continues. For a single vertical line, the scan starts at the top and moves down.

Focus & Scan: clicking this button starts a data acquisition process where signals are simultaneously generated and acquired. With this process, a single point is chosen (either the current laser location, or you specify a location in a dialogue box that pops up) and a focus is generated at that location. With the focus at that location generated repeatedly, the laser jumps to and acquires the velocity at the other scan points, measuring the field at scan locations other than the focus. The location specified for the focus will not be scanned as one of the official scan points, so it would be good to remember or specify where this is before the scan is run.

c) Data Collection

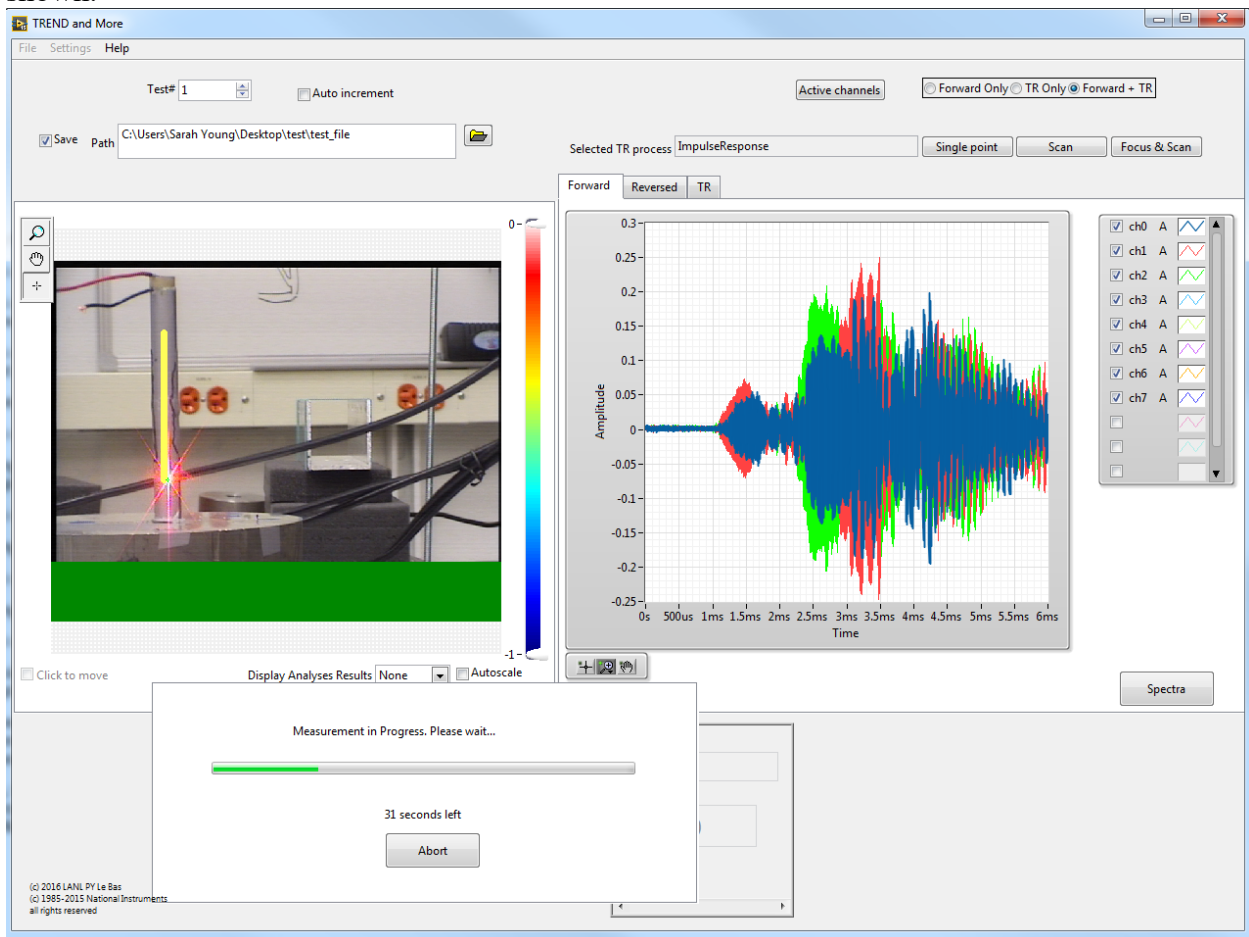
When data collection has started, the following window will pop up and stay until the entire collection process has finished. The remaining time specified above the “Abort” button is fairly accurate. The longer the measurement, the less accurate it becomes.

Incidentally, do not be afraid to Abort the measurement if you need to. The software will not break.

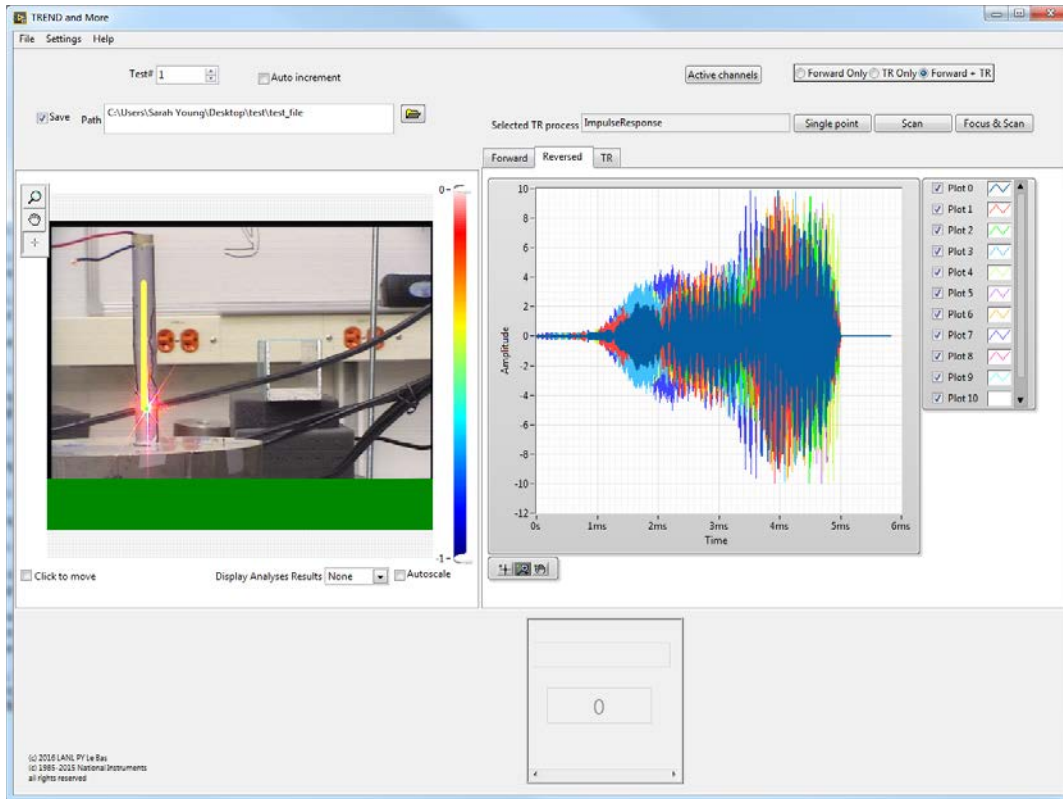


The figure below shows what the entire TREND main screen looks like during data collection. During a scan, the video feed is frozen from the moment the scan is started. So the laser is probably moving as instructed, you just won't see it on the TREND screen.

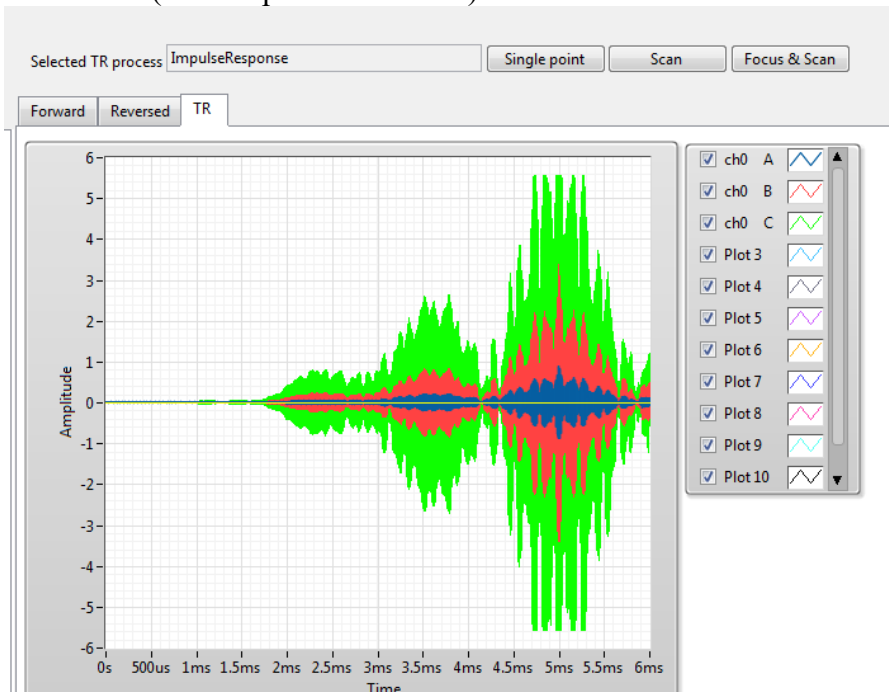
In the box showing the collected data, the "Forward" tab shows the measured response to a chirp or pulse at a single location. If 8 active channels are specified, 8 responses are shown from that location, with the first-measured on top and the most recently collected at the back. The measurements show up as they are taken. In the "Reversed" tab, the calculated and reversed impulse responses are shown. In the "TR" tab, the focus signal(s) are shown at all amplitudes specified. During a scan, only a single location is shown on the screen at a time. When the laser moves to a new location, the previous location's data is removed and the new location's data is shown.



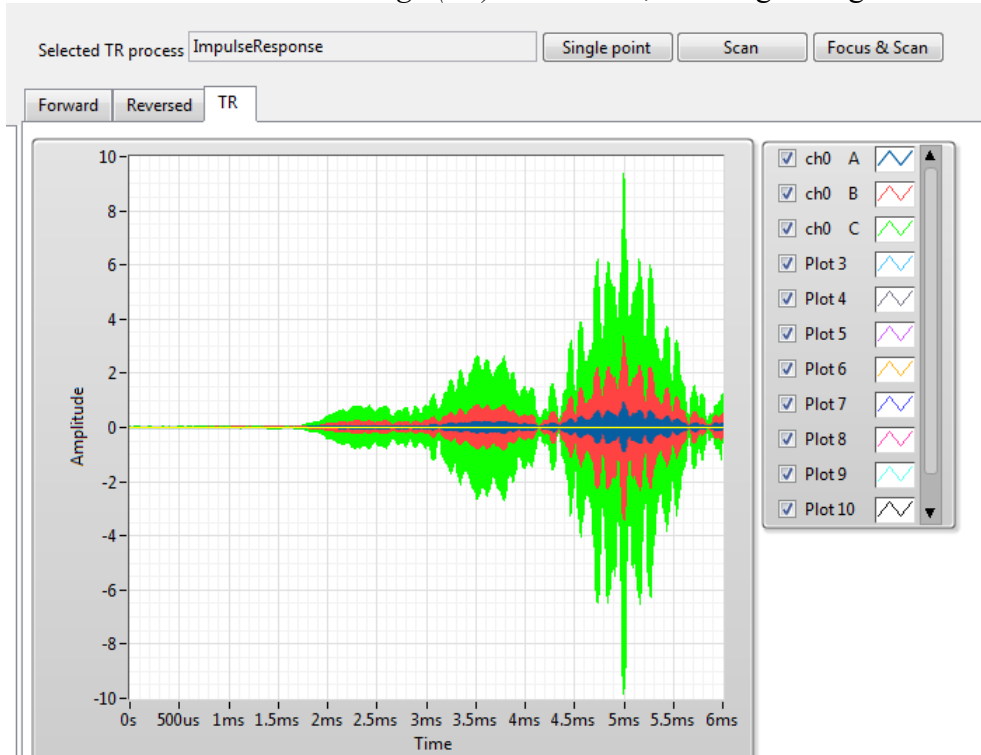
Finished measurement shown below with 8 reversed impulse responses



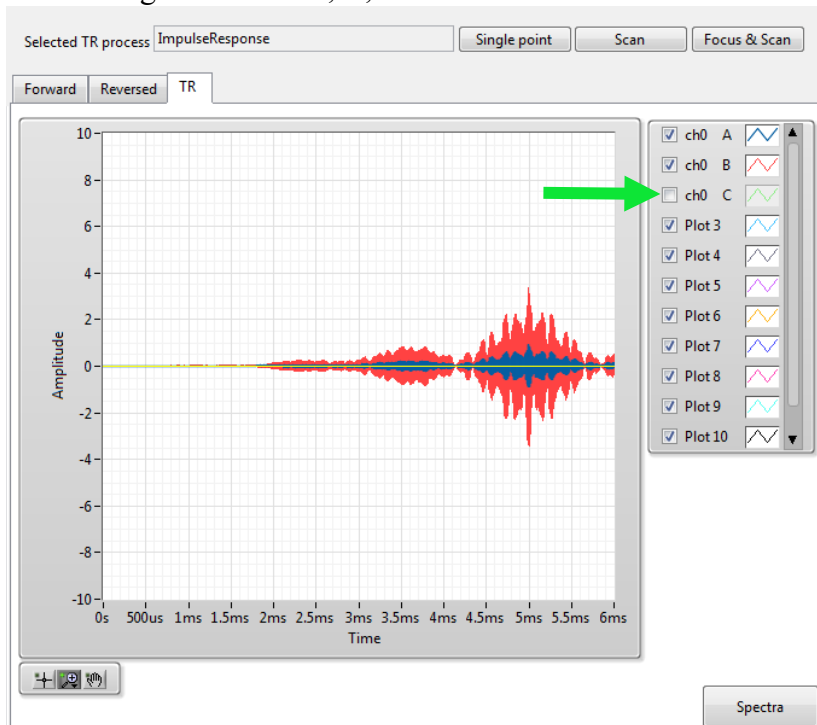
Clipped focal signals. The *Vertical range (TR)* was 10 V in this case, which cuts measurements off at 5.5 V (for inexplicable reasons).



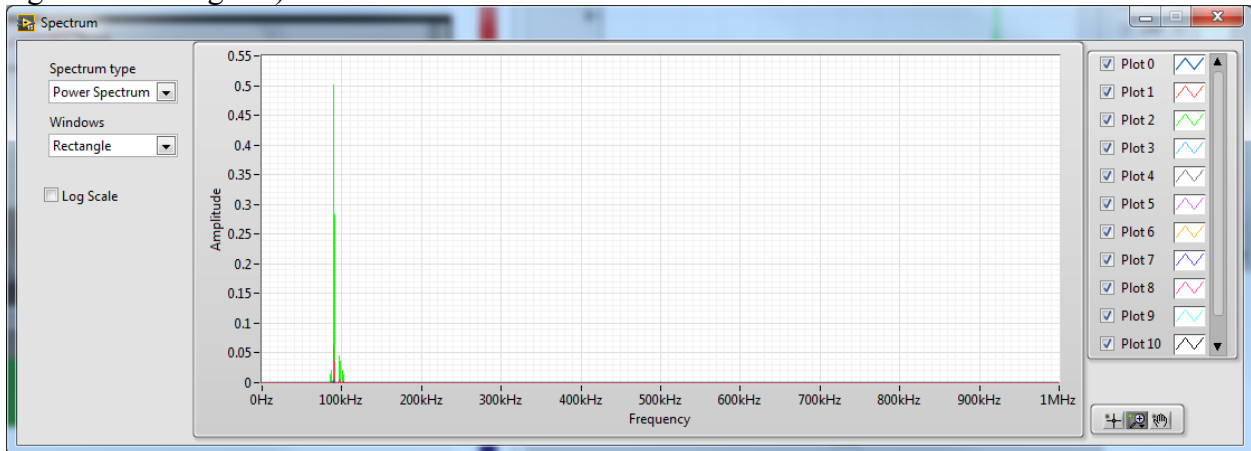
Data retaken with *Vertical range (TR)* set to 15 V, allowing the signal to be measured accurately.



You can remove some of the curves from the figure if you choose by un-checking the corresponding curve's legend box on the right (pointed out with green arrow). I have no idea why the labeling starts with A, B, C.



By clicking the button that says “Spectra” to the right of and below the curves of the measured signals you get the fourier transform of whatever signals are currently shown (either the forward signals or TR signals)

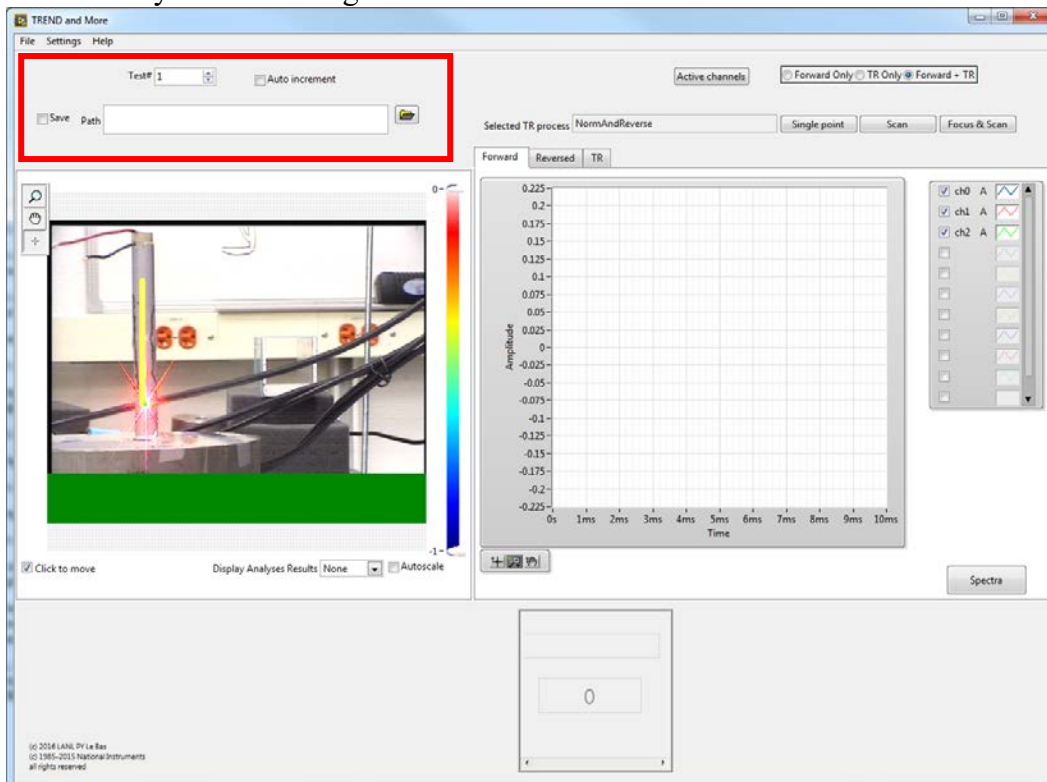


Part 10: Saving Data

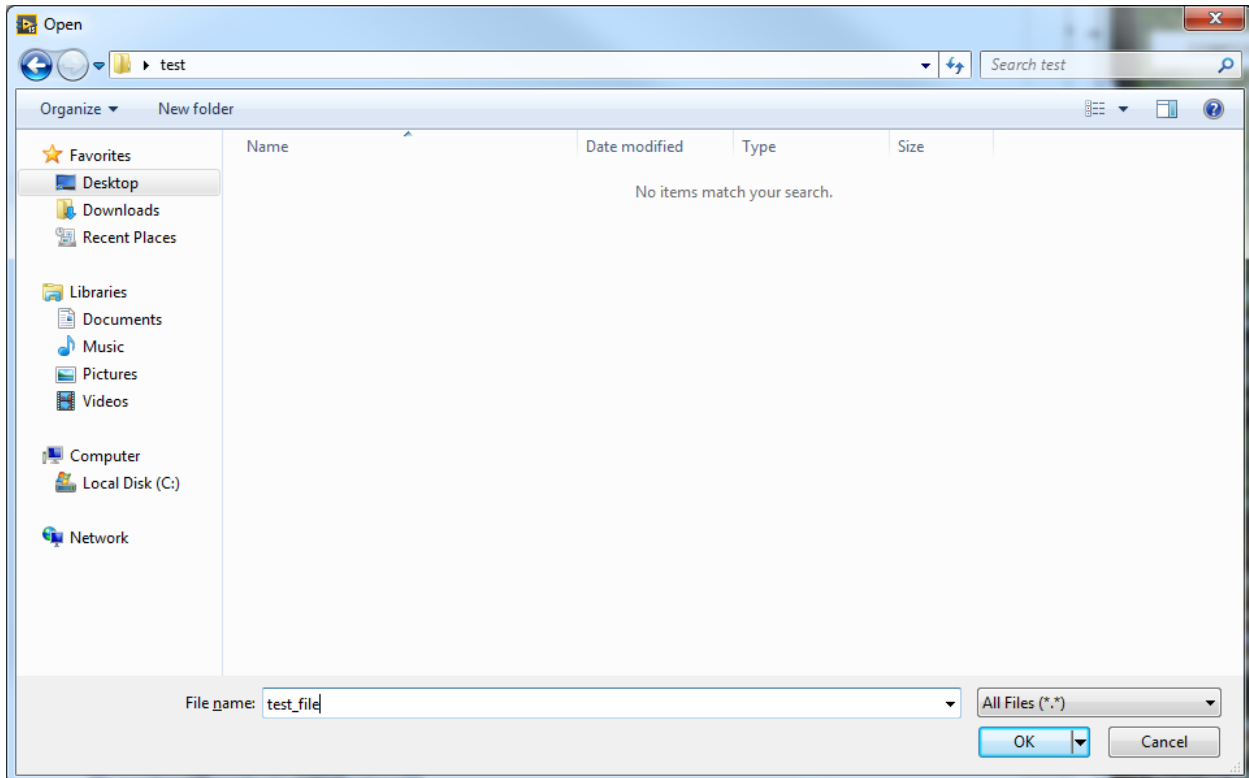
Data can be saved two different ways.

a) Automatic save

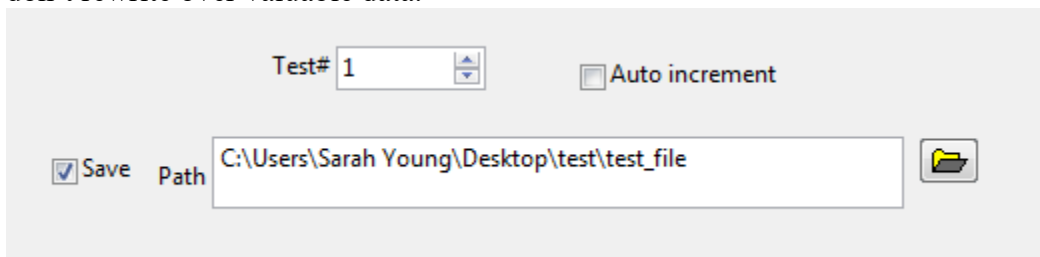
For the first method, the data is automatically saved whenever you collect data, assuming you’ve put in the right info and clicked the save box. In the region boxed in red below, click on the little file folder symbol to the right of the box labeled “Path.”



A dialogue box will open allowing you to select the location of and specify a name for the saved files. If you do not specify a name for the file, you can’t close the dialogue box.

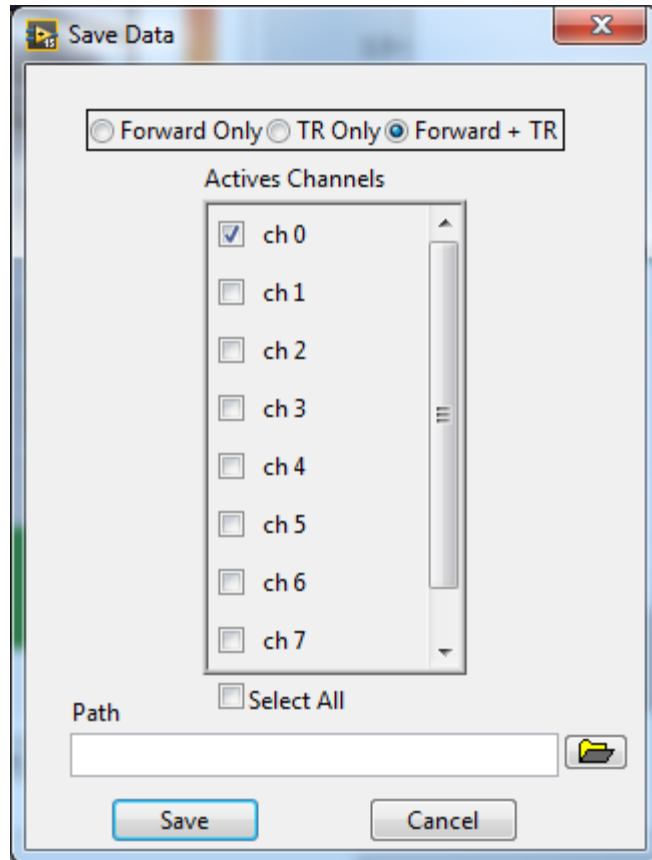
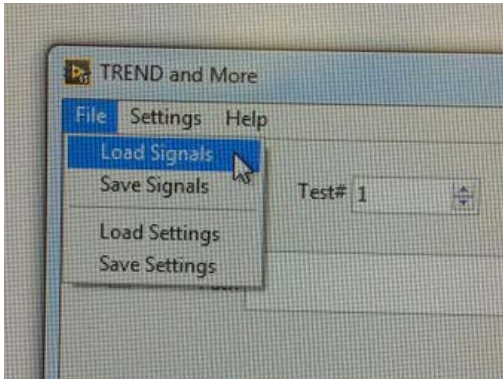


After clicking “OK” the file path and name you chose will show up in the “Path” box. You still need to check the “Save” box for data to be saved though. In the saved data names, the test# will automatically be placed after the name you gave the test, as well as info about whether the file is a forward step (chirp response or pulse response) or a focal signal and which scan point, if you’re saving a scan. If there are multiple focal signals to be saved for a single location, they will be arranged in tab-delimited columns in the same file. The same is true for multiple chirp responses. When starting a scan, there must be a path and file name in the “Path” box or LabVIEW will throw an error. TREND can’t store all of the scan data at once so it must save the data somewhere. In fact, it saves the scan data whether or not the save box is checked. If you check the “Auto increment” box, successive tests will have the same name you specified, but with a different number. This means you don’t have to rename data with each new test but also don’t rewrite over valuable data.



b) on-the-fly save

The second method for saving data can only save the data currently shown on the Forward and TR figures. But this allows you to take data first, look at the data, then save it if you like it. However, this does not work for scans because only the current point is saved using this method. Go into File -> Save Signals and the following box will pop up. It asks which signals you want saved and where (by choosing a path and file name).

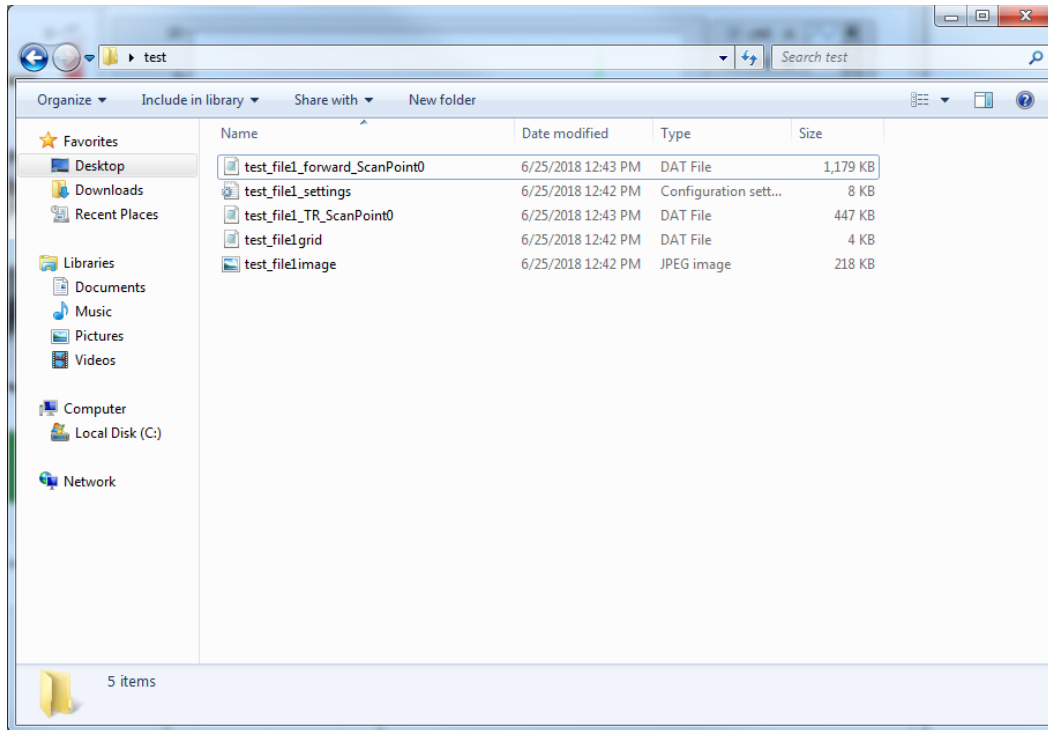


c) What you get when a single point measurement is saved

When saving data from a single point, only the forward steps and focus signals are saved in two '.dat' files. Unlike with scans, a settings file or image is not saved

d) What you get when a scan saves data

When running a scan, three files are saved before data is even collected and are labeled as settings, grid, and image (see below). The grid file saves the location of the scan points as x and y positions in two columns. The numbers are fairly arbitrary (it might be related to pixels...), but it does give the relative position and spacing of the grid points. The image file is a saved picture of the video feed at the beginning of the scan. This figure also shows the first saved scan point with the forward step labeled as "test_file1_forward_ScanPoint0" and the focus data labeled as "test_file1_TR_ScanPoint0."



A settings file looks something like this (shown below). It lists off most of the settings specified in the Generations and Acquisition settings windows. The last entry “Las_sens = 25” was put in by hand and keeps a record of the laser sensitivity used (in mm/s/V). The laser sensitivity is not incorporated into the TREND software anywhere and must be changed on the Polytec PSV software.

DO NOT FORGET TO CHECK THE LASER SENSITIVITY!! Much good data has been lost due to an incorrect laser sensitivity.

Note on weird system bug: every so often the settings file will show 16 generation channels (through ch0-15) instead of the 8 in use. This occurrence correlates with a strange phenomenon wherein none of the forward signals are saved. Files are created for them but they are empty. I recommend that after you start a scan, you immediately open the settings file, check to see if the correct number of generation channels are shown (8 will always be shown, but the ones not in use will =False) and also put in the Las_sens. If more channels than 8 are shown, abort the measurement and try again.

With the settings file as shown (including Las_sens = 25 at the bottom), a Matlab function has been created to automatically read the settings file and put the info into a structure. This code is included in Part 13: Useful Matlab code developed for TREND.

```
test_file1_settings - Notepad
File Edit Format View Help
[Settings]
Signal type = 4.000000
Frequency = 75000.000000
Frequency 2 = 125000.000000
Amplitude = 1.000000
Pulse duration = 0.004000
Pulse delay = 0.001000
Signal duration = 0.006000
Sampling frequency = 500000.000000
Force sampling = TRUE
window = 0.000000
Time between signals = 0.020000
Generator = "\00\00\00\02\11\0FFPGAgen.lvclass\00\00\00\00\01\00\00\00\00\07'
TRparts = 2.000000
ch0 active = TRUE
ch1 active = TRUE
ch2 active = TRUE
ch3 active = TRUE
ch4 active = TRUE
ch5 active = TRUE
ch6 active = TRUE
ch7 active = TRUE
Motion = "\00\00\00\02\17\15ScanningLaser.lvclass\00\00\01\00\00\00\00\00\05\00'
%¥ó"%@f \00\00\00\00\00\00@c)¥ó"»ð@f \00\00\00\00\00@coA@RTe@f \00\00\00\00\00@cup-
\00\00\00\00@h«½\1B\030ú@f \00\00\00\00\00@hNùh3u\10@f \00\00\00\00\00@h-ðµc\0E:
\00\00\00@n-ðBäu$@f \00\00\00\00\00@n5ð\14•:@f \00\00\00\00\00@nz\0cYD.P@f \00\
qxðµc\0E&@f \00\00\00\00\00@që\030úú²@f \00\00\00\00\00@qb\12\02'§<@f \00\00\00\
01ISZ;@f \00\00\00\00\00@t-\0FoëjA@f \00\00\00\00\00@t¿\1D-f7Q@f \00\00\00\00\00

[Acquisition Settings]
Acquisition card = "\00\00\00\02\12\10NI-Scope.lvclass\00\00\00\01\00\00\00\00\00\
TR amplitude#0 = 0.250000
TR amplitude#1 = 1.000000
TR amplitude#2 = 3.500000
Unit/V coefficient = 1.000000
Vertical range (forward) = 2.000000
Vertical range (TR) = 15.000000
Sample rate = 2000000.000000
# averages = 100.000000

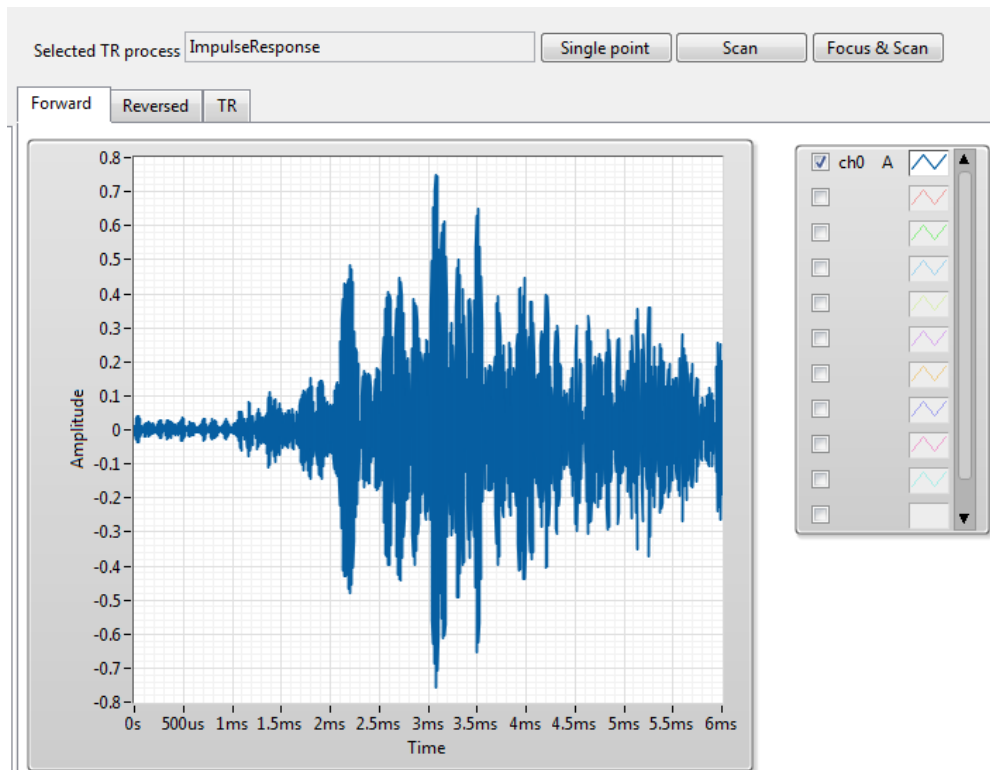
[TR]
Process = "ImpulseResponse"

Las_sens = 25
```

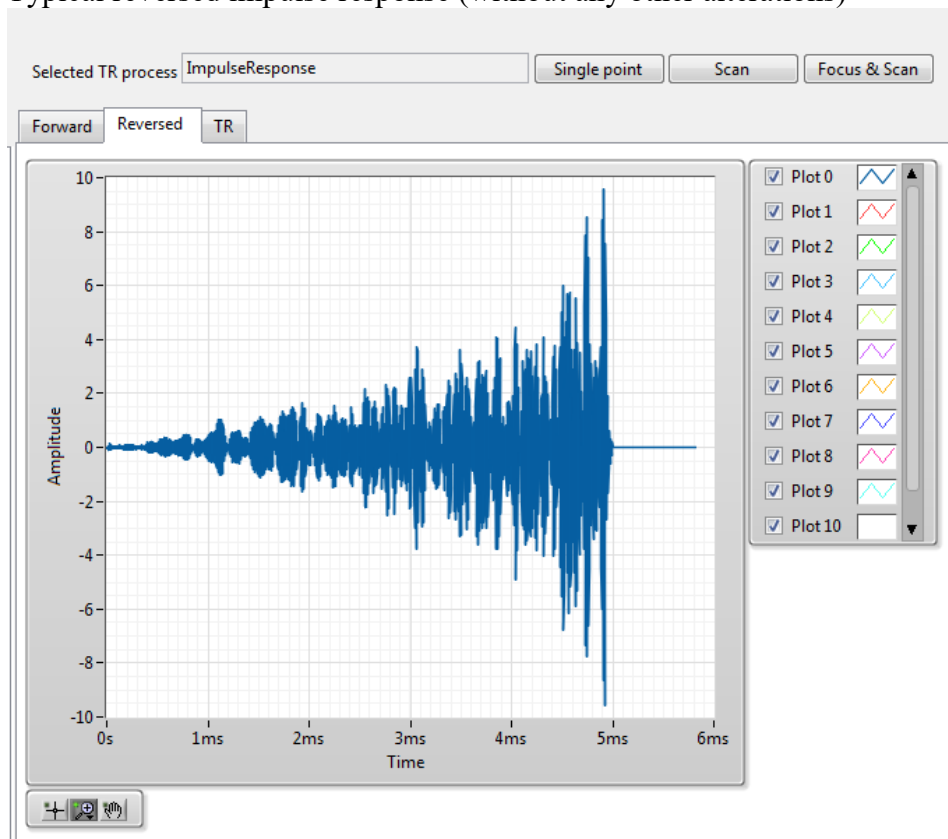
Part 11: Typical Signals

The signals shown above are from a highly resonant system. If the signals you are getting look wrong, they're probably wrong. Sometimes TREND throws weird looking signals for no discernable reason. For a typical nonresonant system operating in solids with ultrasonics, signals should look more like this:

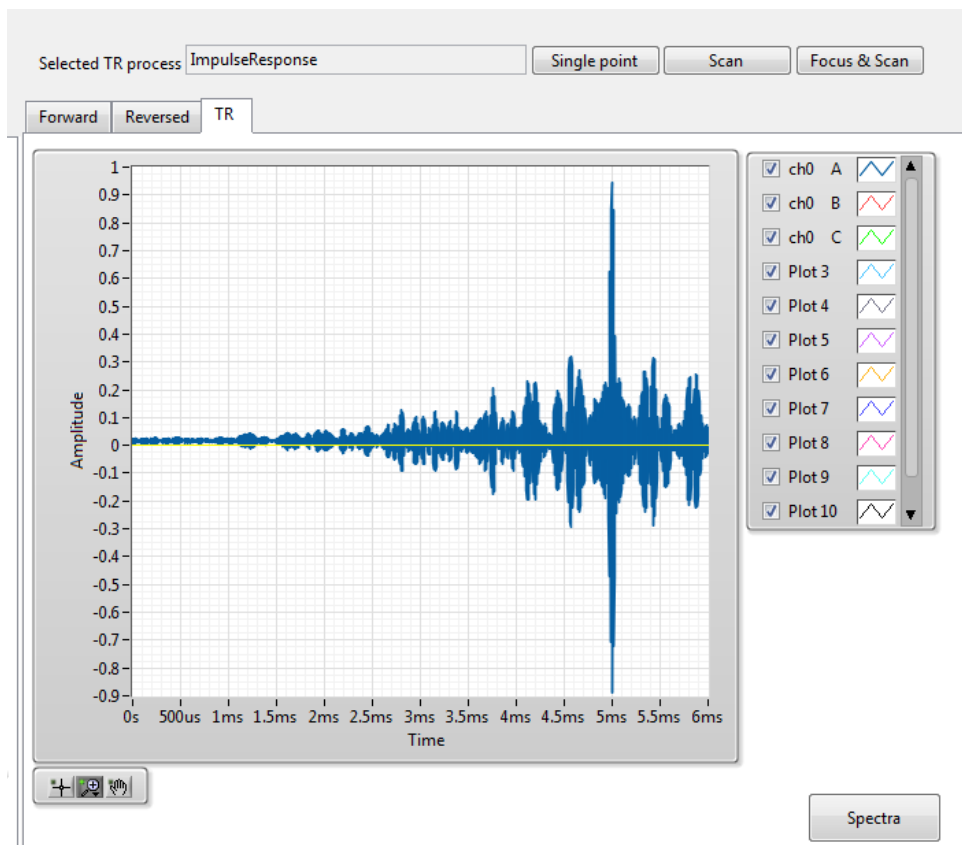
Typical chirp response



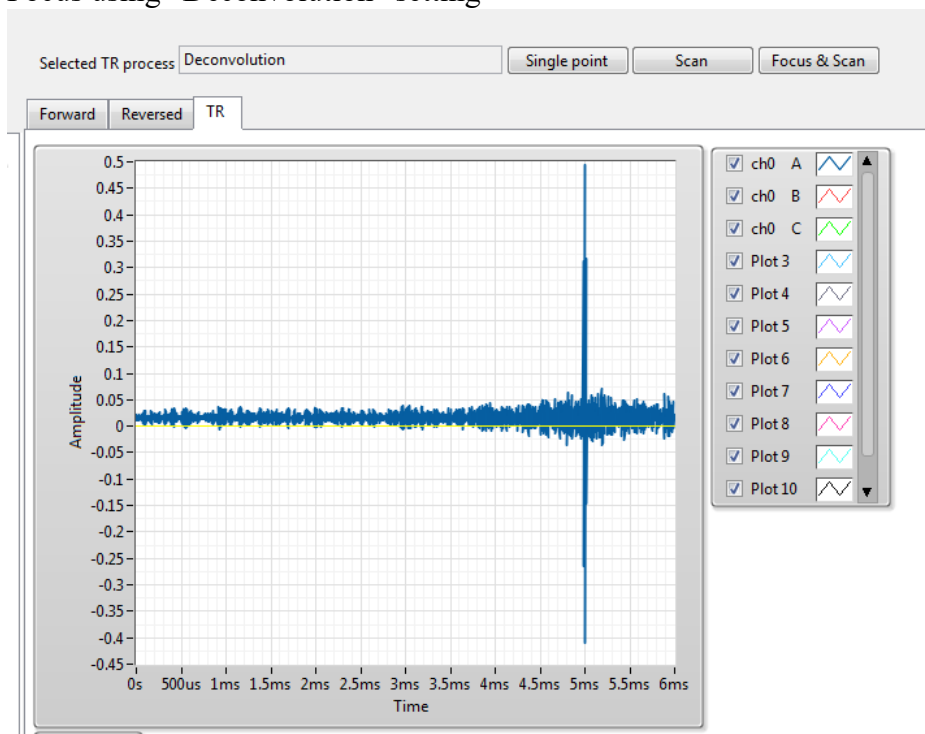
Typical reversed impulse response (without any other alterations)



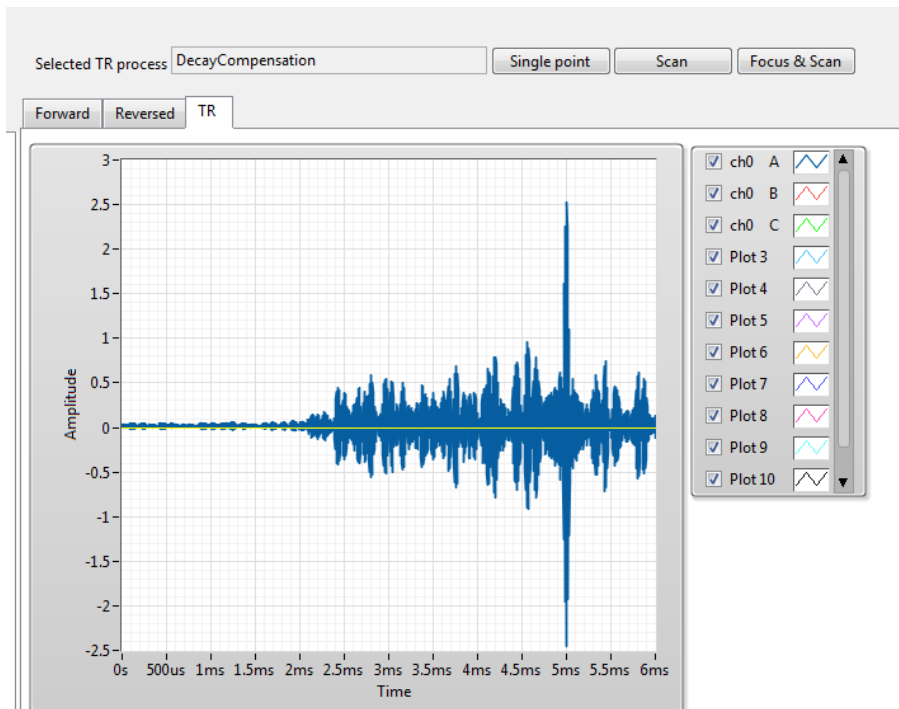
Focus using “ImpulseResponse” setting



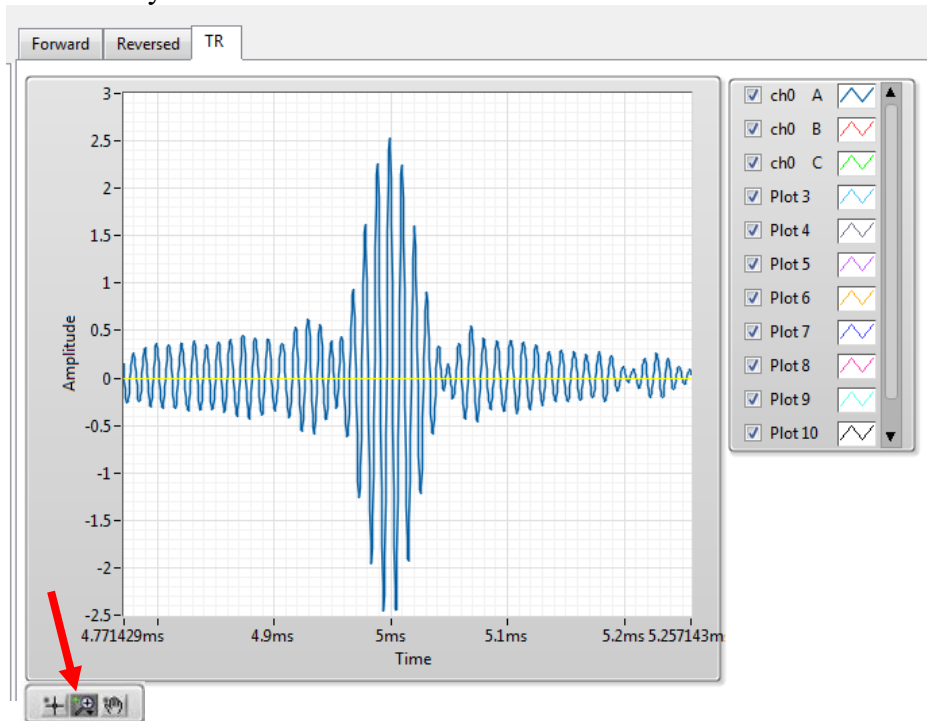
Focus using “Deconvolution” setting



Focus using “DecayCompensation”

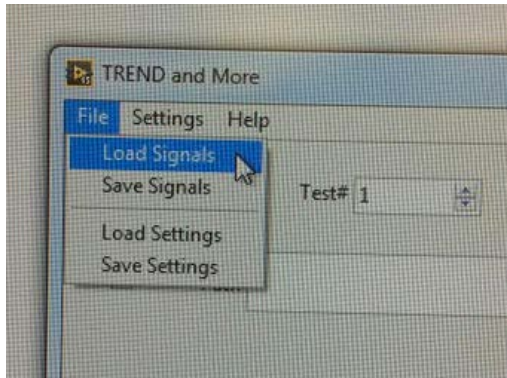


The figure below shows a plot zoomed in over the x-axis time-scale. To adjust the figure either back to its original state or to use a different type of zoom click the button on the bottom left indicated by the red arrow.



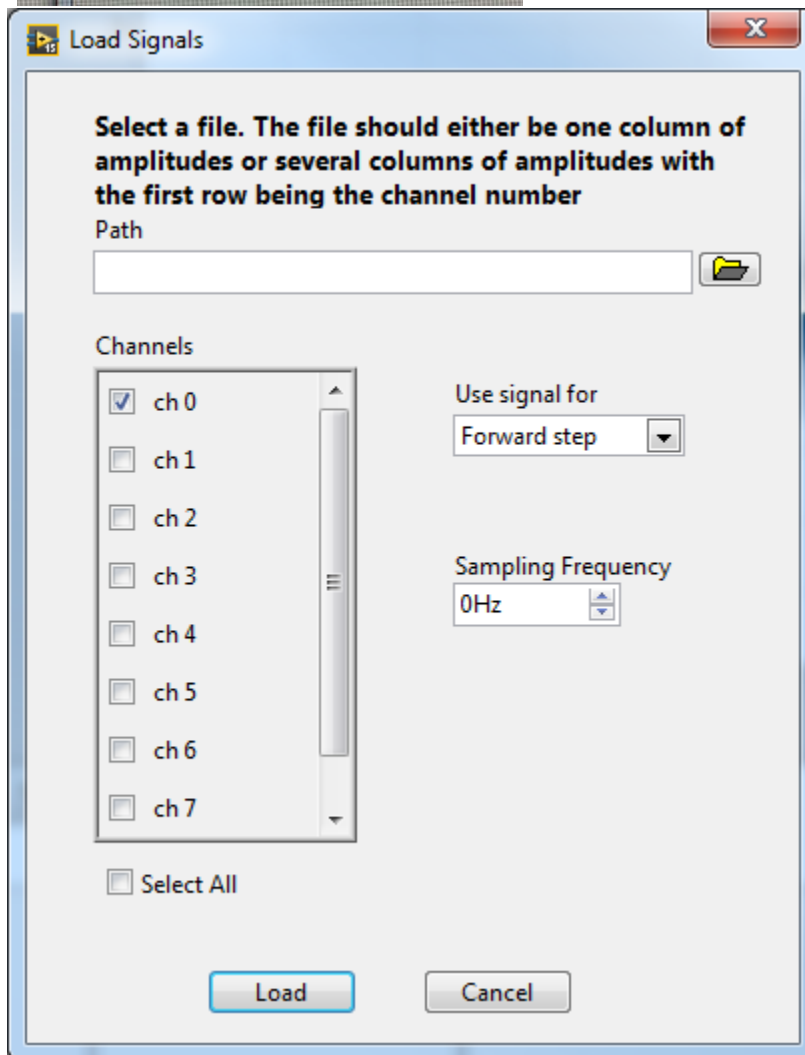
Part 12: Other things

a) Other options under File



Under “File” a couple of options exist that I have never used so don’t know if they have quirky behavioral issues.

File -> Load Signals (shown below) allows you to load previously saved signals

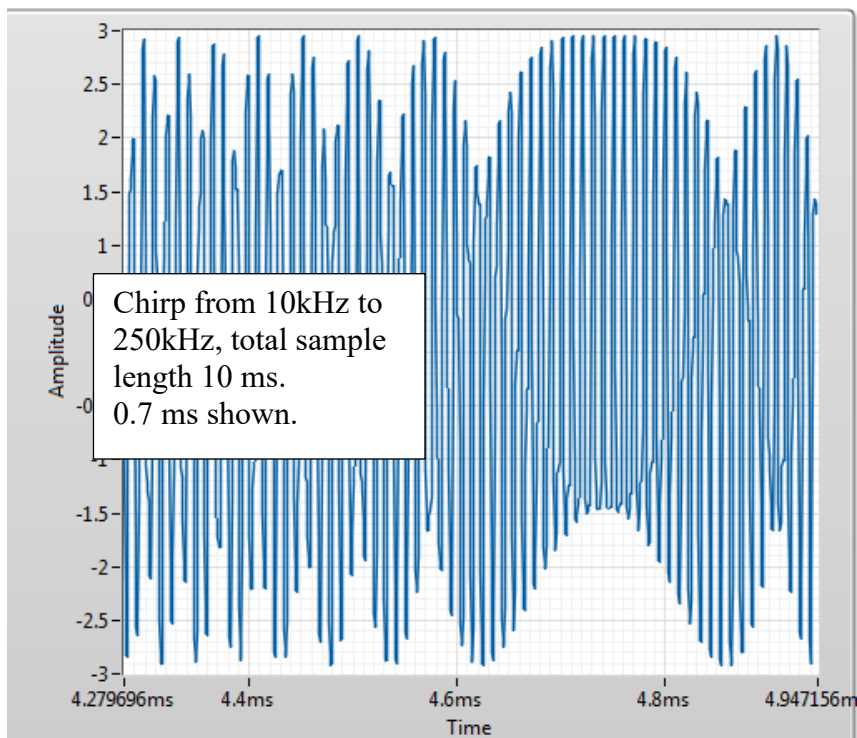
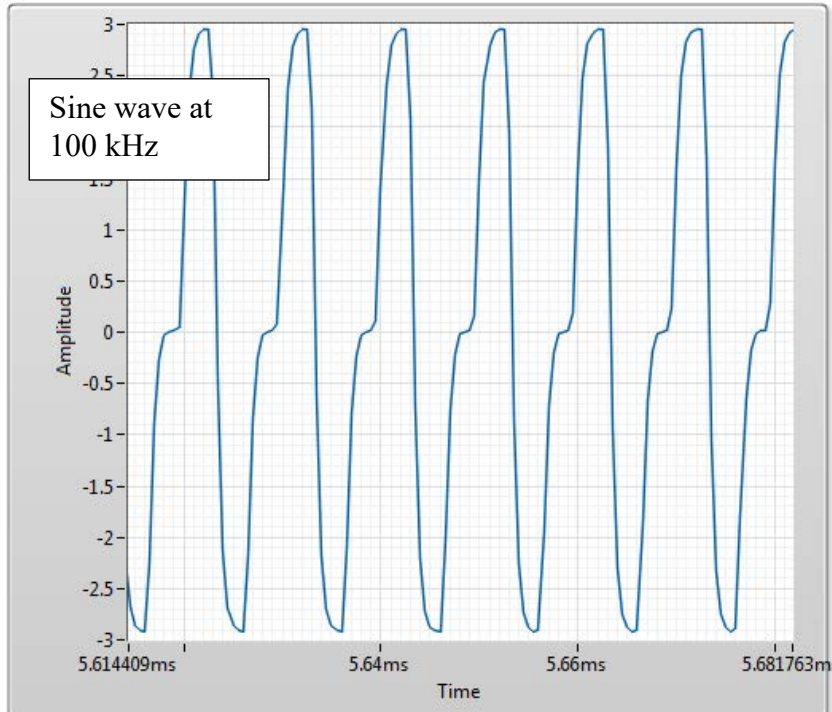


File -> Save Settings and File -> Load Settings hypothetically allows you to save a settings file and load the settings saved in a settings file. It is unknown whether adding “Las_sens” to the settings file breaks this option. Also, it is unlikely that loading settings also connects the software to acquisition and generation cards and mirror controls so that will likely need to be done by hand anyway.

b) Nonlinear characteristics of acquisition and generation cards

In the past, the acquisition card (NI PXIe-5122) has been known to collect data such that higher frequency signals are reduced in amplitude. This may or may not still be the case.

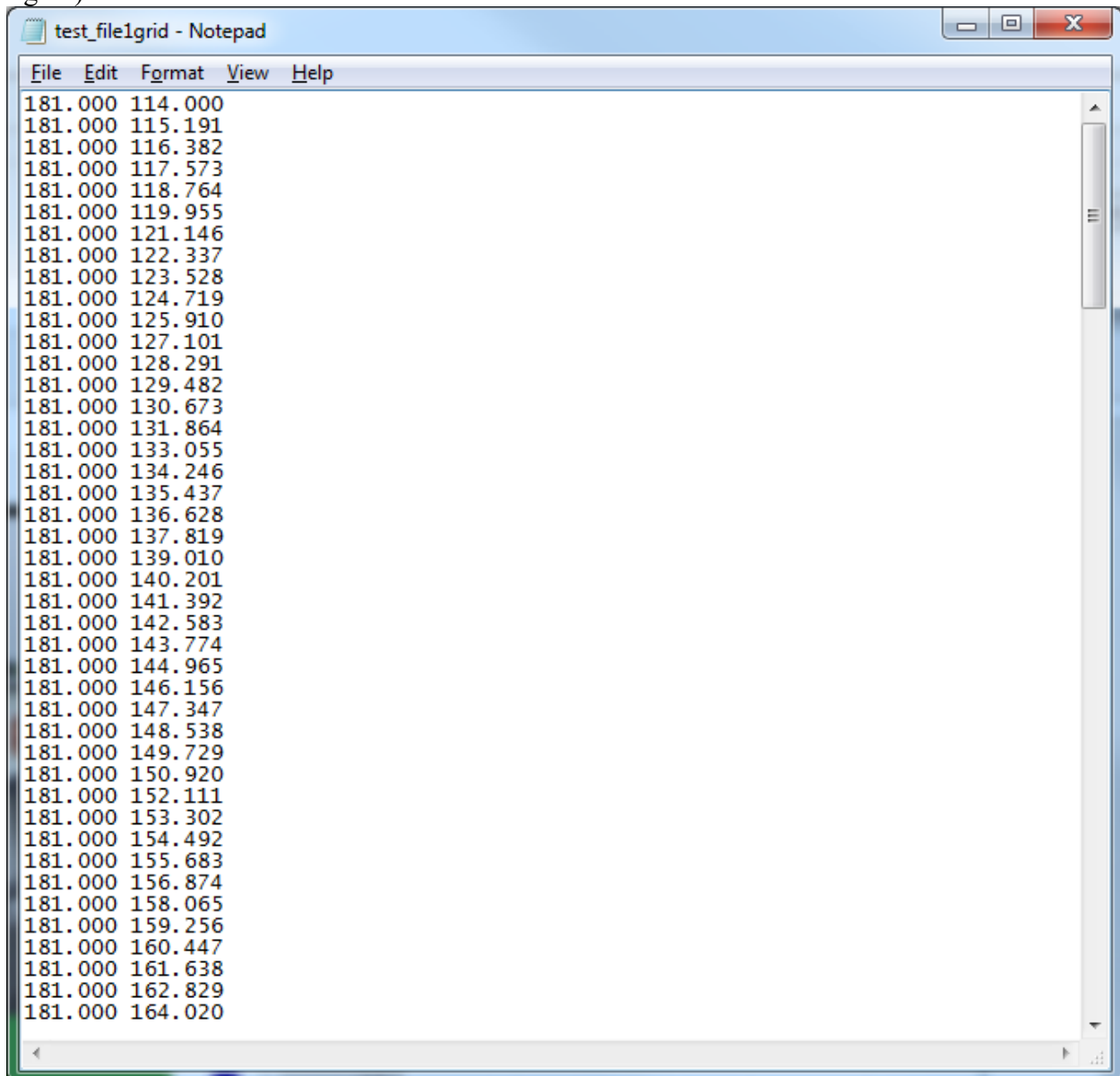
In the past, the generator card (NI PXI-7852R) has been known to emit data with inconsistent amplitude and shape. If you zoom in to signals the amplitudes or signal patterns are not quite sinusoidal. See two examples below.



Part 12: How to load your own scan grid

Despite many efforts, a way has not been determined to create your own grid from scratch. The first problem is that the file type must be very specific. Second, the grid numbering in TREND is somewhat arbitrary, so to build a grid that shows up where you want it to is rather difficult. In this example, we will take a preexisting line of grid points and, maintaining the end points, triple the spatial resolution.

First, set up a grid in TREND and start a scan so it gets saved as a grid.dat file. Abort the scan. Below is a picture of what the grid.dat file looks like for the line scan defined. All the x-coordinates are the same and the y-coordinates increase with point number (as far as I can tell, the (0,0) coordinate position is the upper left corner of the video feed and the coordinate values increase as they move further from it. This means that, assuming the coordinates go in order of scan point with ScanPoint0 at the top, which they do, going down the scan line is an increase in y-coordinate. Go figure).



```
test_file1grid - Notepad
File Edit Format View Help
181.000 114.000
181.000 115.191
181.000 116.382
181.000 117.573
181.000 118.764
181.000 119.955
181.000 121.146
181.000 122.337
181.000 123.528
181.000 124.719
181.000 125.910
181.000 127.101
181.000 128.291
181.000 129.482
181.000 130.673
181.000 131.864
181.000 133.055
181.000 134.246
181.000 135.437
181.000 136.628
181.000 137.819
181.000 139.010
181.000 140.201
181.000 141.392
181.000 142.583
181.000 143.774
181.000 144.965
181.000 146.156
181.000 147.347
181.000 148.538
181.000 149.729
181.000 150.920
181.000 152.111
181.000 153.302
181.000 154.492
181.000 155.683
181.000 156.874
181.000 158.065
181.000 159.256
181.000 160.447
181.000 161.638
181.000 162.829
181.000 164.020
```

Take these values and copy-paste them into an Excel file.

	A	B	C	D	E	F	G	H	I	J	K	L	M	N	O	P
1	181	114														
2	181	115.191														
3	181	116.382														
4	181	117.573														
5	181	118.764														
6	181	119.955														
7	181	121.146														
8	181	122.337														
9	181	123.528														
10	181	124.719														
11	181	125.91														
12	181	127.101														
13	181	128.291														
14	181	129.482														
15	181	130.673														
16	181	131.864														
17	181	133.055														
18	181	134.246														
19	181	135.437														
20	181	136.628														
21	181	137.819														
22	181	139.01														
23	181	140.201														
24	181	141.392														
25	181	142.583														
26	181	143.774														
27	181	144.965														
28	181	146.156														
29	181	147.347														

Determine the current dx (it's supposed to be dy in this case, but whatever), by subtracting the first two scan points.

The screenshot shows an Excel spreadsheet with the following data:

	A	B	D
1	181	114	current dx
2	181	115.191	1.191
3	181	116.382	
4	181	117.573	
5	181	118.764	
6	181	119.955	
7	181	121.146	
8	181	122.337	
9	181	123.528	
10	181	124.719	
11	181	125.91	
12	181	127.101	
13	181	128.291	
14	181	129.482	
15	181	130.673	
16	181	131.864	

Based off of this value, determine what your desired dx is. In this case it's the current dx/3.

The screenshot shows an Excel spreadsheet with the following data:

	A	B	C	D	E	F	G	H	I	J
1	181	114		current dx		desired dx				
2	181	115.191		1.191		0.397				
3	181	116.382								
4	181	117.573								
5	181	118.764								
6	181	119.955								
7	181	121.146								
8	181	122.337								
9	181	123.528								
10	181	124.719								
11	181	125.91								
12	181	127.101								
13	181	128.291								
14	181	129.482								
15	181	130.673								
16	181	131.864								

Starting with the first point the same, create two new vectors of values with the desired dx. In this case, the new vectors will be three times longer than the original grid. That's ok. Make sure they maintain three decimal points.

Book1 - Excel

FILE HOME INSERT PAGE LAYOUT FORMULAS DATA REVIEW VIEW ADD-INS Sign

Clipboard Font Alignment Styles

Calibri 11

Number

Conditional Formatting

Format as Table

Cell Styles

Cells Editing

I2 : \times \checkmark fx =I1+\$F\$2

	A	B	C	D	E	F	G	H	I	J
1	181	114		current dx		desired dx		181.000	114.000	
2	181	115.191		1.191		0.397		181.000	114.397	
3	181	116.382						181.000	114.794	
4	181	117.573						181.000	115.000	
5	181	118.764						181.000	115.397	
6	181	119.955						181.000	115.794	
7	181	121.146						181.000	116.000	
8	181	122.337						181.000	116.397	
9	181	123.528						181.000	116.794	
10	181	124.719						181.000	117.000	
11	181	125.91						181.000	117.397	
12	181	127.101						181.000	117.794	
13	181	128.291						181.000	118.000	
14	181	129.482						181.000	115.000	
15	181	130.673						181.000	115.397	
16	181	131.864						181.000	115.794	

Sheet1

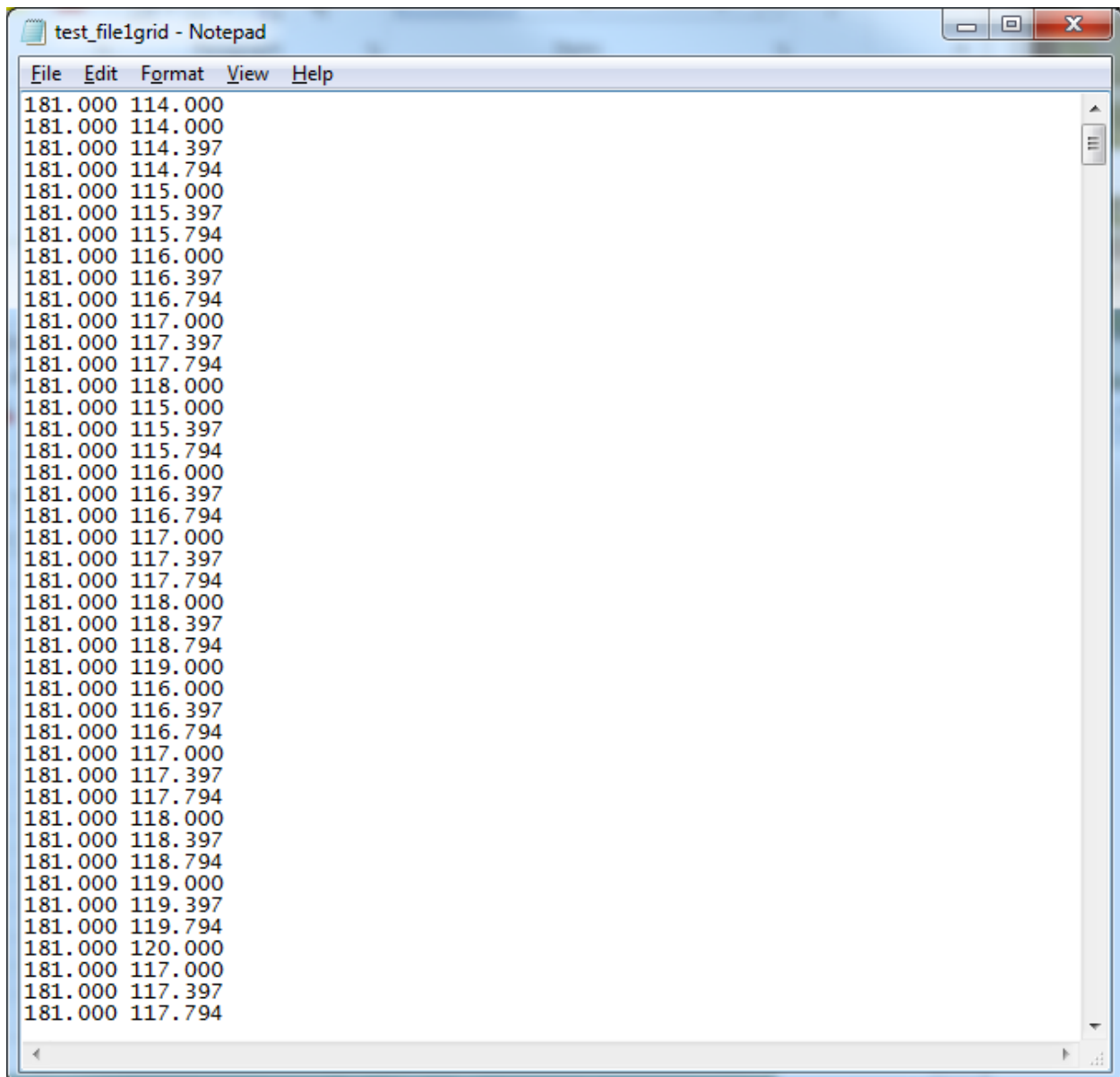
READY 100%

The screenshot shows an Excel spreadsheet with the following data:

	A	B	C	D	E	F	G	H	I	J	K	L	M	N	O	P
1	181	114		current dx		desired dx		181.000	114.000							
2	181	115.191		1.191		0.397		181.000	114.397							
3	181	116.382						181.000	114.794							
4	181	117.573						181.000	115.000							
5	181	118.764						181.000	115.397							
6	181	119.955						181.000	115.794							
7	181	121.146						181.000	116.000							
8	181	122.337						181.000	116.397							
9	181	123.528						181.000	116.794							
10	181	124.719						181.000	117.000							
11	181	125.91						181.000	117.397							
12	181	127.101						181.000	117.794							
13	181	128.291						181.000	118.000							
14	181	129.482						181.000	115.000							
15	181	130.673						181.000	115.397							
16	181	131.864						181.000	115.794							

Copy (see above) and paste the new values into the old grid.dat file (see below) without deleting the first point or last point in the file. For some reason the first and last values define some special formatting allowing the file to be read by TREND. Though I could be wrong about this. Feel free to explore.

Back in “Scan Settings,” choose to “Load grid” and select the file you’ve just created. If it worked your scan points should show up as yellow dots just where you expect them. If it didn’t work the scan points will either not show up, or when you try to run the scan, LabVIEW will throw an error.



```
test_file1grid - Notepad
File Edit Format View Help
181.000 114.000
181.000 114.000
181.000 114.397
181.000 114.794
181.000 115.000
181.000 115.397
181.000 115.794
181.000 116.000
181.000 116.397
181.000 116.794
181.000 117.000
181.000 117.397
181.000 117.794
181.000 118.000
181.000 115.000
181.000 115.397
181.000 115.794
181.000 116.000
181.000 116.397
181.000 116.794
181.000 117.000
181.000 117.397
181.000 117.794
181.000 118.000
181.000 118.397
181.000 118.794
181.000 119.000
181.000 116.000
181.000 116.397
181.000 116.794
181.000 117.000
181.000 117.397
181.000 117.794
181.000 118.000
181.000 118.397
181.000 118.794
181.000 119.000
181.000 119.397
181.000 119.794
181.000 120.000
181.000 117.000
181.000 117.397
181.000 117.794
```

Part 13: Useful Matlab code developed for TREND

a) Settings file turned into a Matlab structure

```
%% Reads the Settings contained in the file generated for TREND scans
% Sarah Young, June 2018

% To call function:
% s = TRENDSettings(test_name);
% or s = TRENDSettings([path,testname]);
% Example:
% BarScan1_settings.ini is the name of the settings file
% BarScan1 is the test_name
% s = TRENDSettings('BarScan1');
% or s = TRENDSettings('C:\Users\Sarah Young\Data\BarScan1');

% A file should also exist called 'test_namegrid.dat'
```



```

% This file needs to exist in the same folder as the settings file so the
% grid values and number of scan points can be extracted

% To work, this function requires the settings file to have the laser
% sensitivity listed at the bottom as shown:
% Process = "ImpulseResponse"
%
% Las_sens = 25

% If the Las_sens is not there, data*s.las_sens=Nan

% This function returns the following settings in a structure 's':
% s.chirp_freq <- bandwidth of the chirp generated
% s.num_channels <- the number of generation channels
% s.fs <- the acquisition sampling frequency
% s.avgs <- the number of data averages
% s.TR_Vinputs <- the voltage inputs for focus excitation
% s.las_sens <- the laser sensitivity in mm/s/V
% s.time <- a time vector corresponding to the collected time data
% s.totaltime <- the time length of each sample (the period)
% s.grid <- the two-column position values saved in grid.dat file
% s.num_points <- the number of scan points

%%
function [settings]=TRENDSettings(test_name)

    filename =[test_name '_settings.ini'];
    fid = fopen(filename);
    c = textscan(fid,'%s','delimiter','\t');
    h=char(c{1,1});
    fclose(fid);

    settings.chirp_freq=[str2double(h(3,13:17)) str2double(h(4,15:20))];
    totaltime=str2double(h(8,19:26));
    settings.num_channels=0;
    for ii=17:24
        if lower(h(ii,18))/32==1
            settings.num_channels=settings.num_channels+1;
        end
    end
    %relies on Las_sens = # being added to the bottom
    settings.fs=str2double(h(end-4,15:end));
    settings.avgs=str2double(h(end-3,13:end));
    num_levels=str2double(h(end-8,14))+1;
    b=num_levels-1:-1:0;
    for ii=1:num_levels
        settings.TR_Vinputs(ii)=str2double(h(end-(8+b(ii)),18:end));
    end
    settings.las_sens=str2double(h(end,12:end));
    settings.time=(0:totaltime*settings.fs-1)/settings.fs;
    settings.totaltime=totaltime;

    gridname=[test_name 'grid.dat'];
    settings.grid = dlmread(gridname);
    settings.num_points=length(settings.grid(:,1));

```

```
end
```

b) Read in .dat files from forward and TR steps

```
%% Efficiently reads in .dat data files generated by TREND software
% (faster than any other method I've explored, including Pierre-Yve's code)
% Sarah Young, June 2018

% To read in chirp response (or forward step)
% forward = importTR_data('test_name_forward_ScanPoint0.dat',0);
% returns matrix with the chirp response from each generator in each column
% (time along rows)
% hardcoded for up to 8 transducers (but can be less)

% To read in focus time data
% TR = importTR_data('test_name_TR_ScanPoint0.dat',1);
% returns matrix with the focus from each excitation amplitude in each column
% hardcoded for up to 12 excitation levels (but can be less)

% test_name is the user-defined portion of the filename with the TREND
% test# tacked on.
% Example: In 'BarScan1_TR_ScanPoint0.dat' BarScan1 is the test_name, 1 is
% the test#
%%
function [vars]=importTR_data(filename,TR)

if TR==0
    fid = fopen(filename);
    forward = cell2mat(textscan(fid, '%f%f%f%f%f%f%f%f')); %hardcoded for up to
8 transducers
    fclose(fid);

    if isnan(forward(end,end)) %removes data that doesn't exist (so you don't
have to know how many transducers there are)

        forward(isnan(forward))=0;
        n=1;

        while sum(forward(:,n))~=0
            n=n+1;
        end

        vars=forward(:,1:n-1);
    else
        vars=forward(2:end,:);
    end

elseif TR==1
    fid = fopen(filename);
    back = cell2mat(textscan(fid, '%f%f%f%f%f%f%f%f%f%f%f%f')); %hardcoded for up
to 12 levels
```

```
fclose(fid);

if isnan(back(end,end)) %removes data that doesn't exist (so you don't have
to know how many levels there are)
    back(isnan(back))=0;
    n=1;

    while sum(back(:,n))~=0
        n=n+1;
    end

    vars=back(:,1:n-1);
else
    vars=back;
end
end
end
```

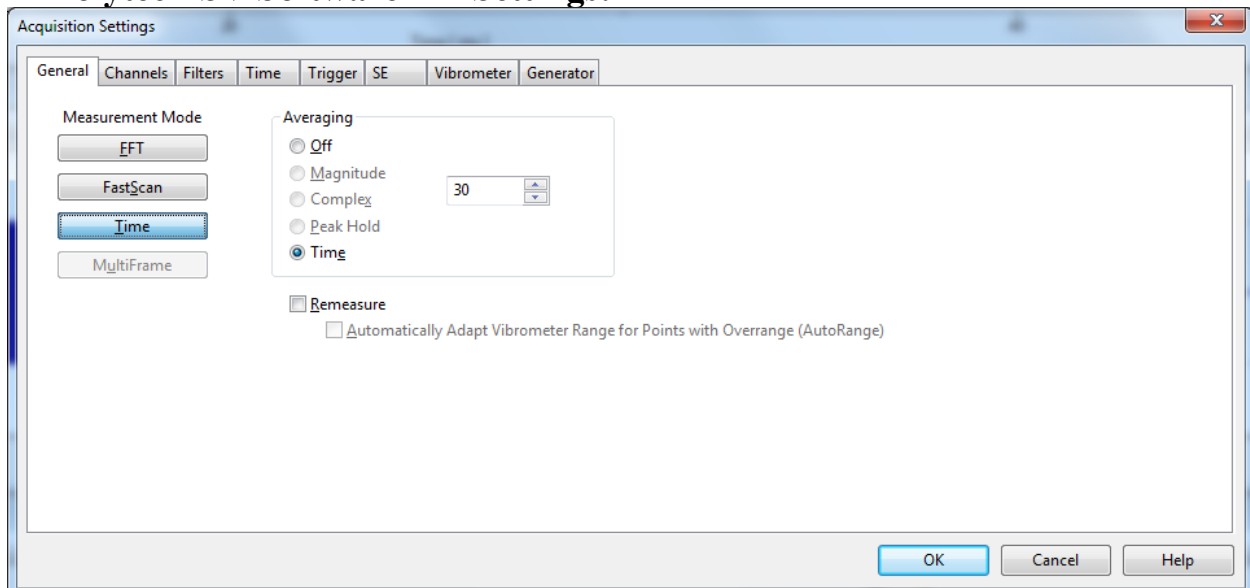
Appendix B

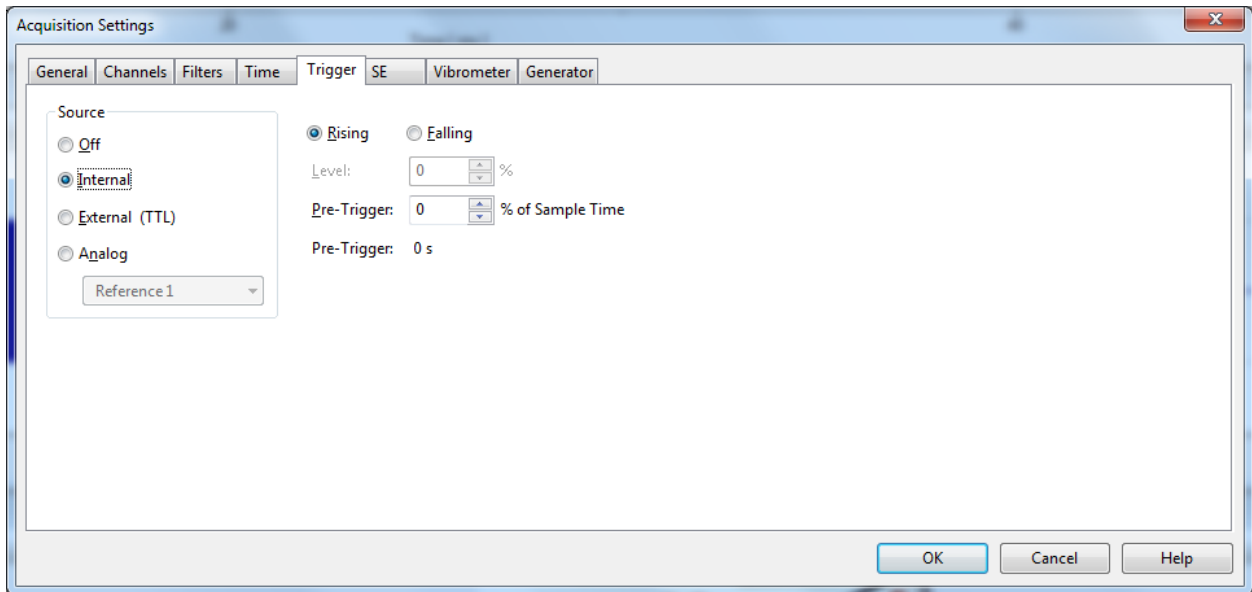
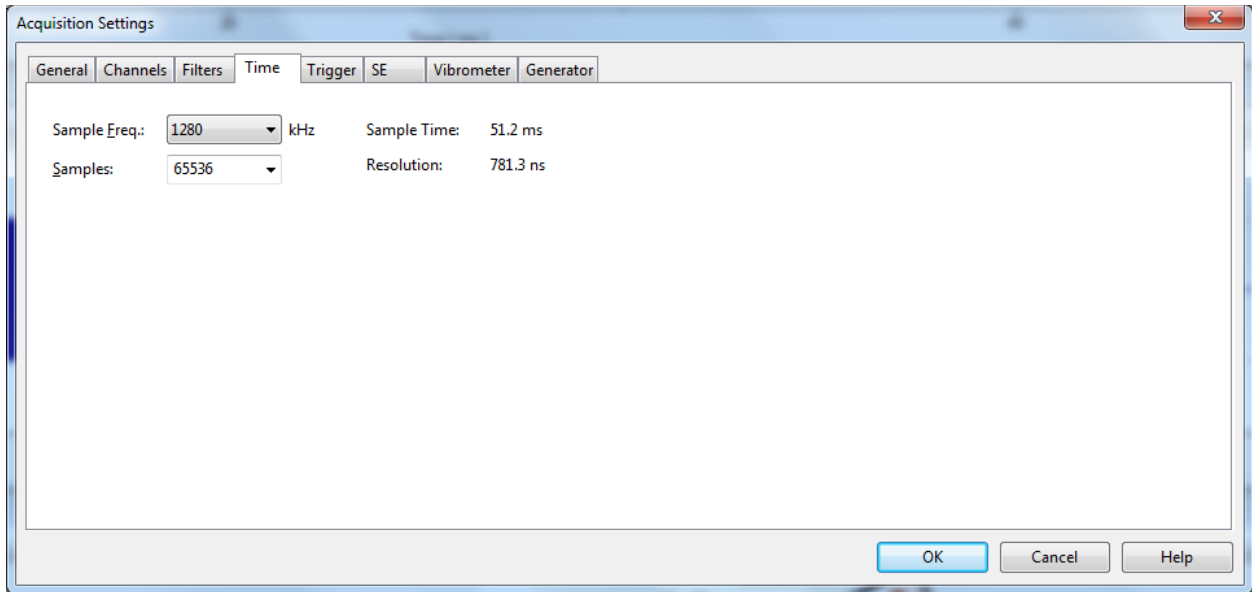
How to Successfully Create a TR focus using Polytec Software

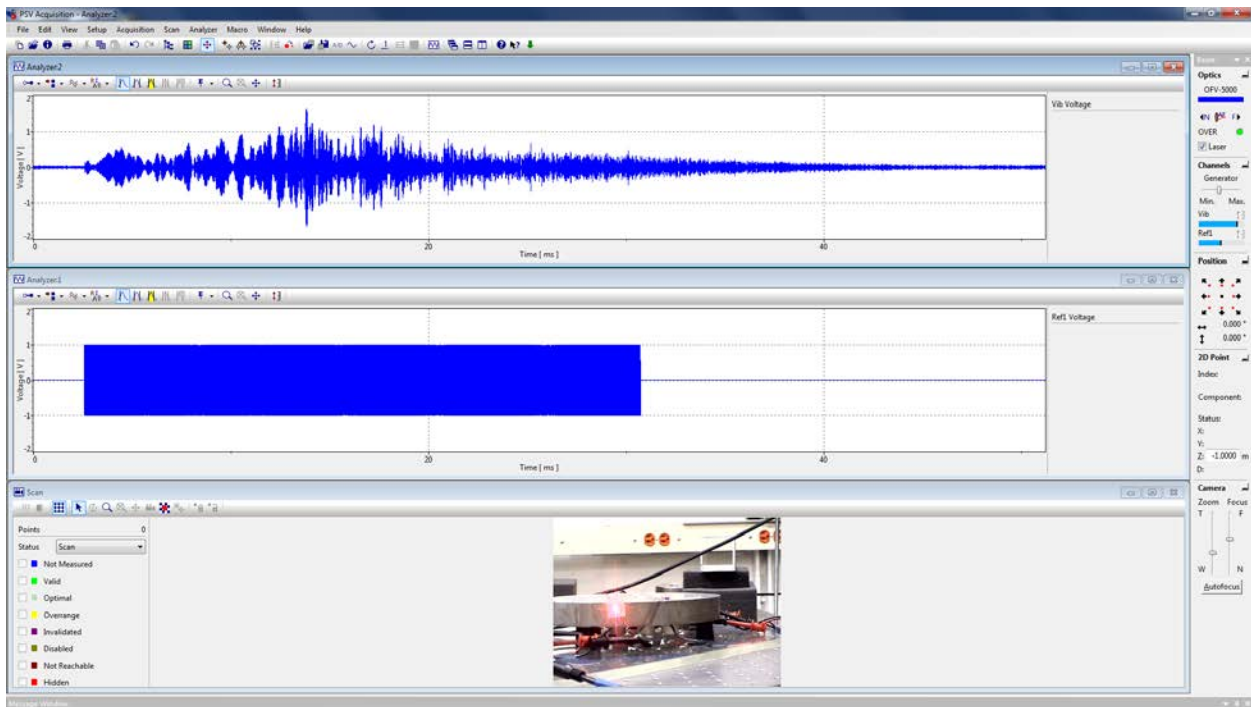
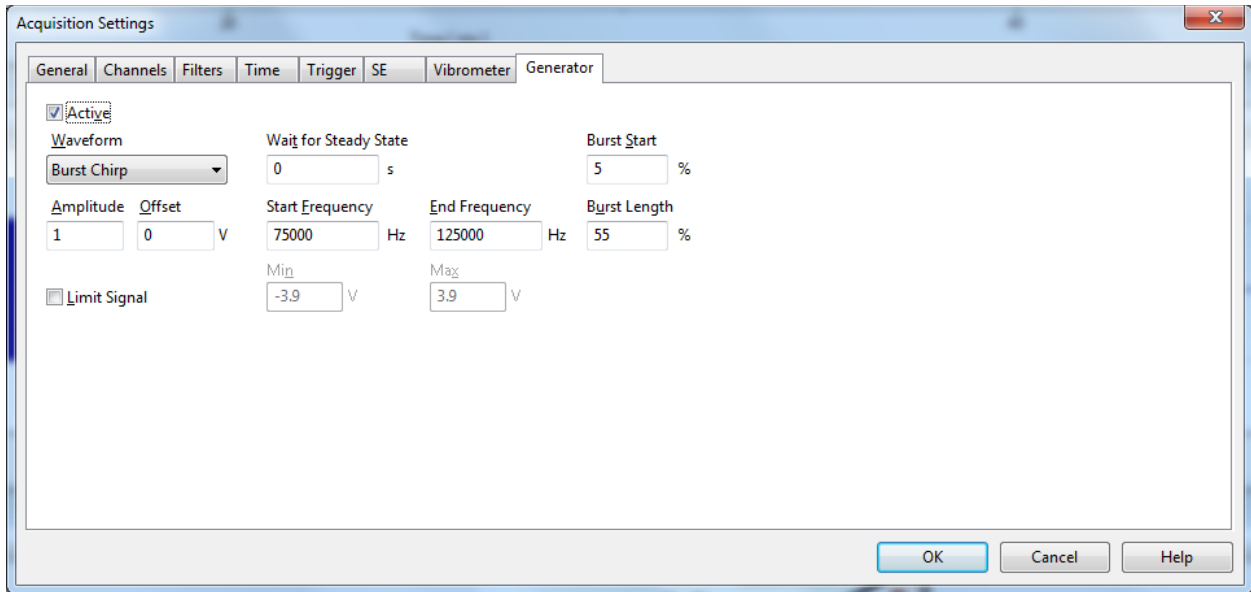
Route the generator output to not only your vibrator, but also into REF 1



In Polytec PSV Software AD Settings:



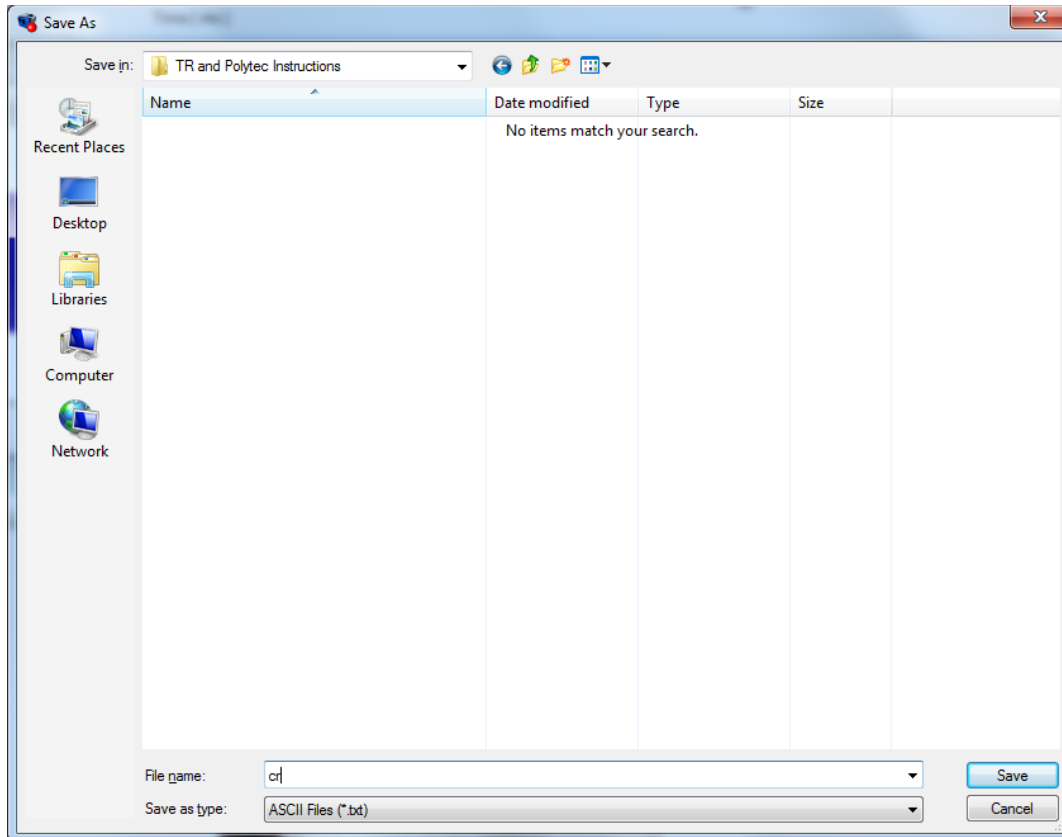




Save chirp response as “cr” and the burst chirp fed into refl as “s” for source (non-vital requirement if you change signal names in Matlab code)

To save ASCII file in Polytec: Click on analyzer window, then Save -> Export -> ASCII

This box will come up.



Code to Generate Special text file of reversed impulse response that works in Polytec User Defined Generator Settings

```
close all;
clear;

% Made to generate file that works with Polytec user defined signal
% specifications

%% Polytec settings and reading in data text files
%Polytec Settings
fs=1280e3;
N=65536;
dt=1/fs;
Ts=N/fs;

fgen=floor(fs/N); %frequency of generator in Polytec user-defined-signal
% options should be 19 for these Polytec settings
Tgen=1/fgen; % Period required for fgen
```

```

extra_time=Tgen-Ts; % extra time that needs to be tacked onto end of TR
% signal so it matches rate of fgen
padding=floor(extra_time/dt); %extra_time translated into a number of
% zeros with which the TR signal will be padded

path='D:\SarahY\TR and Polytec Instructions\';
source=dlmread([path,'s.txt'],'\t',5,0);
s=source(:,2);
cr=dlmread([path,'cr.txt'],'\t',5,1);

%% building time reversed impulse response

ir=impresp(s,cr); % generates impulse response

rtr=flipud(ir); %flip data up down (time reverse impulse response)

rtrn=rtr/max(abs(rtr)); % normalized reversed ir

RTR=zeros(size(rtr)); %array of zeros length of ir
RTR(1:end/2)=rtrn(end/2+1:end); % take the first half of RTR and make it
% equal to the second half of rtrn, the rest will be zeros
% above step places peak of reversed impulse response at time-center of
% signal, such that first half of signal is reversed impulse response and
% second half is zeros (this ensures that focus will be in center of time
% signal)

%%-----
%%implement clipping, decay compensation, deconvolution...etc right here
% threshold = 0.1;
% RTR_clp=clippingTR(RTR,threshold);
% RTR=RTR_clp; %redefine RTR as clipped version
%%-----

RTR(end+1:end+padding)=0; % add padding of zeros to get timing right
TR=RTR;

%% write signal as text file appropriate for Polytec user-defined-signal

filename=[path,'TR.txt'];
header='ArbWave =';
dlmwrite(filename,header,'delimiter',' ','newline','pc')
dlmwrite(filename,TR,'-append','delimiter','\n','newline','pc')

```


Back to Polytec

